

JYU DISSERTATIONS 175

Elmeri Lahtinen

Chemically Functional 3D Printing

Selective Laser Sintering of
Customizable Metal Scavengers



UNIVERSITY OF JYVÄSKYLÄ
FACULTY OF MATHEMATICS
AND SCIENCE

JYU DISSERTATIONS 175

Elmeri Lahtinen

Chemically Functional 3D Printing

Selective Laser Sintering of Customizable Metal Scavengers

Esitetään Jyväskylän yliopiston matemaattis-luonnontieteellisen tiedekunnan suostumuksella
julkisesti tarkastettavaksi yliopiston Ylistönrinteen salissa YlistöKem4
joulukuun 20. päivänä 2019 kello 12.

Academic dissertation to be publicly discussed, by permission of
the Faculty of Mathematics and Science of the University of Jyväskylä,
in Ylistönrinne, auditorium Ylistökem4, on December 20th, 2019 at 12 o'clock noon..



JYVÄSKYLÄN YLIOPISTO
UNIVERSITY OF JYVÄSKYLÄ

JYVÄSKYLÄ 2019

Editors

Matti Haukka

Department of Chemistry, University of Jyväskylä

Päivi Vuorio

Open Science Centre, University of Jyväskylä

Copyright © 2019, by University of Jyväskylä

Permanent link to this publication: <http://urn.fi/URN:ISBN:978-951-39-7994-2>

ISBN 978-951-39-7994-2 (PDF)

URN:ISBN:978-951-39-7994-2

ISSN 2489-9003

ABSTRACT

Lahtinen, Elmeri

Chemically Functional 3D Printing: Selective Laser Sintering of Customizable Metal Scavengers

Jyväskylä: University of Jyväskylä, 2019, 71 p.

(JYU Dissertations

ISSN 2489-9003; 175)

ISBN 978-951-39-7994-2 (PDF)

Growing interest towards making industrial processes and waste management more efficient has created an increasing demand for efficient and easy-to-use metal scavenging methods. Many processes today still operate with the mentality that only the metal of interest should be recovered during the process, while the rest of the metals can be treated as waste. In the long term, this is not a sustainable model. In many cases, the difficulty and cost of incorporating a metal recovery process into an already existing operation are some of the main reasons why metal management often remains on a very basic level.

In this work, Selective Laser Sintering (SLS) 3D printing is suggested as a way to prepare highly customizable metal scavenging filters that could easily be incorporated into already existing processes. Usually, 3D printing is only utilized for the production of objects with mere mechanical or aesthetical properties. However, in this study, the focus was on incorporating chemical functionality into the 3D printed objects. The 3D printing method was evaluated in terms of the usability for metal scavenging processes by studying the ability to alter both the chemical and physical properties of the SLS 3D printed objects. In the introduction section of the thesis, typical metal separation techniques, with a focus on sorption, are discussed and then compared with the advantages and disadvantages of the SLS 3D printed metal scavenging filters. In the original publications discussed in this thesis, different types of chemically functional SLS 3D printed filters are presented.

First, a highly selective method for scavenging gold as tetrachloroaurate from acid leached Printed Circuit Board (PCB) waste was developed. The method utilized SLS 3D printed Polyamide-12 (PA12) filters which achieved nearly quantitative selectivity towards tetrachloroaurate. This was followed by a study where a method for separating palladium and platinum from a similar matrix by using SLS 3D printed filter was developed. Finally, a different approach was taken, where the SLS 3D printed PA12 filters were converted to functional nanocatalysts by first selectively adsorbing the gold from PCB waste and then reducing it into nanoparticles.

Keywords: Metal Separation, Selective Laser Sintering, 3D Printing, Circular Economy, Noble Metals

TIIVISTELMÄ

Lahtinen, Elmeri

Kemiallisesti funktionaalinen 3D-tulostus: Kustomoitavien metallisieppareiden valmistus selektiivisellä lasersintrauksella

Jyväskylä: Jyväskylän yliopisto, 2019, 71 s.

(JYU Dissertations

ISSN 2489-9003; 175)

ISBN 978-951-39-7994-2 (PDF)

Mielenkiinto teollisten prosessien ja jätteiden käsittelyn tehostamiseksi on luonut tarpeen kehittää uusia ja tehokkaita metallisieppareita. Moni nykyisistä prosesseista on suunniteltu toimimaan siten, että vain yksittäiset metallit otetaan talteen, kun taas muita metalleja käsitellään jätteenä. Pitkällä tähtäimellä tämä ei ole kestävä malli. Nykyisten metallien talteenotto prosessien yhdistäminen jo olemassa oleviin prosesseihin on usein haastavaa ja kallista, jonka vuoksi esimerkiksi prosessin sivutuotteena tulevien metallien talteenotto on yleensä heikolla tasolla.

Tässä työssä selektiivisellä lasersintraus (SLS) 3D-tulostuksella valmistetaan kustomoitavia metallisieppareita, jotka voitaisiin helposti yhdistää jo olemassa oleviin prosesseihin. Yleensä 3D-tulostusta käytetään vain mekaanisen tai esteettisen funktion omaavien kappaleiden valmistukseen. Tässä työssä keskityttiin sen sijaan sisällyttämään 3D-tulostettuihin kappaleisiin kemiallinen funktionaalisuus. Valitun 3D-tulostusmenetelmän soveltuvuutta tähän tarkoitukseen arvioitiin tutkimalla mahdollisuutta muokata valmistettujen kappaleiden kemiallisia ja fysikaalisia ominaisuuksia. Tämän väitöskirjan johdannossa esitellään ensin tyypillisimpiä metallien talteenottomenetelmiä, joita verrataan SLS 3D-tulostuksella valmistettujen metallisieppareiden hyviin ja huonoihin puoliin. Tähän väitöskirjaan sisällytetyissä artikkeleissa esitellään erilaisten SLS 3D-tulostettujen metallisiepparisuodattimien valmistusta ja hyödyntämistä.

Ensin kehitettiin menetelmä, jolla kulta voitiin erottaa selektiivisesti elektroniikkaromusta. Menetelmä hyödynsi SLS 3D-tulostettua metallisuodatinta, joka on valmistettu polyamidi-12 (PA12) -polymeeristä. Tämä suodatin saavutti lähes kvantitatiivisen kullan talteenoton hyvin haastavasta matriisista. Seuraavaksi kehitettiin menetelmä, jolla voitiin erottaa palladium ja platina vastaavasta matriisista hyödyntämällä SLS 3D-tulostettua suodatinta. Lopuksi metallien kierrätystä lähestyttiin eri näkökulmasta ja kehitettiin menetelmä, jolla 3D-tulostettu suodatin voitiin muuntaa suoraan funktionaaliseksi nanokatalyytiksi kullan talteenoton yhteydessä.

Avainsanat: Metallien erotus, Selektiivinen lasersintraus, 3D-tulostus, Kiertotalous, Jalometallit

Author's address	Elmeri Lahtinen Department of Chemistry P.O. Box 35 FI-40014 University of Jyväskylä Finland elmeri.e.o.lahtinen@jyu.fi
Supervisors	Professor Matti Haukka Department of Chemistry University of Jyväskylä Finland Professor Ari Väisänen Department of Chemistry University of Jyväskylä Finland Professor Kari Rissanen Department of Chemistry Nanoscience Center University of Jyväskylä Finland
Reviewers	Senior Research Fellow Dr. Tiina Leiviskä Chemical Process Engineering University of Oulu Finland Senior Researcher Dr. Sirpa Peräniemi School of Pharmacy University of Eastern Finland Finland
Opponent	Professor Christian Ekberg Department of Chemistry and Chemical Engineering Chalmers University of Technology Sweden

PREFACE

This work was performed in the Department of Chemistry at the University of Jyväskylä during the period of 2017-2019. Funding for the research was received from Centennial Foundation of Technology Industries of Finland and Jane and Aatos Erkko Foundation as a part of the Future Makers program as well as from the Department of Chemistry, University of Jyväskylä.

I started my PhD studies with the perhaps quite common mentality that I wanted to specialize in something and one day eventually become an expert in my own field. This quickly changed as the 3D printing project went on, and I found myself migrating between the fields of chemistry due to the rather widespread nature of the 3D printing project. Even though this presented me with somewhat of a challenge when it came to identifying myself as a researcher, I enjoyed getting to know several research fields. Looking back, I am happy that I got to do research on such a vast and unexplored field, as it gave me a chance to view chemistry from a broader perspective.

Firstly, I would like to thank my supervisors Prof. Matti Haukka, Prof. Ari Väisänen, and Prof. Kari Rissanen for all the trust and freedom I received when it came to conducting research as well as all the encouraging discussions throughout the years. I am grateful to have been part of their research groups as they are filled with brilliant and motivated people whom I really enjoyed getting to know and to work with. Especially the countless coffee breaks and discussions were a source of inspiration for me. I would like to also thank Dr. Tiina Leiviskä and Dr. Sirpa Peräniemi for their insightful comments on this thesis.

I would also like to thank my family and friends for all the unconditional support I have received for all these years. Finally, I would like to express my gratitude towards my beloved fiancée Katri. You have always been there for me, and this couldn't have been possible without you.

Jyväskylä 18.11.2019
Elmeri Lahtinen

LIST OF ORIGINAL PUBLICATIONS

- I** Lahtinen E., Kivijärvi L., Tatikonda R., Väisänen A., Rissanen K., and Haukka M., Selective Recovery of Gold from Electronic Waste Using 3D-Printed Scavenger, *ACS Omega*, **2017**, 2, 10, 7299-7304.
- II** Lahtinen E., Hänninen M. M., Kinnunen K., Tuononen H. M., Väisänen A., Rissanen K. and Haukka M., Porous 3D Printed Scavenger Filters for Selective Recovery of Precious Metals from Electronic Waste, *Adv. Sustainable Syst.* **2018**, 2, 1800048.
- III** Lahtinen E., Kukkonen E., Kinnunen V., Lahtinen M., Kinnunen K., Suvanto S., Väisänen A. and Haukka M., Gold Nanoparticles on 3D-Printed Filters: From Waste to Catalysts, *ACS Omega*, **2019**, 4, 16, 16891-16898

Author's contribution

The author performed the majority of the design and SLS 3D printing as well as most of the metal separation studies and all of the ICP-OES measurements related to publications **I-III**, participated in the HIM and SEM characterization methods performed for the objects in publications **I-III**, and performed most of the catalytic experiments for publication **III**. The author wrote the initial draft for publications **I-III**.

Other related publications by the author:

- IV Lahtinen E., Precker R. L. M., Lahtinen M., Hey-Hawkins E. and Haukka M., Selective Laser Sintering of Metal - Organic Frameworks: Production of Highly Porous Filters by 3D Printing onto a Polymeric Matrix, *ChemPlusChem*, **2019**, 84, 222.
- V Lahtinen E., Kukkonen E., Jokivartio J., Parkkonen J., Virkajärvi J., Kivijärvi L., Ahlskog M. and Haukka M., Preparation of Highly Porous Carbonous Electrodes by Selective Laser Sintering, *ACS Appl. Energy Mater*, **2019**, 2, 1314-1318.
- VI Lahtinen E., Turunen L., Hänninen M. M., Kolari K., Tuononen H. M. and Haukka M., Fabrication of Porous Hydrogenation Catalysts by a Selective Laser Sintering 3D Printing Technique, *ACS Omega*, **2019**, 4, 12012-12017.
- VII Kukkonen E., Lahtinen E., Myllyperkiö P., Konu J. and Haukka M., Three-Dimensional Printing of Nonlinear Optical Lenses, *ACS Omega*, **2018**, 3, 11558-11561.
- VIII Kulomäki S., Lahtinen E., Perämäki S. and Väisänen A., Determination of mercury at picogram level in natural waters with inductively coupled plasma mass spectrometry by using 3D printed metal scavengers, *Anal. Chim. Acta*, **2019**, 1092, 24-21.
- IX Kukkonen E., Lahtinen E., Myllyperkiö P., Haukka M. and Konu J. Nonlinear Optical Properties of Diaromatic Stilbene, Butadiene and Thiophene Derivatives, *manuscript in preparation*.
- X Lahtinen E., Hänninen M. M., Valjus J., Väisänen A., Tuononen H. M. and Haukka M., Preparation of α -aminomethylphosphonic acid containing filters with polymeric backbone for selective recovery of scandium, uranyl and iron using Selective Laser Sintering 3D printing, *manuscript in preparation*.

CONTENTS

ABSTRACT

PREFACE

LIST OF ORIGINAL PUBLICATIONS

CONTENTS

ABBREVIATIONS

1	INTRODUCTION	13
	1.1 Metals and their circular economy	13
	1.2 Metal separation techniques	14
2	ION-EXCHANGE MATERIALS AND ADSORBENTS	16
	2.1 Ion exchange materials	16
	2.2 Hydrocarbon structure	19
	2.3 Functional groups	21
	2.4 Organic adsorbents	22
	2.5 Physical structure	23
	2.6 Ion exchange processes	25
3	3D PRINTING.....	27
	3.1 Fused Deposition Modelling	28
	3.2 Stereolithography	32
	3.3 Selective Laser Sintering	35
	3.3.1 Printing technique.....	35
	3.3.2 Applications	39
4	AIMS OF THE STUDY	43
5	EXPERIMENTAL	44
	5.1 Chemically functional SLS 3D printing	44
	5.2 Utilization and characterization of the printed objects	46
	5.2.1 Characterization of the SLS 3D printed objects	46
	5.2.2 Metal adsorption experiments	46
	5.2.3 Preparation of the printed nanocatalyst and the catalysis experiments.....	48
6	RESULTS AND DISCUSSION	49
	6.1 Selective recovery of Au from acid leached PCB waste ^I	49
	6.1.1 Preparation and characterization of SLS 3D printed filters	49
	6.1.2 Selective separation of Au.....	51
	6.2 Selective recovery of Pd and Pt from acid leached PCB waste ^{II}	54
	6.2.1 Preparation and characterization of SLS 3D printed filters	54

6.2.2 Separation of the platinum group metals.....	56
6.3 Preparation of Au nanocatalysts from PCB waste derived gold ^{III}	59
6.3.1 Preparation of SLS 3D printed nanocatalysts	59
6.3.2 Characterization and performance of the nanocatalyst	60
SUMMARY.....	65
REFERENCES.....	67

ABBREVIATIONS

21K	Dowex 21K resin
ABS	Acrylonitrile Butadiene Styrene
ASA	Acrylonitrile Styrene Acrylate
CAD	Computer-Aided Design
DLP	Digital Light Processing
FDM	Fused Deposition Modeling
HIM	Helium Ion Microscopy
HKUST-1	Copper(II) benzene-1,3,5-tricarboxylate
ICP-MS	Inductively Coupled Plasma Mass Spectrometry
ICP-OES	Inductively Coupled Plasma Optical Emission Spectroscopy
MOF	Metal-Organic Frameworks
MSFIA	Multisyringe Flow Injection Analysis
PA12	Polyamide-12
PCB	Printed Circuit Boards
PEEK	Polyether Ether Ketone
PETG	Polyethylene Terephthalate Glycol
PLA	Polylactic Acid
PP	Polypropylene
PS	Polystyrene
PU	Polyurethane
PXRD	Powder X-ray Diffractometry
SEM-EDS	Scanning Electron Microscopy Energy Dispersive Spectrometry
SLA	Stereolithography
SLS	Selective Laser Sintering
SPE	Solid Phase Extraction
SP-ICP-MS	Single Particle Inductively Coupled Plasma Mass Spectrometry

1 INTRODUCTION

1.1 Metals and their circular economy

We are utilizing high-tech metals, such as noble metals, at an increasing pace without paying much attention towards their lifecycle.^{1,2} Most of these metals have very limited primary sources, most of which are focused on very specific locations.^{3,4} Industries ranging from technology production to health-care rely on a stable supply of these metals. This makes us, as a whole, very dependent on these critical raw materials, and prolonged supply difficulties would definitely lead to widespread problems.^{3,5}

To promote further utilization of these secondary sources of critical raw materials, novel technologies have to be developed.^{3,6-9} In an ideal situation, these new metal recovery and refining systems would be superior to the current options in terms of efficiency, all while being easy to integrate into any kind of process. However, incorporation of novel technologies into larger scale operations can often lead to unprecedented costs due to the experimental, rather than commercial, nature of the product. Therefore, it would be advisable to come up with a new way of utilizing already existing technologies and materials, while still having the option of incorporating novel materials into the technology.

Selective Laser Sintering 3D printing of chemically active metal scavenging filters would be an ideal example of the aforementioned technology. It has the inherent ability to fabricate objects of any shape or size. Additionally, physical characteristics, such as the porosity of the fabricated objects, can be altered by optimizing the parameters used during the printing process.¹⁰⁻¹³ Already existing materials, such as commercial ion-exchange resins or adsorbents, as well as experimental lab-scale materials can easily be introduced into these highly customizable and porous objects. The metal scavenging filters could be designed to fit already existing processes while also being relatively passively operated.

This thesis first briefly discusses the already existing metal recovery and refining techniques for hydrometallurgical processes, with a focus on sorption

methods. Then, the development and utilization of the Selective Laser Sintering 3D printing method for metal separation are discussed.

1.2 Metal separation techniques

A variety of hydrometallurgical metal separation techniques, ranging from precipitation to solvent extraction and sorption processes, exist. They are widely utilized, for example, as crucial parts of the production processes or as a way to remove harmful metals from waste solutions. Many of these techniques have been utilized for metal separation for hundreds of years at an industrial level. However, even the traditional methods have their challenges, which fuel the search for novel metal separation techniques that could either complete the existing techniques or compete with them.¹⁴

Industrially, the most common metal separation technique is chemical precipitation.¹⁵ It consists of altering the chemical conditions of the target solution in such a manner that the metal of interest forms a solid precipitate. This can be done for example by raising the pH of the solution to form insoluble compounds or by adding complexing ligands into the solution, which then form the insoluble species. Most of the time, the precipitation processes are highly effective when it comes to removing metals from the solution. The disadvantages of the process are the large amount of supplementary equipment and space it requires as well as the inability to easily integrate it into a continuous flow process. Additionally, when it comes to selectivity towards specific metals, precipitation processes usually perform rather poorly. The precipitates often contain a variety of metals unless sufficient pre-treatment of the solution is performed.^{14,16}

Another very common metal separation technique is solvent extraction, which typically includes the use of a metal scavenging compound dissolved in an organic solvent. The feed solution is contacted with the organic phase and thoroughly mixed, followed by separation of the phases.¹⁷ The metals of focus can then be eluted from the organic media to further separate them. Compared to the precipitation process, the solvent extraction often boasts considerably better selectivity towards certain metals, and can, therefore, be utilized as an efficient way to concentrate specific metals. Challenges with solvent extraction rise from the significantly more challenging process, as it often requires very accurate parametric control for optimal operation and a considerable amount of supplementary equipment.¹⁸

The third common method for metal separation is sorption. It consists of sorption of the target metals onto a solid phase^{17,19} This can be done, for example, by utilizing ion-exchange or other interactions. Like the solvent extraction, sorption processes can also have very high selectivities for certain metals and are, therefore, an efficient metal concentration method.²⁰ The challenges faced when using sorption are often similar to the ones encountered with solvent extraction mentioned above: a substantial amount of supplementary equipment and highly

optimized parameters. As with the previous methods, it is also a laborious separation method to implement into an already-existing process.¹⁴

Naturally, there are additional metal separation and refining techniques that can be utilized in hydrometallurgical systems. The sorption processes will be introduced more thoroughly, as they are the most relevant comparison for the novel SLS 3D printing-based process proposed herein. Additionally, several similarities between typical sorbent materials and the SLS 3D printed objects can be observed.

2 ION-EXCHANGE MATERIALS AND ADSORBENTS

Ion-exchange is an exchange of equivalents of charged ions between two or more ionic substances. The key point is that the interaction happens without the formation of covalent chemical bonds. Many reactions and, for example, many solvent extraction systems, are based on ion exchange interactions between the components. However, the term ion exchange material applies to functional polymers, which are usually either ion exchange or chelating resins. The ion exchange resins can be further divided into cation and anion exchange resins, based on the charge of the ions they exchange. Other types of materials relevant to the discussion here include various organic and inorganic sorbents.²¹ These include both absorbents and adsorbents, with the key difference being that the latter refers to materials where the interaction happens at the interface of the different phases, whereas absorption refers to situation where the interaction can also happen within the structure of the material.²² This chapter focuses on briefly describing the different types of ion exchange materials and sorbents, with a focus on their structure and properties.

2.1 Ion exchange materials

Most ion exchange materials consist of an osmotically inactive organic phase that has fixed functional groups, providing the ion exchange properties for the material. The osmotic inactivity means that the carrying matrix cannot migrate to another phase. A simple example of such a system would be carboxylic acid with a structure of $\text{CH}_3(\text{CH}_2)_n\text{COOH}$. The role of the hydrocarbon tail $\text{CH}_3(\text{CH}_2)_n$ is to make the acid, and the resulting metal complex, insoluble to water due to the long nonpolar sections. Carboxylic acids with extensive hydrocarbon tails (e.g. $n=20$) can be considered as an organic polymer with one active carboxylic acid group per molecule. These acids can act as an insoluble phase when submerged into an aqueous solution. When submerged, the functional groups of

the compound retain their active nature and are available for the ion exchange interaction with the matrix surrounding them.²¹

Here, the structure of the submerged solid carboxylic acid should be considered. As it consists of solid particles with immobile functional groups, it is likely that many of the functional groups are located inside the particles and therefore, are not available for interaction with the ions in the solution phase. This means, that only the functional groups close to the inter-phase boundary are available for chemical interactions with the surrounding media. This interaction can be expressed as shown in reaction (1), where R denotes the structural unit of the compound that corresponds to the functional group.²¹



The situation considered here is naturally rather unfavorable if considering the ratio of available functional groups to the mass of the material. Usually, ion exchange materials are utilized as rather large ($\sim 500 \mu\text{m}$) spherical particles. Considering the amount of active functional groups relative to the total number of functional groups present in said particle, a very minimal number of them are available for interactions. This will naturally lead to a rather minimal ion exchange capacity of the material, as the majority of the capacity is lost with the non-reachable functional groups. These kinds of dense polymers have limited usability for conventional ion exchange applications. They can still be utilized in situations in which the maximum capacity of the material is not the main concern.²¹

Luckily, there are solutions to this challenge. As the problem is mainly encountered due to having a rather unfavorable ratio of functional groups to the size of the inactive hydrocarbon chain, it can be countered by increasing the number of functional groups. However, if still considering the carboxylic acid example, a new challenge emerges with the hydrophilic nature of these charged functional groups. If their concentration in the compound is increased too much, the polymeric molecule will become water-soluble. This will reintroduce the problem that was initially solved by merely increasing the length of the hydrophobic hydrocarbon tail of the compound.²¹

This solubility challenge is often solved by cross-linking the polymer chains. This cross-linking can be performed by using short hydrocarbon compounds that act as bridges between the polymeric molecules containing the active functional groups. This leads to a three-dimensional structure that is insoluble to water.²³ Structure of a general cross-linked ion exchange material is depicted in **Fig. 1**. The cross-linked structure allows the material to achieve a high degree of water content while remaining insoluble. Hence, the structure allows the water molecules and ions to migrate inside the swollen structure of the polymer. This leads to most of the functional groups of the polymer being available for ion exchange, which consequently leads to much higher capacity than with the aforementioned dense polymers.²⁴

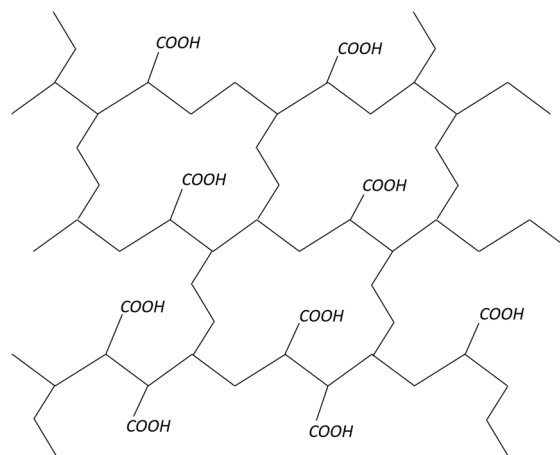
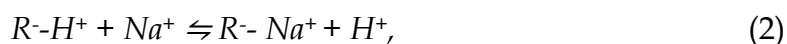


FIGURE 1 General structure of a cross-linked ion-exchange material with carboxylic acid functional groups.²¹

Thus, when the maximum capacity of the material is crucial, the use of cross-linked polymers with a high degree of functionalization is the optimal method. Naturally, this is not always plausible, and even the dense polymers can be effectively used for ion exchange interactions. However, in these applications, the particle size of the dense polymer plays an important role, as by decreasing the size of the dense polymer particles, the ratio of surface area to the mass of the polymer increases. With small particles, reasonable capacities can be often achieved. However, they still cannot directly compete with the capacity of the cross-linked polymers.²¹

Ion exchangers can be viewed as insoluble polymeric networks possessing reversibly attached ions. The attached ions are called counterions, as they possess the opposite charge of the functional groups of the ion exchange material. The counterions can move within the swollen polymeric network of the material. However, their movement has to be compensated by the movement of other ions with the same charge to meet the electroneutrality principle.²¹

Moreover, the ionic form of the ion exchanger has an important impact on the performance of the material. The ionic form describes the counterions present within the ion exchange material, which compensate the charge of the functional groups. The counterions can be shown as follows:



where the material can be seen to initially possess H^+ ions and is thus in hydrogen form. This is followed by a conversion to sodium form (2). Even though ion exchange materials are often referred to as being in a specific ionic form, they often contain a mixture of different counterions. This is evident as the ionic form of the ion exchange material is inherently not an unchangeable property but rather a way of expressing the presence of specific counterions inside the structure.²⁵

The reaction (2) depicts the basic operation principle of a cation exchange material. These materials bear functional groups with a negative charge and,

therefore, carry cations as counterions. Consequently, anion exchangers have functional groups with a positive charge and interact with anions. Hence, the polymeric structures of cation and anion exchange materials can be viewed as macromolecular polyanions and polycations, respectively. In specific materials, functional groups with both positive and negative charges can be present. These materials are called amphoteric ion exchangers. Additionally, some of the ion exchange materials are able to form chelate structures with the counterions. These types of materials are called chelating resins and the chelate structures are typically formed with metal ions. Strictly differentiating ion exchange resins from chelating resins can be troublesome as some polymers can possess both chelating and non-chelating properties. These properties are often altered based on the nature of the chemical environment in which the material is placed.²¹

Adsorbents are another material type pertinent to discussions regarding ion exchange. Ion exchange closely resembles adsorption, since in both processes, the solid phase scavenges dissolved species from the solution phase.²⁶ However, the main difference between the two phenomena is that the ion exchange follows stoichiometric behaviour. For each ion removed from the solution, the equivalent number of other ions with the same charge are moved into the solution phase. Whereas, in adsorption processes and more specifically in physisorption, the solute is being bound by the adsorbent in a non-stoichiometric way, without necessarily being replaced by anything. There are, however, exceptions to these definitions, as some ion exchange materials can possess adsorption-like nature and some adsorption processes can also follow stoichiometry in their behavior.²¹

2.2 Hydrocarbon structure

The aforementioned organic ion exchange materials always possess a three-dimensional polymeric structure. This framework is referred to as a matrix. The functional groups are then either directly incorporated in the polymeric chains or later attached to the framework. Another option of functional group attachment is via short hydrocarbon links, which are often called spacers.²¹

As discussed earlier, usually the structure of the organic ion exchange material consists of polymeric chains of molecules that are then cross-linked into each other via short hydrocarbon chains. Divinylbenzene is the most commonly utilized cross-linking agent. It is typically used to cross-link styrene polymers to develop styrene-divinylbenzene matrices, which are widely used due to their mechanically and chemically stable nature.²⁷ Perhaps the most common type of ion exchange material is a sulfonated styrene-divinylbenzene matrix (**Fig. 2**), where the sulfonyl group can act as a cation exchanger.²³

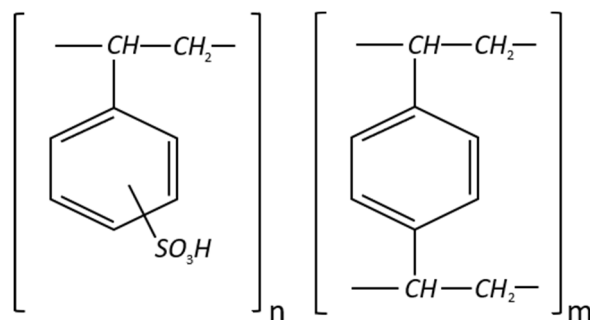


FIGURE 2 Components of sulfonated polystyrene-divinylbenzene resin.²¹

Another way of bringing diversity to the polymeric framework is by altering the choice of cross-linking agent. Even just by altering the length - and inevitably the flexibility of the cross-linker - the properties of the framework can be greatly altered. A more flexible framework is often easier for the ions to migrate through, and the more open structure also makes it possible for larger ions to enter the framework for ion exchange interactions.²⁴ The disadvantage of using long cross-linkers is the reduction of the ratio of functional groups to the mass of the material, which leads to a reduced maximum capacity of the material. Even though the altering of the cross-linking agent might make it possible to perform ion exchange with larger ions due to less steric hindrance, the choice of cross-linker is typically not meant to alter the functionality of the functional groups.²¹

Aside from choosing the cross-linker, the amount of cross-linking in the material should also be considered. The degree of cross-linking can affect the structure of the framework and thus the mobility of ions inside it.²⁵ Materials with a high degree of cross-linking are harder and often more stable, whereas materials with a low degree of cross-linking can resemble gels.²³ Ion exchangers with a high degree of cross-linking often suffer from slower reaction kinetics if compared to materials with a lower degree of cross-linking. Both materials have their use cases and the alteration of the degree of cross-linking also gives the user yet another option of altering the performance of the material.²¹

However, cross-linking is not the only method of decreasing water solubility of polymers with a high amount of hydrophilic functional groups. Often a big factor contributing to the stability and water insolubility of these materials is their physical knotting and tangling. Furthermore, a wide diversity of weak interactions, such as hydrogen bonding and van der Waals interactions, also take place and contribute to the stability of the polymers. Although a variety of these kinds of polymers are known, their utilization is rather limited if compared to more traditional cross-linked ion exchange materials.²¹

2.3 Functional groups

Ion exchange materials and non-functional polymers mainly differ due to the presence of functional groups in the structure of the polymeric ion exchange materials. A wide diversity of functional groups have been introduced into the polymeric frameworks to acquire material with ion exchange properties. However, if only commercially available materials are considered, the variety of these materials is reduced greatly.²¹

The properties of a specific ion exchange material are mostly defined by their functional groups. The different types of functional groups can be roughly divided into cation and anion exchangers, based on the charge they bear. Another way to classify functional groups is to divide them into strong and weak exchangers, based on their dissociation properties. An example of a strong cation exchange group would be an acid that is completely ionized in the surrounding aqueous solution. The analogue of sulfuric acid, $-\text{SO}_3\text{H}$, group is often completely ionized in the aqueous medium; therefore, the material associated with $-\text{SO}_3\text{H}$ groups is a strong cation exchanger. Materials that have a specific working pH range, due to that only specific pH range allows the functional group to exist in ionized form, are considered as weak ion exchangers.²⁴

In the case of cation exchangers, the most common groups are the sulfonic acid and the weakly acidic materials with the carboxylic acid $-\text{COO}^-$ groups.²⁵ Other types of cation exchangers are, for example, phosphonic and selenonic acid groups.²⁴ It should also be noted that different ion exchange materials with the same functional groups can possess different chemical behaviors as the hydrocarbon part of the ion exchanger can also impact the chemical properties of the functional group. In the case of the anion exchange materials, most of them contain nitrogen atoms as the proton acceptor to yield the positive charge. Weakly basic anion exchangers often contain functional groups, such as $-\text{NH}_3^+$, while strong-base anion exchangers often have the general structure of $-\text{N}^+(\text{CH}_3)_3$. Aside from the nitrogen-based anion exchangers, tertiary sulphonium $-\text{S}^+(\text{CH}_3)_2$ and quaternary phosphonium $-\text{P}^+(\text{CH}_3)_3$ are also utilized.²¹

Besides the cation and anion exchangers, chelating polymers are also a very common group of ion-exchange materials. However, not everyone considers chelating polymers as a type of ion-exchange resins, as they do not obey all classical definitions of ion exchange materials. While this may be true, many of the functional groups that are categorized as chelates can possess exchange functionalities without the chelating properties in certain situations. For example, materials with iminodiacetic functional groups can act as chelates or as ion exchangers as shown in **Fig. 3** (top); classical cation exchange functionality, where Na^+ ions are exchanged by K^+ ions, is shown for the iminodiacetic material. The **Fig. 3** (middle) shows typical behavior for weakly acidic cation exchange materials, as the functional groups are protonated and the Na^+ ions are removed. This interaction is also considered to be ion exchange. The **Fig. 3** (bottom) represents the chelating properties of the iminodiacetic acid group, where the

complex is formed by the two coordinating $-COO^-$ groups and the Cu^{2+} ion. This interaction, as well as the ion exchange reactions, can be seen to follow stoichiometry in a similar fashion.²¹

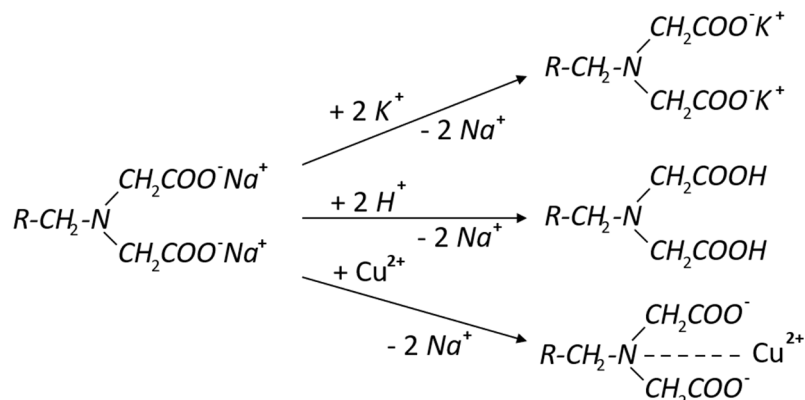


FIGURE 3 Different chemical interactions involving iminodiacetic functional groups: ion exchange (top), protonation (middle), and chelating interaction (bottom).²¹

2.4 Organic adsorbents

Besides the typical ion exchange materials, organic adsorbents are also a compelling option when considering sorption processes. In addition to ion exchange and other interactions, these materials rely on the use of a myriad of different weak interactions. The most common weak interactions include van der Waals forces, hydrogen bonds, and π - π interactions. These sorption processes are often based on physical adsorption of the compounds to the material. Therefore, the specific surface area of organic adsorbents is crucial for their performance. However, not all organic adsorbents possess high surface area and instead rely on, for example, specific functional groups for interaction with their surroundings. The organic materials can be used as obtained, but a more common way of utilization is to enhance their adsorption properties by either physical or chemical treatment.²⁸

Activated carbon is perhaps the most commonly utilized organic adsorbent even though its use as a powdery or granular material on a larger scale is rather challenging. While readily available, it is a rather expensive additive and has thus led researchers to investigate the utilization of various waste streams as a source for activated carbon. Several waste sources ranging from households to industry wastes have been identified as potential options for activated carbon production. The production method typically consists of two steps: carbonization and activation. The carbonization is usually a multi-step pyrolysis process, which can be optimized to yield carbonic material possessing different kinds of physical properties. The carbonization process affects factors such as the pore structure

and the surface area. After carbonization, the material has to be activated, which can be done via physical or chemical methods.²⁸

A popular example of another potentially promising adsorbent is chitin. It is widely available in nature and is already produced at high quantities by variety of industrial processes. Especially promising factor about chitin is that it can be converted into chitosan, which has been demonstrated to be a rather effective adsorbent for various applications. It has been reported to be a well-functioning additive for both organic compound²⁹⁻³¹ as well as metal ion³²⁻³⁵ adsorption from aqueous media.²⁸

The wide range of organic adsorbents³⁶⁻⁴² and inorganic adsorbents⁴³⁻⁴⁷ exist, but they will not be further reviewed here as properties of specific materials do not fit the rather general scope of this introduction. As the work here is primarily focused on the development of the method for anchoring the powdery material onto an SLS 3D printed framework, a thorough inspection of the materials themselves does not appear relevant. Moreover, a fundamental point is that most of the organic adsorbents also suffer from the same challenges encountered when trying to handle powdery materials.

2.5 Physical structure

As initially discussed above, the general structure of a typical ion exchange resin consists of a three-dimensional, irregular, macromolecular framework of hydrocarbon chains with attached functional groups. Both the framework and the functional groups define the chemical characteristics of the material. The physical structure of the polymer has a major effect on the chemical performance of the material affecting properties such, as surface area, resistance to liquid flow and mechanical stability of the material. Even kinetic and thermodynamic properties of the ion exchange material are affected by the macroscopic structure of the polymer.²¹

Gel resins (**Fig. 4**) are a conventional type of resin that have relatively homogeneous density throughout the polymer beads. They do not have a well-defined pore structure as the porosity within these gel beads consists of the voids present between the hydrocarbon chains.²⁵ When the gel is swollen, the voids are filled with solvent molecules. Conversely, when the gel is completely dry, the pores collapse and are practically non-existent. Consequently, the degree of swelling also affects the properties and even the size of these materials.²²

Another type of widely utilized materials nowadays are macroporous resins. Contrary to gel resins, the macroporous resins consist of two different phases. The first phase consists of gel regions containing the dense polymer chains and a small amount of the solvent. The second phase is the permanent, macroscopic pores that contain the solution from the surrounding media. The diameter of the permanent pores typically ranges from 20 to 200 nm, whereas the pores between the adjacent hydrocarbon chains are usually only about 0.5-20 nm in diameter. Another significant difference between these two types of materials

is that the macroporous materials possess rather consistent shape and that their larger pores are unaffected if the material is dried.²¹

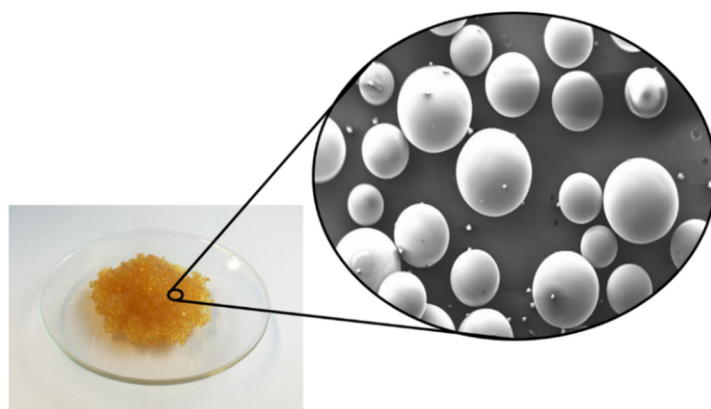


FIGURE 4 Image of a gel-type resin with SEM image of the structure.

The structure of the macroporous resins can be highly advantageous if the process is limited by the rate of diffusion because the diffusion of the solution through the material is much faster in the case of the macropores, inside which the solution is practically similar to the surrounding solution. The gel resins display much slower diffusion kinetics, due to their physical structure. Another advantage of the open structure of macroporous resins is the possibility for larger molecules diffusing through the polymer.²² They are able to participate in the ion exchange reaction in the macropores without having to try to diffuse into the gel region. Another advantage of the rigid macroporous resins is their chemical stability.²¹

The density of the ion exchange materials is usually above 1 g cm^{-3} . When comparing different types of swollen resins, cation exchange resins typically have a higher density than anion exchange resins. Estimated densities for these materials are $1.10\text{-}1.40 \text{ g cm}^{-3}$ and $1.01\text{-}1.10 \text{ g cm}^{-3}$, respectively. This difference in densities can be utilized to separate cation and anion exchange resins from each other. Challenges may arise, especially with anion exchange resins, if the density of the resin is below that of the solution. This makes their utilization rather inconvenient, especially in packed bed reactors.²¹

Different processes often set specific requirements for the ion exchange resins. Many of the packed bed techniques, such as the expanded bed technique, require the exchanger resin to have a higher density than the surrounding media. Researchers have tackled the problem with different approaches, with incorporating dense inorganic material into the ion exchange material being one of them. For example, TiO_2 particles have been combined with cellulose-based material, to make it usable for anion exchange in an expanded bed process. In this type of solution to the problem, the nature of the inorganic additive needs to be carefully considered to avoid the introduction of unnecessary impurities to the surrounding solution. Another way of solving the challenge would be using

material with a dense inner core and porous exterior. However, these materials are rare, and a more promising answer could be imprinting the whole ion exchange material into another framework, which would hold the polymer beads in place. This could remove the whole consideration about the density of the material.²¹

2.6 Ion exchange processes

Typically, ion exchange processes utilized on an industrial scale use either batch or various types of resin bed-based processes, while ion exchange on a laboratory scale is often conducted by using packed columns (**Fig. 5**). All of these methods have the basic operation cycle of sorption, elution, and regeneration in common but differ in the practical operation of the process. The simplest of these is the batch method, where the ion exchange resin and the solution are mixed in a tank. The reaction is allowed to reach equilibrium and the resin is separated from the tank. After the process, the resin has to be either regenerated or disposed and replaced by new resin. Batch processes are far less popular than the flow-based processes when it comes to industrial applications, which could be due to their challenging incorporation into already existing processes. Another issue is the laborious operation of the batch process, since the ion exchange resin has to be constantly removed from the solution and either regenerated or replaced in order to process the next batch of the solution. Especially when dealing with large quantities of solution, this becomes a crucial concern.⁴⁸

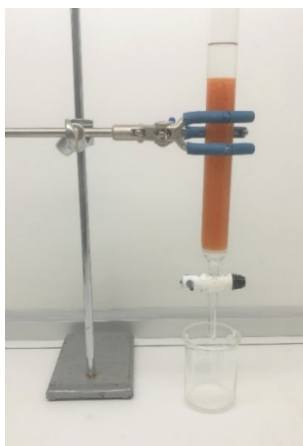


FIGURE 5 Image of a typical ion exchange column used on a laboratory scale.

Contrary to the batch process, the most widely utilized ion exchange process type on an industrial scale is the fixed bed. These types of fixed bed processes usually differ in how the solution flows through the bed. It can be either simply flown from the top or bottom or by using a counterflow process, with the top-down being the most common. Consequently, the up-flow process has the solution flowing upwards from the bottom, through the fixed resin bed. The counterflow

process combines the two types, by having the treatable solution flowing downwards through the bed, whereas in the regeneration phase, the flow is upwards from the bottom of the resin column. The fixed bed processes are common due to their good throughput and operational simplicity. However, usually the problems arise when the treated solution contains solid particles, which hinders the flow of the solution through the column.⁴⁸ Another challenge, which is not limited to just fixed bed operation, is fouling of the resin. For example, larger organic compounds can get entangled within the structure of the resin, therefore hindering its capabilities. This can however be combated by adjusting the amount of cross-linking in the resin or, for example, by treating the resin with chloride solution between the operation cycles.²⁵

The solution containing high concentrations of dissolved solids can be treated by utilizing a fluidized bed column. This process combats the presence of solids in the feed solution by having free pass ways for the solid particles through the resin beads. This is achieved by passing the raw solution with relatively high speed from the bottom of the column into the resin bed. This causes the resin beads to start moving and swirling around the column, which then creates space for the solid particles to move past the resin bed without significantly hindering the flow of the process. Another type of ion exchange process, where the resin bed is not strictly stationary, is the moving bed process, in which the ion exchange beads and the solution are brought to flow through the system. This type of process requires a lot less supplementary equipment and less space for operation but also suffers from the instability of the process and the possible mechanical deterioration of the ion exchange beads.⁴⁸

Naturally, the described processes do not represent all possible operation types of ion exchange materials (e.g., membranes^{49,50}) but serve as a brief introduction to the traditional ion exchange processes. What should also be considered here are the challenges that are imposed upon these processes by the wide variety of materials being available. Different types of resins are more practical and economical to utilize in specific approaches; therefore, each process has to be optimized for a specific material. Other common problems for all column-based processes also include factors such as channelling, which is also a concern in ion exchange processes.

3 3D PRINTING

Three-dimensional printing technologies have seen a major boost in development due to growing interest in the field during the last decade.⁵¹⁻⁵⁴ Many of the techniques have become widely available even on a consumer level, and awareness of the techniques has increased tremendously.⁵⁵ These days, it is not uncommon to see three-dimensional printers utilized even in elementary education.⁵⁶

Applications of three-dimensional printing have expanded vastly. Previously, it was primarily used to make objects with mere aesthetic or mechanical properties. Objects were usually small and of relatively rough quality. However, these days, even entry-level machines are able to produce commercial grade parts with relatively large dimensions.⁵⁷ Nowadays, buildings can also be 3D printed.^{53,54,58-60} This further shows the interest in exploring additional use cases for 3D printing, aside from just small mechanical parts or aesthetic objects. The importance of these applications should not be underestimated but there is also a widespread inspiration to study additional, out-of-the-box applications for the 3D printing techniques.

This search for novel applications has further been accelerated by the myriad of 3D printing techniques available today.⁵⁴ Whereas other techniques offer possibilities of fabricating transparent objects⁶¹, or objects with highly customizable chemical compositions^{62,63}, others make it possible to 3D print metal⁶⁴⁻⁶⁶. However, although 3D printing techniques have seen a major development boost during the last decade, they are not meant to replace existing production techniques. They should be viewed as supplementary production techniques that can complete traditional production techniques and push them forward.⁵⁵ Therefore, the utilization of 3D printing techniques should also be critically assessed and compared to traditional techniques to determine ideal applications.

Typical 3D printing workflow can be split into four different sections. The first section is the generation of the three-dimensional model of the object, traditionally carried out by using a Computer-Aided Design-program (CAD) to design the object to be printed. Another option is to download the model from a

range of free file repositories available. The second step in the workflow is to convert the three-dimensional model into a file format that the 3D printer is able to read, namely G-code. This is done by using a slicer program, which essentially splits the three-dimensional model into two-dimensional layers using the settings defined by the user. The generated file is then transferred onto the 3D printer to print the object. The last section, which is also widely dependent on the 3D printing technique utilized, is the post-processing of the printed objects. In some techniques, no post-processing is needed, whereas in other techniques, the post-processing is a crucial part of the workflow.

In the following sections, three different techniques of 3D printing will be shortly reviewed. Even though there is a wide variety of techniques, the following three can be viewed as the core techniques from which many others derive. Additionally, chemistry-related applications of these techniques will be shortly reviewed.

3.1 Fused Deposition Modelling

Fused Deposition Modelling (FDM) 3D printing is perhaps the most widespread 3D printing technique at the moment. The technique utilizes plastic filament as the building material. The material is pulled from a spool into a hot end, where it is extruded typically through a brass nozzle and is then laid down onto the build plate. (Fig. 6) By moving either the build plate or the hot end, the object can be built on a layer-by-layer basis.⁵⁴ There are different types of FDM 3D printers, which basically differ by which part of the printer is actually moving during the printing process. For example, in a Cartesian FDM 3D printer, the build plate only moves on the vertical axis, and the hot end moves along the horizontal axes.

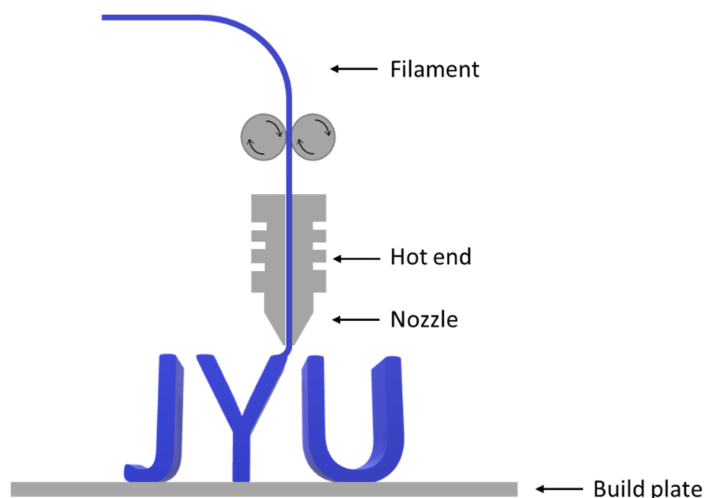


FIGURE 6 Operating principle of an FDM 3D printer.

As for the printable materials, FDM 3D printing has seen a major development in the availability of materials. In the past, only very basic materials, such as acrylonitrile butadiene styrene (ABS) or polylactic acid (PLA), were available. PLA still remains the most utilized material due to being an inexpensive and a beginner-friendly material, but the selection of different materials has widened to also include plastics, such as polyethylene terephthalate glycol (PETG), acrylonitrile styrene acrylate (ASA), and polyether ether ketone (PEEK).⁶⁷ Additionally, a new trend in these materials is the introduction of various additives into the 3D printing material.⁶⁸⁻⁷² Filaments containing a wide range of additives are readily available even on a consumer level. This further shows the interest in the field to develop novel ideas for the techniques.

The reason why FDM 3D printing is the most commonly utilized technique consists of a couple of key factors. The first one is ease-of-use and availability of introductory guides. Moreover, entry-level FDM 3D printers are relatively easy to use and widely available commercially.⁵⁴ Additionally, FDM 3D printers are usually rather compactly sized, and this, together with advancements in 3D printing technology that have lowered costs for consumers - another key factor - has further widened their usability and popularity.⁷³ Another attraction to the FDM is that the built objects are often usable straight after the printing process, without requiring much additional post-processing.⁷⁴

FDM 3D printing has traditionally been used to fabricate small mechanical components and prototypes. It is still widely used for producing pieces that would otherwise be challenging to fabricate. The availability of different materials and improved technology of the machines have made the technique capable of producing high-quality parts with helpful properties, such as extremely good mechanical durability⁷⁵ or even antimicrobial properties⁷⁶. The aforementioned advancements in the availability, technology and the range of available materials have made it possible to produce finished end products, instead of mere prototypes, using FDM 3D printing. The utilization of the technique has seen a major interest in a wide variety of different fields that could make use of extrusion-based methods, such as the construction industry, which is now looking into combining such methods into their line-up of building techniques.⁵⁸

The chemistry-related applications utilizing FDM 3D printing are being reported at an accelerating pace.⁷⁷⁻⁸⁰ The pure FDM 3D printing polymers are often not optimal for chemical applications due to the low surface area, non-porous structure, and poor thermal properties. Therefore, in many reported applications that utilize extrusion-based methods, novel materials have been developed with a specific application in mind. Catalysis is an example of a field that has seen a major interest in the utilization of customizable, extrusion-based, heterogeneous catalysts. In one case, a novel Cu/Al₂O₃ catalyst was prepared by combining Al₂O₃ powder with an aqueous solution of Cu(NO₃)₂ · 2.5 H₂O along with viscosity modifiers. This resulted in a viscous ink which could be extruded using a custom extrusion-based 3D printer to form cylindrical woodpile (Fig. 7). After the extrusion, the printed object was post-processed by sintering the

catalyst. It could then be successfully utilized for Ullman reactions to yield imidazoles, benzimidazoles, and N-aryl amides. The 3D printed catalyst showed mostly great yields (78-94 %) under relatively mild conditions.⁸¹ It should be noted that when 3D printed catalysts are discussed, the ease of use and the reusability of the catalyst are also key performance factors because - aside from the customizable structure - they are the main practical factors that distinguish the use of 3D printed catalysts from plain catalyst powder scenarios. In the case of the Cu/Al₂O₃ catalyst, the 3D printed catalyst showed excellent reusability, as the performance did not significantly decrease over the ten cycles performed.⁸¹ The approach is not limited to just Ullman reactions as cycloaddition⁸², crosscoupling⁸², and even Biginelli⁸³ and Hantzsch⁸³ reactions have been reported using catalysts that have been produced using extrusion-based methods.

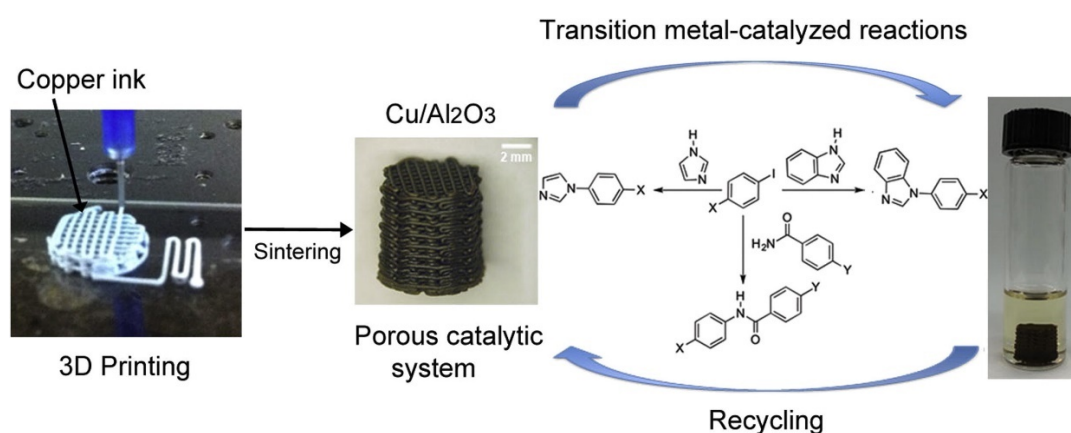


FIGURE 7 3D printed Cu/Al₂O₃ catalyst utilized for Ullman reactions. Reprinted from Tubío *et al.* with kind permission from Elsevier.⁸¹

The capabilities of the FDM 3D printing have also been noticed in many applications that are indirectly related to chemistry. Examples of these are situations where the printing method was used to produce highly customizable reactionware. The technique was used to develop a protocol for fabrication of the reactionware, which could be utilized for multistep organic synthesis. The sealed reactor could be customized to fit the required reaction conditions and could even include the catalysts for the reactions within the printed object.⁸⁴ This approach has also been extended to include the purification step of the synthetic procedure within the one-piece reactor (**Fig. 8**) by compartmentalizing the structure to allow controlled flow of the starting materials through the device. The actual purification was performed by controlling the flow of the material through a silica bed inside the reactor.⁸⁵ Furthermore, this type of procedure has also been extended to include the ability for in-situ monitoring by the use of printed-in components for spectroscopic and electrochemical analyses of the reaction.⁸⁶ If considering practical applications outside the laboratory environment, the ability to fabricate versatile and customizable reactionware which are able to produce organic compounds, such as pharmaceuticals, could allow for local drug manufacturing.⁸⁷

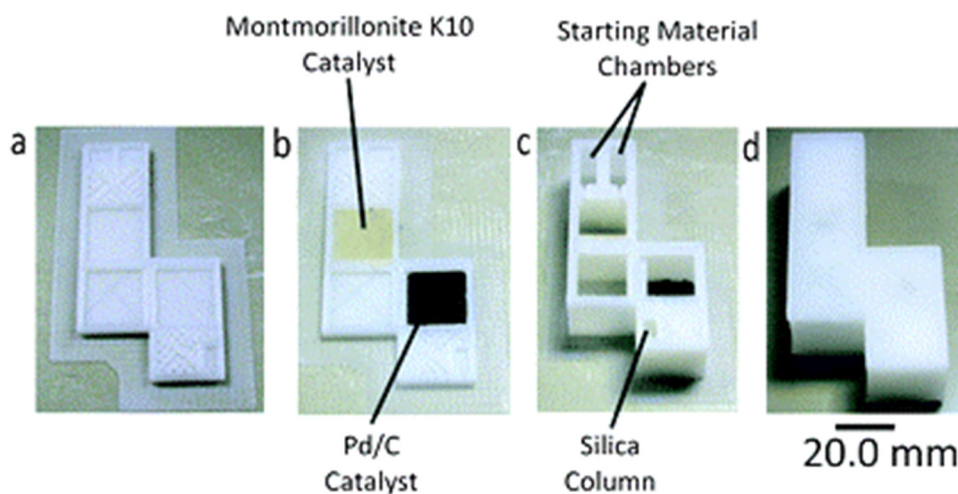


FIGURE 8 3D printed reactionware with integrated catalysis and purification sections.⁸⁵ Reproduced from Kitson *et al.* with kind permission from the Royal Society of Chemistry.⁸⁵

Extrusion-based 3D printing methods have also been utilized in the field of separation sciences even though as a field it has seen far less attention when it comes to implementing 3D printing.⁸⁸ Regardless, there have been some reports, for example, for small molecule separation by utilizing FDM 3D printed separators. This was demonstrated by using a composite filament, with part of it being water-soluble. After the printing process, the object was rinsed with water to dissolve the soluble portion of the object, thus leading to a porous object. Then, researchers separated glimepiride from a water solution with great recovery efficiency (82.24 %). Another significant point here is the ability to produce porous materials, particularly given that FDM 3D printing usually produces objects with smooth surfaces and non-porous structure. However, even by using the composite material and dissolving one of the components to increase the porosity, the specific surface area of the material remained rather low, as it was reported to be around $1 \text{ m}^2 \text{ g}^{-1}$.⁸⁹

Another field of research that has really embraced 3D printing technology is electrochemistry. There has been a vast range of reports regarding various electrochemical applications.⁹⁰⁻⁹³ Especially, the development of 3D printable Li-ion batteries⁹⁴⁻⁹⁶ and electrodes^{97,98} by using extrusion-based printing methods have seen major interest lately. While many of these reports do not use FDM 3D printing, the techniques utilized (e.g., Direct Ink Writing) can still be viewed as extrusion-based. The focus of these reports has often been on the development of novel, lightweight and ubiquitously available devices. The 3D printed objects can range from Li-ion batteries to supercapacitors or even personalized electronics.^{91,92}

3.2 Stereolithography

Stereolithography (SLA) was the first 3D printing method developed and still remains one of the most utilized 3D printing methods today. Unlike FDM, SLA utilizes photopolymerization reaction to produce the objects. This places certain limitations to the materials and applications available for the method. The printing process consists of build plate lowering into a vat containing the highly viscous photopolymerizable resin. The first layer of the object is formed as the laser, operating at the UV-region, hits the resin, thereby initializing the polymerization reaction, which turns that part of the resin solid. Subsequently, the build plate is lifted and lowered, after which the process is repeated until the object is built.⁹⁹ (Fig. 9)

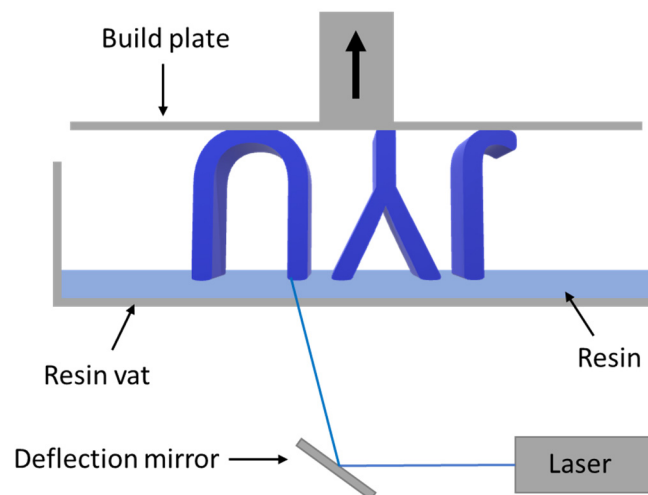


FIGURE 9 Operating principle of an SLA 3D printer.

As mentioned earlier, different 3D printing methods differ vastly in the amount of post-processing required after printing. SLA is one of the methods requiring a significant amount of processing after printing. After the object is built, it is still covered in the unpolymerized resin and has to be washed extensively. Washing is often done by using a series of ethanol or isopropyl alcohol and water rinses. After washing, the object is still rather soft, and the polymerization process must be finished - typically by inserting the objects into a UV-light containing chamber, where the UV-light ensures the completeness of the polymerization process. After this, the object is ready to be used.⁹⁹

The requirement of the post-processing can be viewed as one of the main challenges when considering the widespread use of SLA 3D printing. Another factor is the safety-related challenges faced when handling the resin used as the building material. This places requirements on the environment in which the technique can be utilized in. While the aforementioned FDM 3D printer could be usually comfortably placed even on an office table, the SLA 3D printer probably should not be handled in an office environment.

Another challenge with the utilization of the SLA 3D printer is the limited amount of materials available for the technique. Naturally, the polymerization process places requirements on the material: it must consist of appropriate monomers and initiators at suitable concentrations. There are a variety of commercial materials available, but many of them consist of modified acrylate monomers and oligomers combined with a photoinitiator; therefore, the actual variance between the available materials is quite limited. However, new types of materials are continuously being developed.⁹⁹ As with the FDM 3D printing, some variety to the available materials has recently been introduced by the utilization of additives that give the resin new properties. One example of such application is the introduction of nanoparticles into the resin, which leads to nanocomposite objects.¹⁰⁰ The utilization of additives is, however, much more common when it comes to filaments made for FDM 3D printing.

However, SLA 3D printing also has advantages over other printing techniques. One of these is the high resolution obtained with the use of the laser. The resolution is often considerably better than, for example, if comparing to a part that has been produced using FDM 3D printing.⁵⁴ The great resolution allows for specific use cases, where the end result must have good surface finish without visible layer lines. A good example of this is the jewelry industry, which sometimes uses SLA 3D printing to fabricate a customized model of jewelry before casting it in other material based on the model.⁷⁹ Another advantage of the technique is the ability to print transparent objects (**Fig. 10**). The transparency is naturally related to the printing process and the post-processing of the object, but it is made possible by the often inherently transparent nature of the resin. This feature has made it possible to even fabricate lenses with great optical quality using SLA 3D printing.¹⁰¹

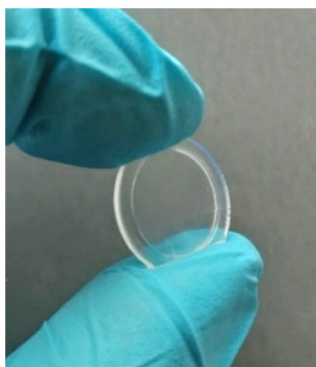


FIGURE 10 Image of an SLA 3D printed transparent lens.

As can be seen from the previous examples, the SLA 3D printing is a technique that is often utilized on a commercial, rather than on a consumer level. This is due to the safety challenges and because the price of the machines is often considerably higher than entry-level FDM 3D printers. However, there is another 3D printing technique available that utilizes a very similar process to SLA 3D printing and is often more affordable. This technique is called Digital Light

Processing (DLP) 3D printing, where the laser is replaced with high power LED sources, which are used to cure an entire layer of the object at once. This makes the technique often faster, usually at the cost of resolution, than traditional SLA 3D printing.^{56,102,103}

If considering the possible applications of the technique within the field of chemistry, the nature of the resin places some limitations on what can be done. However, it also makes it easy to incorporate either chemically active or passive components into the resin or modify the composition of the resin to fit a specific application.¹⁰⁴ This has been exploited in many different approaches ranging from optical devices¹⁰⁵ to metal separators⁸⁸. The SLA 3D printing method has actually seen quite a significant use when it comes to separation sciences.^{78,88,106}

A good example of this is the preparation of a preconcentrator device for trace elements from seawater. This approach was used to tackle the problem of accurate determination of metal concentrations from as challenging a matrix as seawater. Analytical methods, such as Inductively Coupled Plasma Optical Emission Spectrometry (ICP-OES) or Inductively Coupled Plasma Mass Spectrometry (ICP-MS), allow high-resolution analytics to be performed, but even then, the trace amounts of metals present in the seawater might require preconcentration methods to be accurately determined. This problem was solved by utilizing acrylate-based 3D printing resin to fabricate the preconcentrator device. The chemical functionality of the carboxyl groups was used to extract a series of metals (Mn, Ni, Zn, Cu, Cd and Pb) from the seawater. The method managed to remove the challenging salt matrix from the sample as the metals of interest were held up by the preconcentrator, while the rest of the solution flowed through. This was followed by the elution and analysis of the metals. As a whole, the utilization of the preconcentrator allowed the accurate analysis of the metals with detection limits rivaling those of the more conventional methods available.¹⁰⁷

A similar approach has been utilized to prepare a solid-phase extraction (SPE) device for accurate analysis of iron from water samples by using a multisyringe flow injection analysis (MSFIA) system. The method utilized SLA 3D printing to produce part of the SPE device containing a commercial chelating disk (3M Empore), responsible for the scavenging of the Fe(III) after the oxidation process. Next, Fe(III) was eluted from the 3D printed SPE disk and analyzed by using a spectrophotometric detector connected to the MSFIA system. The analysis method achieved a remarkable detection limit of 7 ng for the total iron present in the samples.¹⁰⁸

In addition to the iron determination, a similar approach has also been used for preconcentration and determination of Cr(VI). Here, SLA 3D printing was utilized to produce an SPE device that could be used in combination with the MSFIA system. In the reported system, the Cr(VI) is first complexed with 1,5-diphenylcarbazide, which is then bound by the sulfonic acid groups present in the SPE disk. The method achieved a detection limit of 1 ng for the total Cr(VI) in the sample.¹⁰⁹ In summary, these kinds of systems aim at the automation or the improvement of the analysis method by utilizing 3D printing. And while 3D

printing is utilized in the studies, the role of the method is often rather indirect when it comes to actual chemistry being performed.

Another application, utilizing essentially SLA 3D printing is the so-called 4D printing of materials. The fourth dimension often relates to an additional property, such as the ability of the material to return to its original shape under certain conditions. This has been demonstrated by the preparation of tailorable shape memory polymers. The materials were able to alter their shape in response to temperature. When the temperature was lowered, the object would take up a certain shape, followed by the return to the original shape after the heating process. This was made possible by tailoring the chemical composition of the printing material and therefore serves as a good example of successful targeting of specific applications by altering the chemical characteristics of the printing material.¹¹⁰

3.3 Selective Laser Sintering

3.3.1 Printing technique

The third, and final, 3D printing method that will be shortly reviewed here is Selective Laser Sintering (SLS) 3D printing. Like SLA 3D printing, it utilizes a laser in the printing process, but instead of polymerization it uses the laser to sinter the building material. The material used is in the form of small, spherical polymer beads. The printing process includes the heating of the chamber containing the building material near to materials melting point, after which the high-powered laser is used to selectively sinter layer of the object. Next, a thin layer of the powdery building material is laid down on the build plate, containing the previously sintered layer, and the whole process is repeated. (Fig. 11) In the end, the whole object is built into the powder bed.⁵⁶

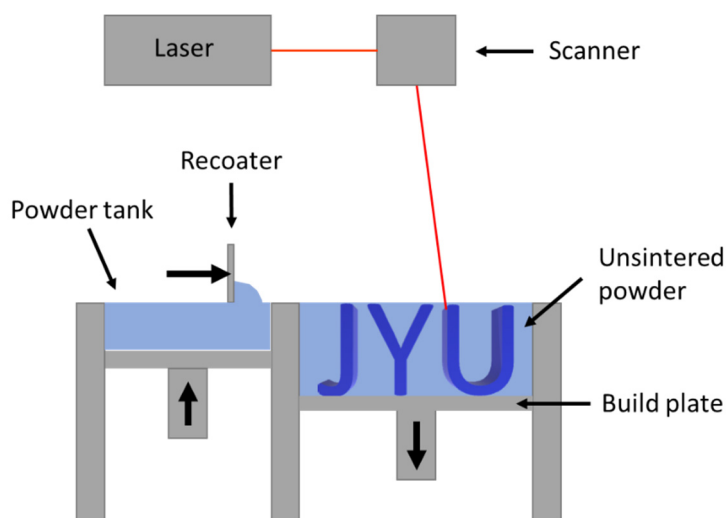


FIGURE 11 Operating principle of an SLS 3D printer.

Building the object into the excess powder comes with both advantages and challenges. The main advantage is the fact that SLS 3D printed objects do not need any support structure. This is not the case with most of the other printing methods. For example, if using FDM or SLA 3D printing and the object has steep overhangs, they have to be supported by building specific support structures as the printer cannot insert building material mid-air. These support structures are removed after the printing process. As the whole object is built into the surrounding powder, SLS 3D printing does not require any supports. However, the use of excess powder also provides challenges. As the whole build plate must be filled for the whole height of the object, the printing process often requires significant amounts of material if compared to the mass of the object being built. Luckily, the excess building material can often be reused, at least to a certain extent.⁵⁶

The material selection for SLS 3D printing was previously heavily dominated by the use of polyamide-12 (PA12). Due to its affordability, wide availability, good mechanical properties, and easy printability, it was an industry standard for a long period of time and remains one of the most utilized materials alongside polypropylene (PP), polyurethane (PU), and polystyrene (PS), which are also gaining popularity. As with FDM and SLA 3D printing materials, SLS materials have also been customized with special additives. Anything from carbon fibers to small glass beads have already been introduced into the commercially available materials. This is a rather easy process, as the main requirement for the additive is a suitable melting point range so that it would not disturb the melting process of the powdery polymer. Another requirement is the grindability into relatively small particles as the spherical polymer particles used are often around 50 μm of diameter.⁵⁶ However, with these requirements met, the so-called material synthesis is as simple as merely mixing the two materials at the desired concentrations. This makes the SLS 3D printing a very attracting printing technique if the customizability of the material is of interest.

Naturally, SLS 3D printing is not without its challenges. If from the previously reviewed techniques, FDM 3D printing can be used in an office setting and SLA 3D printing requires a bit more specific space, SLS 3D printing definitely requires a dedicated space for its use. This is mainly due to the use of the powdery starting material. Even though the materials themselves are often harmless, everyday polymers, such as PA12, the use of the 50 μm particles requires special attention when it comes to factors such as ventilation. Such a consideration is particularly important given that the handling of the powder is not just in the beginning of the printing process, as the SLS 3D printer is also filled with the powder. When the process is done, the printed object has to be dug from the powder. At this point, the object is still completely covered in unsintered powder, which must be removed (**Fig. 12**). This naturally places requirements even on the place where the parts can be cleaned, as excess spreading of the building material should be avoided. Therefore, SLS 3D printers are often utilized in an industrial setting or in specific laboratories. The considerably

higher price of SLS 3D printers also limits their use to commercial or research environments.

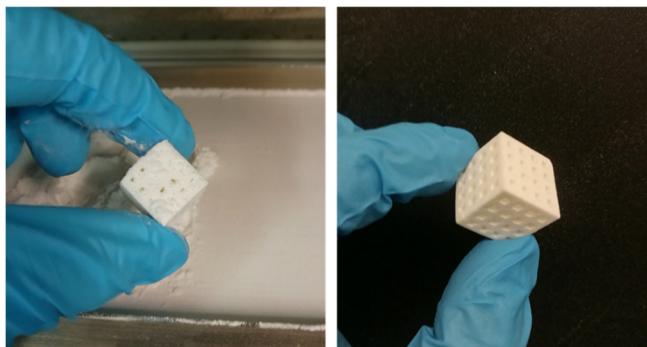


FIGURE 12 Image of the SLS 3D printed object prior to and after the removal of the unsintered powder left from the printing process.

One major advantage of SLS 3D printing is the customizability of the objects. Due to the inherent ability to customize the physical shape of 3D printable objects, different structures can be designed into the objects, but SLS 3D printing enables an even finer level of control over the structure. This control is achieved through altering the level of sintering by adjusting the printing parameters, such as laser power, laser speed, and temperature. This will alter the degree of melting within the material. By using high laser power and high temperature, and therefore high energy density, the material can be completely molten, producing a dense structure. Consequently, by using settings that result in a lower energy density, objects with porous interior structure can be produced. Depending on the application, this feature can be rather crucial, as it allows the fabrication of objects that can, for example, allow fluid to pass through them.^{11,111-115}

This alteration of the interior structure of the SLS 3D printed objects is what makes the technique an appealing option if compared to the aforementioned two techniques. With FDM 3D printing, the inner structure of the produced objects is inherently non-porous as the filament used as the building material is completely molten during the extrusion process. The same problem remains with SLA 3D printing: the physical inner structure cannot be controlled as the polymerization process leads to completely dense objects without the ability for solvent permeability without designed flow channels. SLS 3D printing provides the user with the ability to alter the physical structure by both designing the object and by altering the utilized energy density and, therefore, the degree of sintering during the printing process.^{114,115}

In addition to this, the degree of sintering and thus the porosity of the object can be controlled even within a single object. For example, higher energy density could be utilized for the outer parts of an object to produce a solvent impermeable layer around the object. This could be combined with the use of low energy density, by which one could produce porous structures for the inner parts of the object. This would allow the production of solvent permeable structures.

(Fig. 13) Hence, the solvent flow through the object could be controlled by determining which parts of the object are permeable and to what degree.¹¹⁶

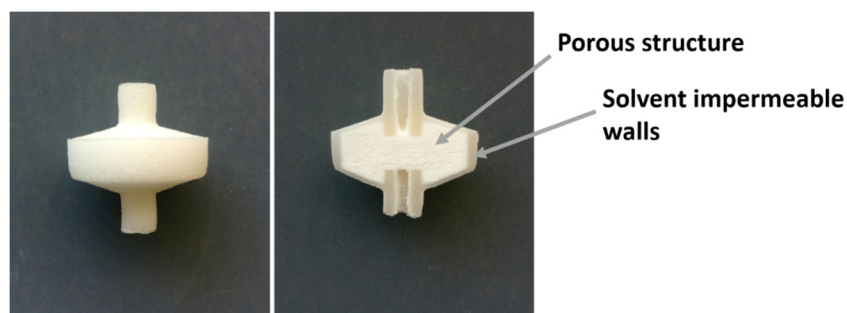


FIGURE 13 Image of the SLS 3D printed object where the walls have been printed using high energy density, thus making them solvent impermeable. The core of the object has been printed using lower energy density which leads to porous structure.

Due to the highly alterable inner structure of the objects, SLS 3D printing gives the user immense control over the physical properties of the printed objects. When the high level of control is combined with the easy customizability of the building material, even more control over both physical and chemical characteristics of the object is gained. This allows the objects to be fully customizable to specific applications. Especially, if chemistry-related applications are considered, a high degree of customizability makes the SLS 3D printing technique a rather tempting choice.

If the SLS 3D printed objects are compared to typical sorbents discussed throughout section 2, a myriad of similarities can be observed. In a sense, SLS 3D printing enables the fabrication of larger-scale sorbent materials, with much of the same properties as typical sorbents. Whereas with classical ion exchange resins the degree of cross-linking is discussed as a way to alter the porosity and flow properties, with SLS 3D printing, those characteristics can be controlled by customizing the printing parameters; the same applies for the discussion regarding the functionalization. With classical sorbents, the material is either functionalized by preparing the resin from functional components or by performing post-processing steps for functionalization. In the case of SLS 3D printing, the object is also either fabricated from already functionalized material or functionalized after the printing process. The added ability of being able to customize the physical characteristics makes the technique essentially a fabrication method for highly customizable sorbents, just on a larger scale than the more traditional materials. In addition to separation processes, SLS 3D printing has already been utilized for a variety of other applications.

3.3.2 Applications

Although the SLS 3D printing technique appears promising, it has received far less attention when it comes to chemistry-related research than the other previously discussed 3D printing techniques. This is probably not so much because of the characteristics of the technique, but more due to its availability and higher price of the technique. Regardless of the improvements, the technique is still considerably more expensive than the other 3D printing techniques. However, lately as the technique has become more available, there has been increasing interest for its use due to the unique characteristics it has in terms of the control of the structure of the printed objects. There have been reports discussing the use of SLS 3D printing for personalized medicine, microfluidic devices, and biotechnology,^{12,103,117-119} while other chemistry-related fields are yet to receive the same level of attention.

Lately, the SLS 3D printing has been reportedly introduced into several chemistry-related applications, such as electrochemistry¹²⁰, gas adsorption¹²¹, and catalysis¹²². From these, the report focusing on the fabrication of customizable electrodes (**Fig. 14**) utilizes a similar approach than the previously discussed extrusion-based methods. It combines the base building polymer with graphite, thus forming a conductive composite material that can be printed by using SLS 3D printing. The advantage this method has over the extrusion-based methods is the inherently customizable porosity (**Fig. 14**) of the physical structure of the printed objects as well as the immensely easy material synthesis. The process of generating the material simply consists of mixing the polymer powder with the graphite powder. By altering the polymer used and by changing the concentration of the graphite in the material, the conductivity of the printed objects could be altered. The optimal mixture reported was 60 wt-% PS, combined with 40 wt-% of graphite. By combining the optimized printing parameters with the optimized material, highly macroporous objects with conductivities of up to 4.3 S m^{-1} were observed. While the reported conductivity is rather low, it could potentially be improved by changing the graphite to another carbon-based material with better electric conductivity. Additionally, it was mentioned that the method could produce flexible electrodes if PU was used as the host polymer. The electrodes were able to alter their conductivity based on the mechanical stress they were placed under. This would make it possible to utilize the electrodes as sensors. Furthermore, it shows how both the properties of the carrying matrix polymer and the additive can be combined to produce novel objects for electrochemical applications.¹²⁰

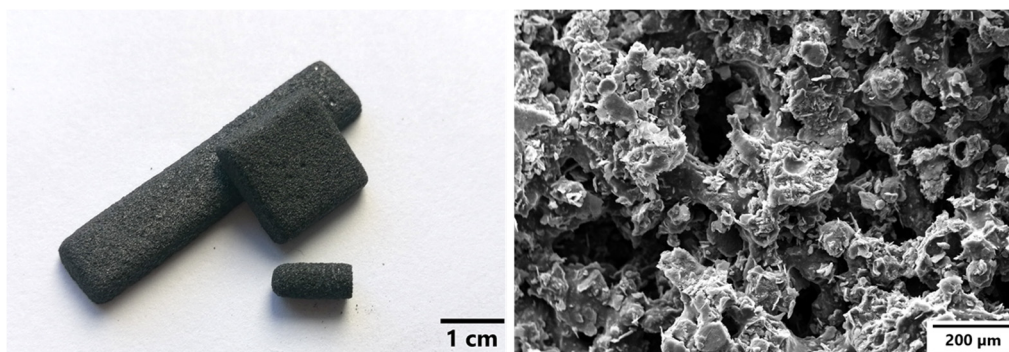


FIGURE 14 Image of the SLS 3D printed highly porous electrodes and SEM image of the porous structure of the surface of the electrode.

Another potential reported application is SLS 3D printed gas adsorbents. This approach incorporated Metal-Organic Frameworks (MOFs) into the printing material (**Fig. 15**). This work utilized commercial copper(II) benzene-1,3,5-tricarboxylate (HKUST-1) as the MOF which was combined with the PA12 polymer by simply mixing the two components together to form the building material for SLS 3D printing. The MOF was shown to be evenly distributed throughout the structure of the 3D printed objects. Additionally, the structure, activity, and the morphology of the MOF crystals were shown to be unaffected by the printing process. The printed objects were shown to be able to act as CO₂ scavengers under laboratory conditions. The report further demonstrates the ability of the technique when it comes to easy incorporation of lab-scale materials into actual macroscopic objects. New MOFs or other synthetic materials could easily be prepared on a lab-scale and incorporated into customizable objects. This would considerably shorten the development cycle needed for a lab-scale material to be implemented in practical applications.¹²¹

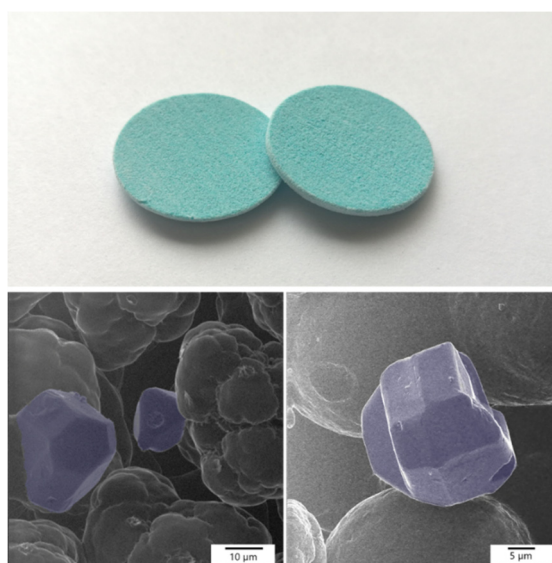


FIGURE 15 Image of the SLS 3D printed PA12-MOF object. HIM images show the MOF crystals in the porous structure of the PA12-MOF object. Reproduced from Lahtinen *et al.* with permission from John Wiley & Sons.¹²¹

Fabrication of highly porous hydrogenation catalysts using the SLS 3D printing has also been reported. This study combined the highly inert polypropylene powder with SiO₂ powder that contained palladium particles. Together they formed effective hydrogenation catalysts that were shown to be efficient in the hydrogenation of styrene, cyclohexene, and phenylacetylene. The objects were printed in the shape of stir bar sleeves (**Fig. 16**) so they could be utilized by simply inserting them onto a stir bar when the catalytic reaction was taking place. The performance of the 3D printed stir bar sleeves was compared to the performance of the SiO₂ powder with the palladium particles. The study found that the SLS 3D printing did not negatively affect the hydrogenation activity of the catalyst. Furthermore, the reusability of the 3D printed catalyst was also studied and found that it does not significantly reduce on consecutive reactions. Therefore, the SLS 3D printing seems like a promising candidate for the preparation of customizable catalytic objects of any shape or size.¹²²

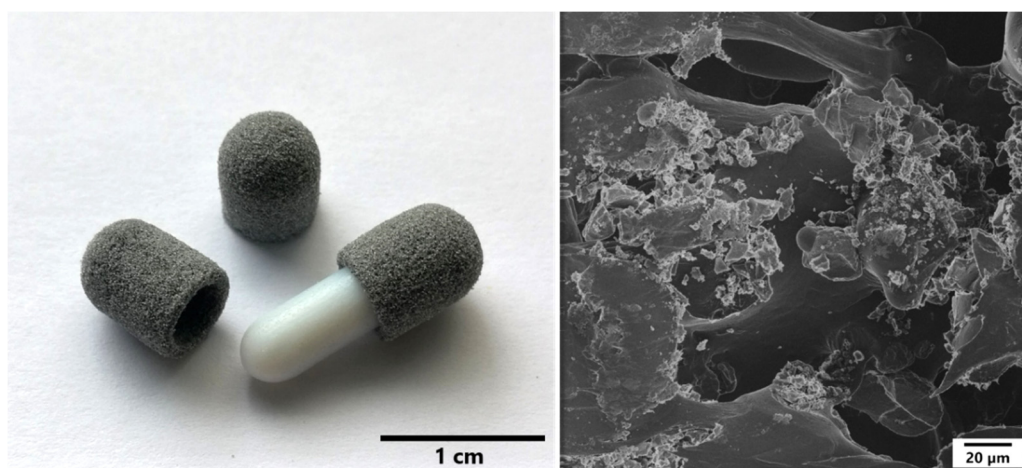


FIGURE 16 Image of the SLS 3D printed hydrogenation catalysts in the shape of stir bar sleeves. HIM image of the structure of the printed catalyst. Reproduced from Lahtinen *et al.* with kind permission from the American Chemical Society.¹²²

With the variety of applications discussed here, it seems evident that SLS 3D printing can be effectively utilized in several ways, even with rather rudimentary approaches. The effectivity of such simple approaches also further suggests that SLS 3D printing boasts more potential when it comes to chemistry-related applications. Further applications relating to the metal separation studies will be discussed in the results section of this thesis.

To conclude, all the different printing methods all have their advantages and disadvantages, and as their utilization in the field of chemistry becomes more prominent, each technique is likely to find its most suitable application. The printing principle and their strengths and weaknesses are concluded in **Table 1**.

Table 1. Advantages and disadvantages of different printing methods.

Printing method	Principle	Pros	Cons
FDM	Filament extrusion	<ul style="list-style-type: none"> • Simplicity • Inexpensive equipment • Easy to get started • Wide range of materials 	<ul style="list-style-type: none"> • Filament harder to customize • Resolution • Objects typically nonporous
SLA	Laser induced photopolymerization of resin	<ul style="list-style-type: none"> • High resolution • Objects can be optically transparent • Easy to introduce additives • Inexpensive equipment 	<ul style="list-style-type: none"> • Material handling • Requirements set by photopolymerization • Objects typically nonporous
SLS	Laser induced sintering of particles	<ul style="list-style-type: none"> • Customizability of the material • Adjustable porosity and structure • Wide range of materials 	<ul style="list-style-type: none"> • Material handling • Cost of the equipment

4 AIMS OF THE STUDY

The aim of this thesis was to further explore the potential of chemically functional 3D printing. Other printing techniques have seen some interest in research regarding chemical functionality of printed objects, while SLS 3D printing has been mostly underutilized technique, despite of its potential. Therefore, the use of the SLS 3D printing in the development of highly customizable metal separation devices was studied. This included investigating the following aspects:

- ability to fabricate chemically functional devices with SLS 3D printing;
- introduction of desired functionality into the building material via the use of additives;
- metal separation efficiency of SLS 3D printed objects;
- customizability of the microscopic structure of printed objects with parameter optimization;
- separation of platinum group metals from the PCB waste; and
- ability to use PCB waste as the gold source for preparation of printed catalysts.

5 EXPERIMENTAL

This chapter briefly introduces the workflow of chemically functional SLS 3D printing as well as some of the experimental procedures that were employed throughout papers I-III.

5.1 Chemically functional SLS 3D printing

The general workflow of preparing chemically active SLS 3D printed objects consisted of three steps: designing the object, preparing the building material, and the actual SLS 3D printing. The first step was rather similar across printing different materials, as the objects to be tested on a lab-scale were rather simple. Generally, cylinder-shaped filters were used for metal separation studies. However, for paper I, objects with a designed mesh structure were utilized (**Fig. 17**). After the CAD design process, the objects were sliced into G-code by utilizing a slicer program. While the CAD design phase made it possible to plan out the structure, shape, and size of the object, the slicing phase gave more control over the fine structure of the object, as features such as layer height can be determined.

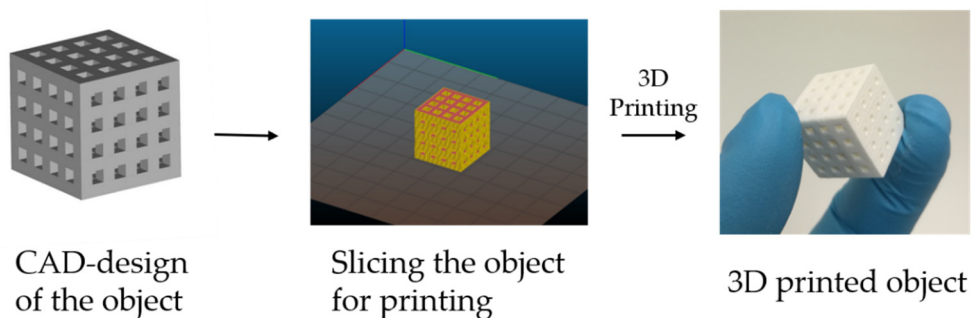


FIGURE 17 Workflow of the 3D printing starting with CAD-design of the object and followed by generation of G-code via slicing and 3D printing.

The preparation of the building material for an SLS 3D printing process is often relatively simple. Typically, the hybrid material consists of chemically-passive carrying polymer and a chemically-active additive. However, it is also possible to use chemically functional carrying polymers. The components are then simply mixed together. Nearly anything can be utilized as a functional additive, as long as the melting point of the additive is higher than that of the carrying polymer. Even this limitation can often be circumvented due to the range of different printing polymers. Another requirement for the additive is that the particle size should be rather small. As the printing is usually done using a layer height of around 100 μm , the particle size should be less than that.

Once the object for the 3D printing has been designed and the building material has been prepared, the printing parameters have to be determined. These parameters greatly affect the physical characteristics of the result and thus should be optimized for the targeted application. Typically, parameters, such as the laser power and speed as well as the temperature and cooling rate, are adjusted to obtain chemically functional objects with the desired physical characteristics. The parameters affect the physical structure of the printed object especially in terms of porosity. After printing, any unsintered powder from the printing process that might remain on the surfaces of the objects is simply cleaned off. They are then ready to be utilized without further post-processing. The general workflow of SLS 3D printing of chemically functional objects is shown in Fig. 18.

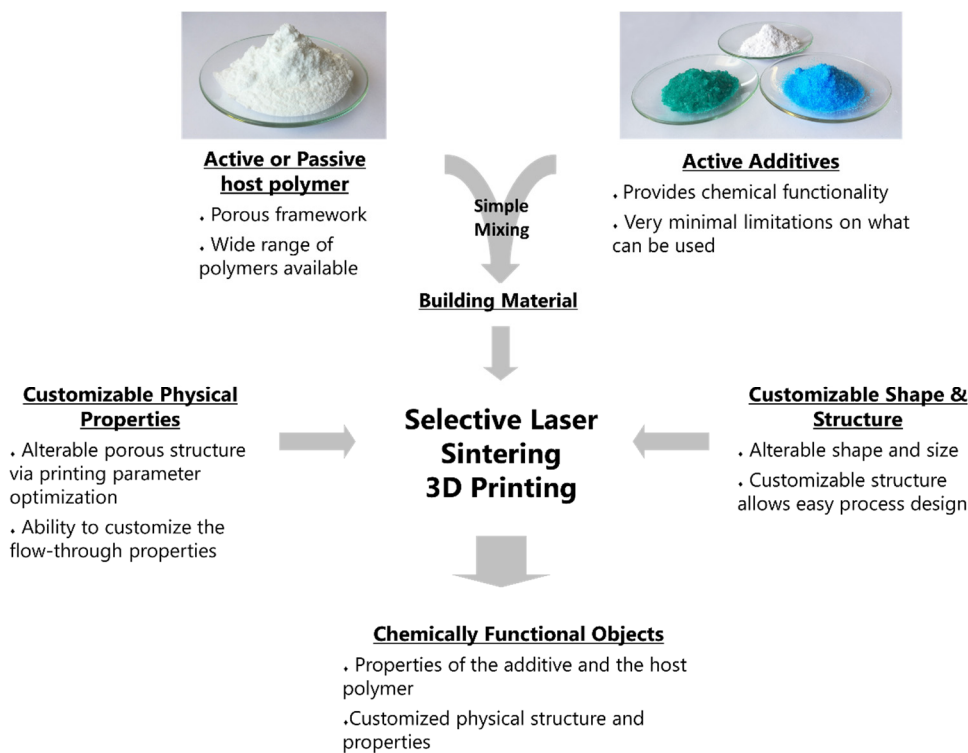


FIGURE 18 Scheme of the workflow of the chemically functional SLS 3D printing.

5.2 Utilization and characterization of the printed objects

5.2.1 Characterization of the SLS 3D printed objects

The characterization of the printed objects was done using several different methods. The porosity and the overall visual structure of the objects were examined by using both Scanning Electron Microscopy (SEM) and Helium Ion Microscopy (HIM). They both allowed the study of the general physical characteristics of the objects. As for the printed objects with additives included, especially HIM was utilized to study the distribution and attachment of the additive particles onto the carrying polymer matrix.^{I-III}

Further insight about the structure and in particular the porosity of the object was gained via X-ray tomography. It was used to further study the homogeneity of the printed object in terms of the porosity and additive distribution. With further analysis, the total volume of the pores, as well as the average diameter of the pores could be determined.^{II}

When studying the printed nanocatalysts, several techniques were utilized to gain information about the size and distribution of the particles. First, HIM was used for high-resolution imaging to obtain a rough estimate of the size of the nanoparticles as well as to study the dispersion of the nanoparticles on the surfaces of the objects. Next, Powder X-ray Diffractometry (PXRD) was applied to further confirm the estimation about the particle sizes. This was followed by Single Particle Inductively Coupled Plasma Mass Spectrometry (SP-ICP-MS), which allowed for more accurate determination of the sizes of the nanoparticles. Additionally, Scanning Electron Microscopy Energy Dispersive Spectrometry (SEM-EDS) was utilized as spectral profiling was found to be a rather conclusive method of studying the dispersion of the gold nanoparticles on the surface of the object.^{III}

5.2.2 Metal adsorption experiments

For the metal adsorption experiments, both synthetic and authentic samples were utilized. The synthetic samples were prepared by diluting metal stock solutions. The authentic PCB samples were first milled down to fine particles followed by thermal treatment at 950 °C for 4 hours. The ashed PCB sample was then dissolved by using ultrasound assisted aqua regia leaching. The dissolved PCB sample was diluted with ultra-pure water prior to use for metal adsorption tests.^{I-III}

In general, a known volume of the sample solution was flown through the printed object for the metal adsorption tests. As for the batch processes, the printed objects were placed in a shaker with the sample solution. The adsorption efficiencies were determined by measuring the initial metal concentrations in the

solution and by comparing them to the metal concentrations observed after the experiment. ^{I-III}

All metal concentrations were measured with a PerkinElmer Optima 8300 Inductively Coupled Plasma Optimal Emission Spectrometer (ICP-OES) using an argon gas flow of 8 L min⁻¹, nebulizer gas flow of 0.6 L min⁻¹, auxiliary flow of 0.2 L min⁻¹, and a sample flow rate of 1.5 mL min⁻¹ with a radio frequency power of 1500 W. For the measurements, the ICP-OES was equipped with a cyclonic spray chamber and a GemCone low flow nebulizer. For paper **I**, the analyzed metals, the wavelengths, and other method details are represented in **Table 2**.

Table 2. ICP-OES measurement method details. ^I

Metal	Wavelength (nm)	Axial/Radial view	Calibration range for synthetic solutions (mg L ⁻¹)	Calibration range for leached PCB (mg L ⁻¹)	R value
Au	242.795	Axial	0.1-10	0.1-10	≥0.9999
Pd	340.458	Axial	0.1-10	0.1-10	≥0.9999
Pt	265.954	Axial	0.1-10	0.1-10	≥0.9999
Ni	221.648	Radial	0.2-20	1-100	≥0.9999
Al	396.153	Radial	0.1-10	0.5-50	≥0.9999
Cr	267.716	Axial	0.1-10	0.5-50	≥0.9999
Pb	220.353	Axial	0.1-10	0.5-50	≥0.9999
Zn	206.200	Radial	0.2-20	1-100	≥0.9999
Sn	189.927	Axial	0.1-10	0.5-50	≥0.9999
Fe	238.205	Radial	0.2-20	1-100	≥0.9999
Cu	327.393	Radial	0.2-20	1-100	≥0.9999

For paper **II**, the ICP-OES operating parameters were identical but small alterations were made to the measurement methods and calibration ranges of the metals as shown in **Table 3**. These modifications were made to avoid unnecessary dilutions and to allow the study of specific methods for recovery and elution studies. ^{II}

Table 3. ICP-OES measurement method details. ^{II}

Metal	Wavelength (nm)	Axial / Radial view	Calibration range for elution studies (mg L ⁻¹)	Calibration range for recovery studies (mg L ⁻¹)	Calibration range for leached PCB sample (mg L ⁻¹)	R value
Au	242.795	Axial	0.1-10	0.1-10	0.1-10	≥0.9999
Pd	340.458	Axial	0.1-10	0.1-10	0.1-10	≥0.9999
Pt	299.797	Axial	0.1-10	0.1-10	0.1-10	≥0.9999
Ni	221.648	Radial	0.1-10	1-100	1-100	≥0.9999
Al	396.153	Radial	0.1-10	1-100	0.5-50	≥0.9999
Cr	267.716	Axial	0.1-10	1-100	0.5-50	≥0.9999
Pb	220.353	Axial	0.1-10	1-100	0.5-50	≥0.9999
Zn	206.200	Radial	0.1-10	1-100	1-100	≥0.9999
Sn	189.927	Axial	0.1-10	1-100	0.5-50	≥0.9999
Fe	238.205	Radial	0.1-10	1-100	1-100	≥0.9999
Cu	327.393	Radial	0.1-10	1-100	1-100	≥0.9999

5.2.3 Preparation of the printed nanocatalyst and the catalysis experiments

The printed nanocatalysts were prepared by adsorbing tetrachloroaurate onto the printed PA12 plates. The plates were then reduced to produce the nanocatalyst. This was done by contacting the plates with different reducing agents, namely NaBH₄, ascorbic acid, and H₂O₂. Additionally, thermal treatment at 110 °C and UV-light reduction were also utilized as reduction methods. The reduction time was altered for each reductant depending on the reduction efficiency. After the reduction, the printed nanocatalysts were rinsed with water prior to use.^{III}

For the catalysis experiments, a 0.1 mM 4-nitrophenol solution was prepared. For the reactions, known volume was taken and combined with excess of NaBH₄, and a printed nanocatalyst was added. The reactions were stirred for 2 hours, after which the completeness of the reduction into 4-aminophenol was monitored by a UV-Vis spectrometer, as 4-nitrophenol has a characteristic absorption peak at 400 nm, which diminishes as it is reduced into 4-aminophenol.^{III}

6 RESULTS AND DISCUSSION

This chapter discusses the results and findings from the three papers included in this thesis. Papers **I** and **II** focused on selective separation of gold, palladium, and platinum from acidic leachate of PCB waste by utilizing SLS 3D printed filters. In paper **III**, a different approach was taken, where waste-derived gold was adsorbed into SLS 3D printed filters, followed by direct conversion into functional nanocatalysts.

6.1 Selective recovery of Au from acid leached PCB waste¹

6.1.1 Preparation and characterization of SLS 3D printed filters

The preparation of SLS 3D printed filters for selective recovery of gold as tetrachloroaurate included following the general printing procedure by using pure PA12 as the building material. The filters were designed to have an inner mesh structure that was controlled by CAD design (**Fig. 19**). The inner structure of the filters allows for a high flow rate of the passing fluid while still disturbing the flow enough to enhance the contact of the fluid with the chemically active surfaces of the printed PA12 filter. The filter components were designed to be interconnectable to be able to easily alter the amount of gold scavenging material present in the flow application. In addition to the filter-shaped object, cubic mesh structures were also designed for batch process testing (**Fig 17** and **22** (right)). After the design, the objects were manufactured using pure PA12 as the building material. Parameters were optimized so that they led to durable, yet highly porous objects.

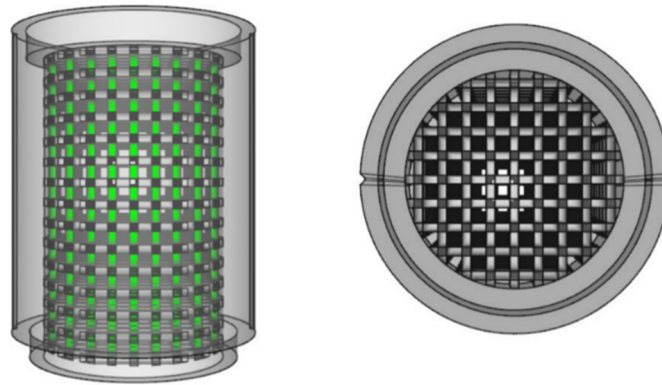


FIGURE 19 CAD drawings of the PA12 filters.

SEM and HIM were utilized for the characterization of the produced objects. The SEM analysis of the material was initially carried out. Due to the highly nonconductive nature of the printed objects, the objects had to be covered with gold to reduce the charging effect observed due to the imaging technique. Regardless of the remaining charging effect, the structure of the 3D printed PA12 filters can be seen to have a highly porous structure (**Fig. 20 a.**). If the structure is inspected more closely, the PA12 particles can be seen to have retained their particle-like nature and only be partially sintered to each other to form the solid object (**Fig. 20 b.**)

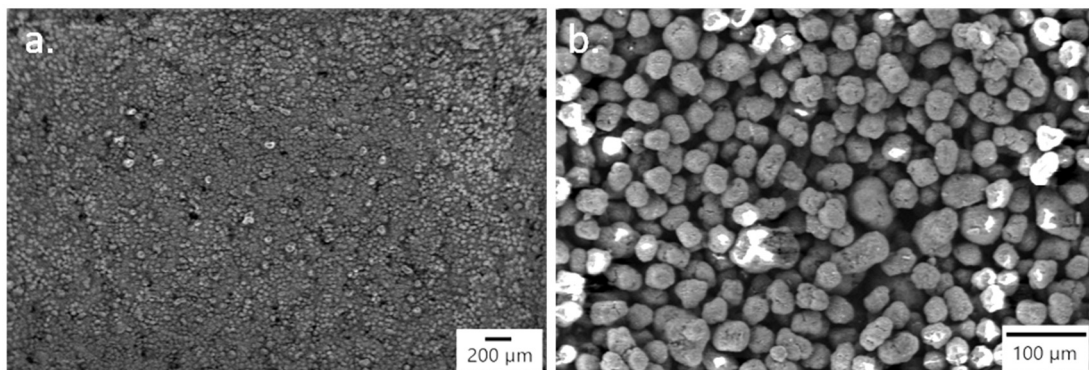


FIGURE 20 Overall (a.) and zoomed in (b.) SEM images of the surface of the SLS 3D printed PA12 objects.

HIM imaging typically allows for more resolution, even with nonconducting samples. From the HIM images, the structure could be observed more clearly. It is evident, that the PA12 particles still retain their roughly spherical shape when optimal printing parameters were utilized. It could even be seen, that by altering the amount of laser power, the porosity of the structure could be altered significantly. As the lower laser power is utilized, the lower energy density leads to a highly porous structure (**Fig. 21 a.**). When using higher laser power, a practically nonporous structure is obtained (**Fig. 21 b.**) Thus, the structure of the

SLS 3D printed filter could be controlled on two separate levels: on a macroscopic level by altering the design of the object in CAD, and on a microscopic level by optimizing the printing parameters to match the desired porosity of the object.

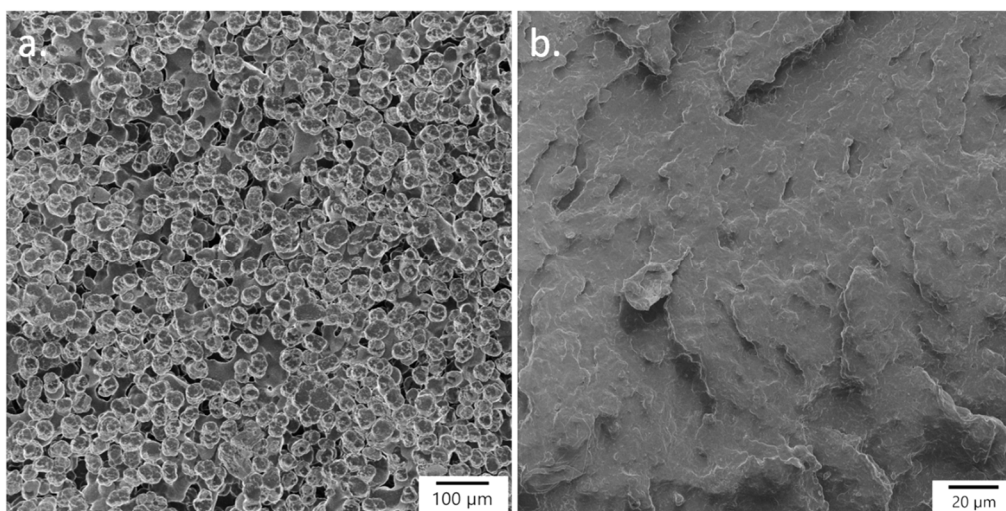


FIGURE 21 HIM images of the surfaces of PA12 objects that have been printed using lower laser power (a.) and higher laser power (b.).

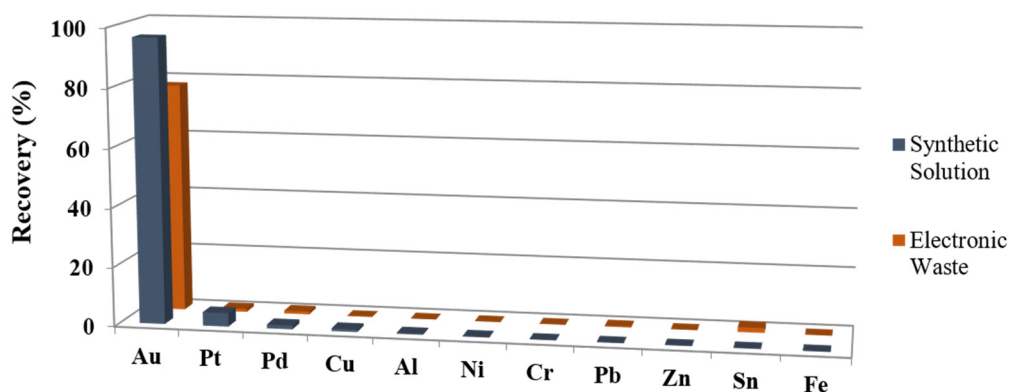
6.1.2 Selective separation of Au

As the idea of developing the chemically functional SLS 3D printing method was that the resulting objects would possess the chemical functionalities of its components, the testing of the properties of the components can also be carried out prior to the actual printing of the material. Therefore, the functionality of the PA12 powder was analyzed as it is the most commonly utilized SLS 3D printing polymer. The experiment was performed by contacting the powdery PA12 material with both synthetic and authentic acid leached PCB waste. The synthetic leachate was prepared to roughly simulate the metals concentrations present in acid leached PCB waste. The synthetic sample was used for most of the experiments as the authentic PCB waste can be highly heterogeneous; therefore, the use of synthetic solution allowed more reliable estimation of the performance of the SLS 3D printed filters. The authentic sample was prepared by performing ultrasound-assisted leaching of crushed and ashed PCB waste with aqua regia. The obtained leachate was then diluted in a 1:1 ratio prior to the metal adsorption experiments. The metals and their concentrations in both of the samples are represented in **Table 4**. After the experiments, ICP-OES was utilized to determine the metal concentrations before and after the treatment of the solution with the PA12 as described in section 5.2.2.

Table 4. Metal concentrations of the synthetic and authentic PCB leachates.¹

Metal	Concentration synthetic solution (mg L ⁻¹)	Concentration PCB leachate (mg L ⁻¹)
Au	5	70
Pd	5	40
Pt	5	<5
Cu	100	25 000
Fe	100	2700
Ni	100	1600
Zn	100	1700
Al	50	500
Cr	50	190
Pb	50	500
Sn	50	850

For both the synthetic and authentic sample, PA12 was found to be extremely selective towards gold as tetrachloroaurate. It was observed to adsorb the gold nearly quantitatively (96.4 %) while only adsorbing trace amounts of the platinum (4.6 %) and none of the other metals present in the samples (Fig. 22). The material was found to perform in a rather similar manner in synthetic and authentic samples. All in all, PA12 was found to be highly efficient in separating tetrachloroaurate from extremely challenging media containing high concentrations of competing cations and anions.

**FIGURE 22** Metal recovery profiles of the PA12 powder from synthetic and authentic electronic waste solution.¹

As the powdery material had desirable performance, it was SLS 3D printed into the aforementioned filter shaped objects and mesh cubes for batch process testing (**Fig. 23**). The mesh cubes were tested for batch processes by contacting them with the synthetic sample solution. They were found to perform identically to the unprinted PA12 powder as they selectively and nearly quantitatively (90.4 %) adsorbed the gold from the solution without significant adsorption of any of the other metals. In addition to the batch process, the usability of the SLS 3D printed objects in flow applications was tested by first passing a sample through one 3D printed PA12 filter (as shown in **Fig. 23** (left)). This resulted in 27.2 % of the gold being adsorbed. As the number of filters was increased to 3 and 10, the gold adsorption efficiency increased to 47.8 % and 82.7 %, respectively. Even with the longest filter consisting of 10 separate filter pieces, the contact time with the solution and the filter remained under 30 seconds. Therefore, the performance of the filters could be even further improved by either making the column longer or by altering the flow-channel structure of the filters. The gold could be eluted from the filter by utilizing 7 M HNO_3 , which allowed the reuse of the printed filters.



FIGURE 23 Image of the SLS 3D printed PA12 filter objects with one (left) and three (middle) filter units attached. Image of the SLS 3D printed PA12 mesh cube (right).

Based on the obtained results, PA12 acts as extremely selective material for gold adsorption from chlorine-containing acidic media. It enables the separation of gold from both common matrix elements such as Cu, Ni, and Fe, as well as other platinum group metals such as Pd and Pt. Furthermore, the objects made out of PA12 by using SLS 3D printing were found to possess the chemically functional properties of the unprinted PA12 powder. Therefore, SLS 3D printing can be seen as an effective way to prepare highly customizable objects for selective gold adsorption in both batch and flow-through processes.

6.2 Selective recovery of Pd and Pt from acid leached PCB waste^{II}

6.2.1 Preparation and characterization of SLS 3D printed filters

As the gold was selectively separated from the PCB leachate by using PA12 filters, the separation of the rest of the remaining noble metals present was tackled next by incorporating a chemically functional additive into the SLS 3D printed filters. The functional additive was chosen to be a typical anion exchange resin Dowex 21K with a benzyltrimethyl ammonium functional group. As it is a classical gel-type material, resin had to be dried first to make it more easily compatible with the powdery printing material. Therefore, the resin was dried at 90 °C overnight followed by grinding into finer particles via ball-milling. The now powdery 21K resin was then incorporated into polypropylene (PP) powder via mechanical mixing. The mixture was adjusted to contain 10 wt-% of the 21K. The PP was chosen as the host polymer due to its chemically stable and inert nature. Unlike for the gold separation, filters without any interior structure were designed and printed (**Fig. 24**). These filters allowed for better utilization of the observed porous nature of the objects, which in turn allowed the fluid to pass through the filter even without any specific flow channels. The functional filters were printed according to the aforementioned process with optimized printing parameters.



FIGURE 24 Image of the PP-21K filters (left) and of the 10 mL syringe with three PP-21K filters that was used for the adsorption experiments (right).

The PP-21K filters were then characterized by HIM as well as X-ray tomography. The HIM images show the porous structure of the object as well as the homogeneous distribution of 21K (**Fig. 25 a**). Additionally, it can be seen that the 21K particles are only attached to the surfaces of the partially sintered PP particles and not encapsulated by the polymer (**Fig. 25 b**). This means that they remain available for interactions with the fluid passing through the pores of the filter. The images also show how the PP particles are only partially sintered and are therefore attached onto each other only via a small percentage of their total surface area.

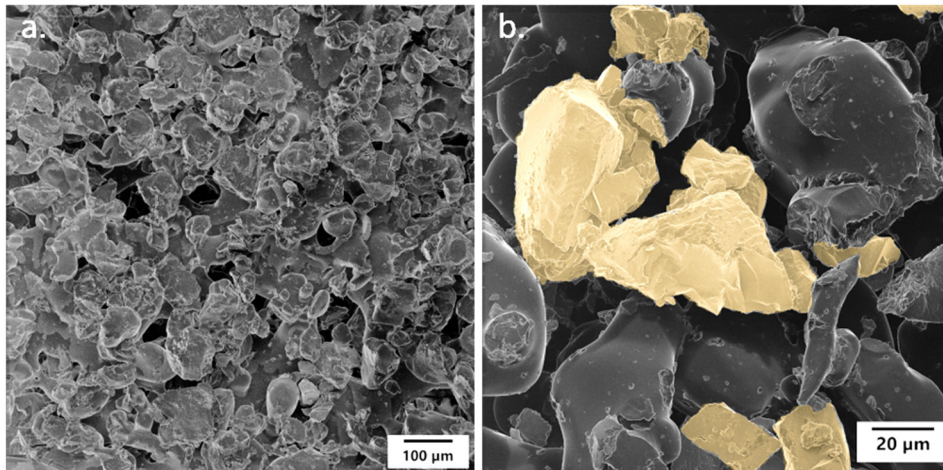


FIGURE 25 HIM image of the structure of the PP-21K filter (a.) and zoomed-in image of the surface of the filter with highlighted 21K particles (b.).

The X-ray tomography imaging was conducted for a small cylindrical object prepared from the same PP-21K material. The horizontal and vertical tomography images (**Fig. 26**) further confirm the observations from the HIM imaging as they show that the distribution of the pores in the object is homogeneous throughout the entire object. The resin can be seen in the images as white particles. Their distribution can also be seen to be rather homogeneous even at the relatively low additive concentration of 10 wt-%. Additional analysis of the tomography images showed that the pores make up around 32 % of the total volume of the filter, with most of the pores being between 20 and 60 μm in diameter in size. The combination of HIM and X-ray tomography analysis proves that additive materials can be effectively utilized in SLS 3D printed objects by simply mixing them with the powdery material, as the resulting objects will have a homogeneous distribution of the additive particles.

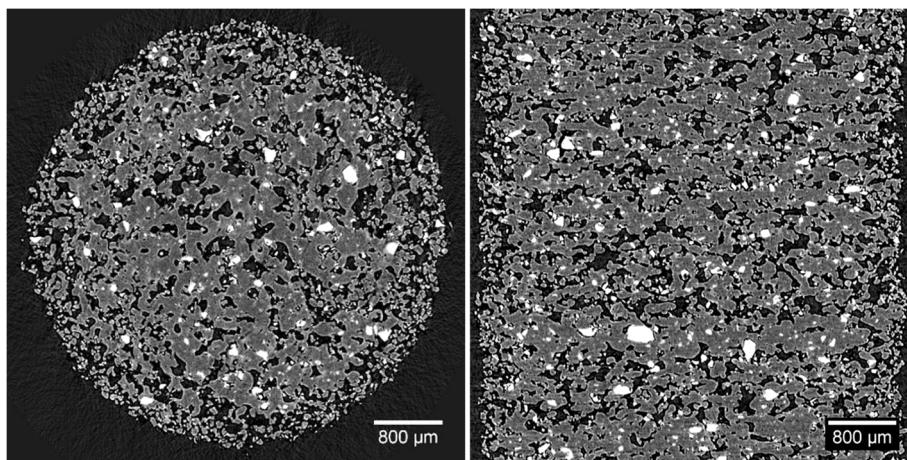


FIGURE 26 Vertical and horizontal x-ray tomography images of the PP-21K filters.

6.2.2 Separation of the platinum group metals

Next, the adsorption performance of the PP-21K filters was evaluated by utilizing the same synthetic PCB leachate solution as in paper I, with the main difference being that platinum concentration in synthetic solution was lowered to 1 mg L^{-1} . This was done to better mimic the often-lower amount of platinum present in PCB waste. The authentic PCB leachate was roughly similar in metal concentrations as shown in **Table 4**, with some differences in the matrix element concentrations due to heterogeneity of the PCB waste. The samples were analysed by utilizing ICP-OES as described in section 5.2.2 combined with the calibration ranges and other measurement details represented in **Table 3**.

The filters were utilized by placing them into a 10 mL syringe and gently pushing the sample solution through the filters. For the adsorption studies, three PP-21K filters were placed in a syringe. For the synthetic solution, this resulted in effective adsorption of 96 % and 98 % of palladium and platinum, respectively. However, also 50 % of tin as well as around 10-22 % of zinc and lead was adsorbed onto the PP-21K filter (**Fig. 27**). Due to the amount of different metals in the filter, further separation of the elements was needed via elution studies.

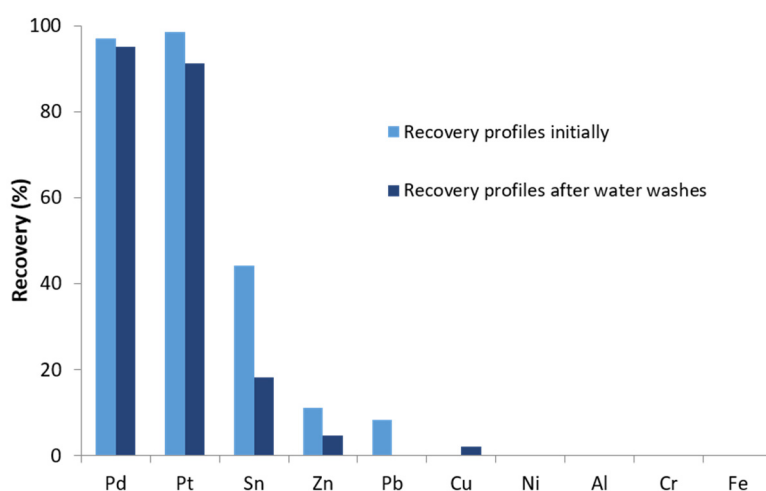


FIGURE 27 Recovery profiles of the metals after being treated with PP-21K filters and the recovery profiles after the elution with water. ^{II}

First, the zinc and lead were selectively eluted from the PP-21K filter by passing water through the filter. The water washes also eluted around 50-60 % of the tin that was adsorbed onto the PP-21K filter. Next, the elution of the noble metals was performed by first eluting most of the palladium with using a 0.1 M thiourea solution, followed by platinum elution using a 0.3 M thiourea solution. The one-by-one elutions of palladium and platinum lead to elution efficiencies of 83 % and 85 %, respectively. Even though the separation of palladium and platinum is not complete (**Fig. 28**), it could be improved via further optimization. Finally, the part of the tin that could not be eluted with the water washes could be effectively eluted by using 4.5 M HNO_3 . After the elution cycle, the filter could be

regenerated by 0.1 M HCl and reused without significant loss of activity. Similar adsorption process was also performed by using authentic PCB leachate. The filters were observed to behave similarly than what was observed with the synthetic solution.

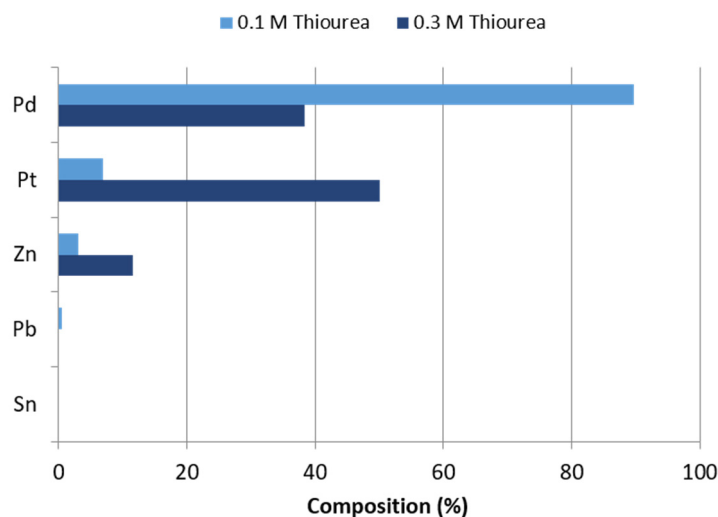


FIGURE 28 Metal composition of the thiourea elution fractions.^{II}

The capacity of the PP-21K filter was evaluated in a batch process with a solution containing much higher palladium and platinum concentrations (400 mg L^{-1} of both Pd and Pt in 5% *aqua regia*) than what was present in the PCB leachates. It was tested by placing a single PP-21K filter in a 10 mL syringe and passing the sample of the test solution through the filter five times. To monitor the effect of the printing process on the capacity of the material, a similar test was performed by placing an equal weight of unprinted PP-21K powder onto a container with the sample solution and monitoring the adsorption behavior. The SLS 3D printed PP-21K filter showed a palladium and platinum capacity of around 11 wt-% relative to the amount of functional material in the filter unit, while the unprinted powder showed a 13 wt-% capacity. The small difference in results can be attributed to the part of the surface area of the 21K particles being utilized for effective anchoring onto the PP matrix. The result demonstrates that the SLS 3D printing process has only a minimal effect on the capacity of the material. While the performed capacity experiment is not the optimal way of determining the maximum capacity of the material, it was found to be sufficient for roughly monitoring the effect of the SLS 3D printing process on the capacity of the material.

The gold adsorption process described in section 5.2.2. was also tested by utilizing a similar test setup and solid filter objects that were utilized for the palladium and platinum separation. As expected, the “solid” PA12 filters without any designed flow-channels were able to selectively and quantitatively

6.3 Preparation of Au nanocatalysts from PCB waste derived gold^{III}

6.3.1 Preparation of SLS 3D printed nanocatalysts

Even though the metal separation process described in previous sections returns the metals from waste to circulation, it might not be the optimal solution in all cases. Another approach to a circular economy-related solution would be converting the metals from waste straight into functional products, therefore eliminating the need for extra processing. Here, the PCB waste-derived gold is adsorbed onto PA12 objects (as described in section 5.2.2) followed by the conversion of the whole object into a functional nanocatalyst. The conversion is done by reducing the adsorbed gold into nanoparticles, which can then be further utilized, for example, in catalysis.

As the process utilizes plain PA12 as the building material, SLS 3D printing was performed in a similar manner to what was described earlier. The printed PA12 objects were then allowed to adsorb gold from a synthetic tetrachloroaurate solution. After the adsorption, the objects were rinsed thoroughly with water before being used in reduction experiments. The reduction process was carried out using a series of different reduction methods. The reducing agents included NaBH_4 , ascorbic acid, and even H_2O_2 , a more unconventional reducing agent, that is known to produce gold nanoparticles¹²³. In addition to the chemical reduction methods, UV-light, as well as heating induced reduction were also tested. Different reduction methods and reaction times were also experimented with and were found to lead to different colors of the PA12-Au objects as shown in Fig 30.

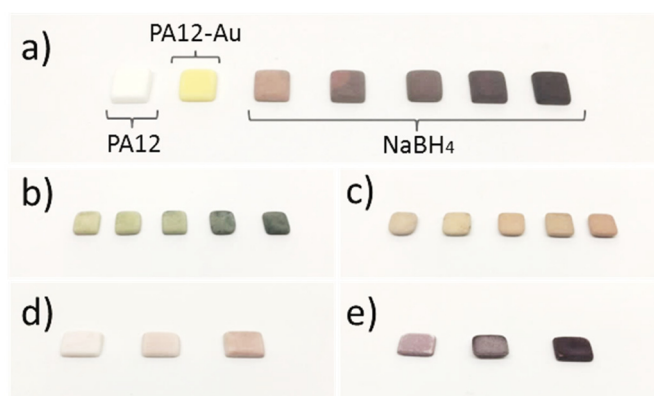


FIGURE 30 Images of the printed PA12-Au filter plates (10x10x2 mm). a) Plain PA12 filter and PA12 filter straight after the gold adsorption as well as PA12-Au filters reduced with NaBH_4 for 1, 3, 5, and 15 minutes, respectively. b) Series of PA12-Au filters that were reduced using 0.5 M ascorbic acid for 1, 3, 5, 10 and 15 minutes, respectively. c) Series of PA12-Au filters that were reduced using 30% H_2O_2 for 5, 10, 15, 30 and 60 minutes, respectively. d) Series of PA12-Au filters reduced using UV light (405 nm) for 20, 40, and 60 minutes. e) PA12-Au filters reduced using thermal treatment (110 °C) for 30, 60 and 90 minutes. Reproduced with kind permission from the American Chemical Society.^{III}

Additionally, an auto-reduction process was also observed to take place when the gold adsorbed PA12-Au objects were left without any additional reduction process for an extended period of time. And even though the Au in the PA12-Au objects shown here is derived from synthetic solution, the similar process was also shown to work with authentic PCB leachate derived Au. Furthermore, regardless of the simple shape of nanoparticle-functionalized objects, the inherent ability of the 3D printing is to customize the objects. Therefore, the nanocatalysts can be fabricated into any shape and size with highly customizable structures (**Fig. 31**).

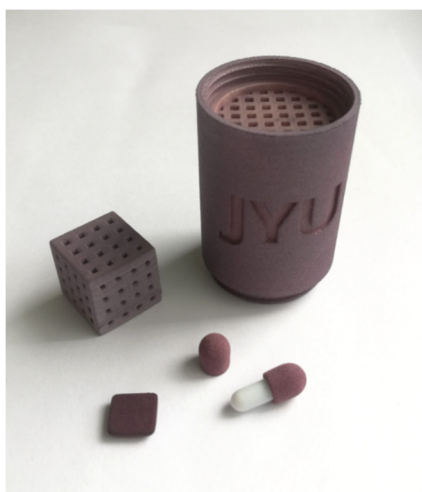


FIGURE 31 Image of different SLS 3D printed PA12 objects that have been functionalized with gold.

6.3.2 Characterization and performance of the nanocatalyst

The PA12-Au objects with the nanoparticles were first characterized by using HIM imaging. The PA12-Au objects prepared by using different reduction methods were imaged and were found to have a homogeneous distribution of the Au nanoparticles. The **Fig. 32** shows the HIM images of the PA12-Au filters, which were reduced using H_2O_2 (a and b) and ascorbic acid (c and d). The nanoparticles can be seen to have an even coverage of the whole granular structure of the object. Even though HIM is not an optimal method of determining the size of the observed nanoparticles, they can be seen to be roughly between 10 and 100 nm in size. The PA12-Au plates prepared with other reduction methods were observed to have a similar structure as shown in **Fig. 32**.

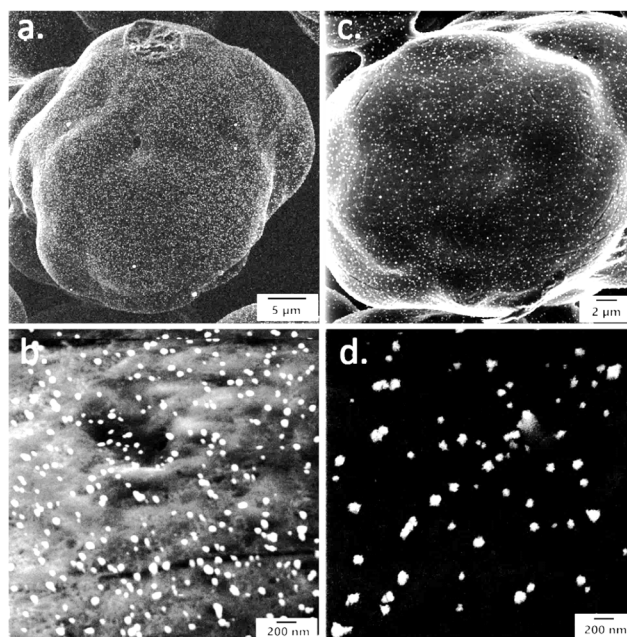


FIGURE 32 HIM images of the H_2O_2 reduced PA12-Au filters made using synthetic gold solution (a and b) and of the PA12-Au filters with PCB derived gold followed by ascorbic acid reduction (c and d). Reproduced with kind permission from the American Chemical Society.^{III}

The distribution of the Au nanoparticles was also studied by performing spectral imaging analysis of the objects' surfaces by using SEM-EDS. The surface was imaged in relation to the Au locations, and the images clearly show that the Au is evenly distributed throughout the surface of the object (Fig. 33). However, this was expected, as the object consists solely of PA12. Still, the results show that only minimal agglomeration of Au nanoparticles takes place during the reduction process. This suggests that there is most likely interaction between the surface of the PA12 and the gold nanoparticles that prevents excessive agglomeration during the reduction process.

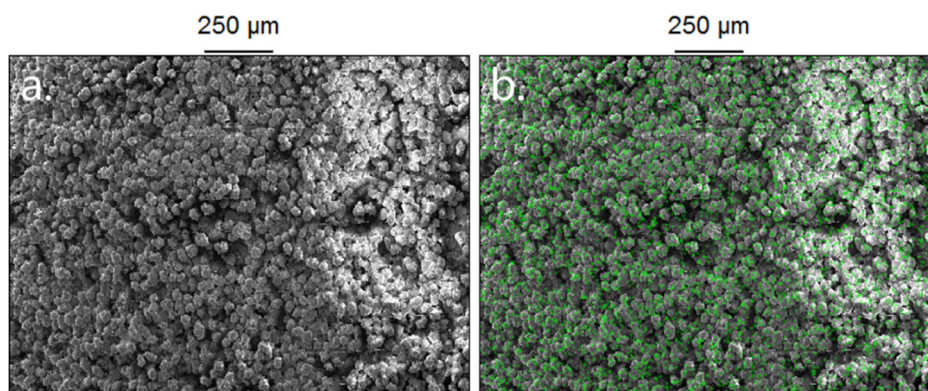


FIGURE 33 Ascorbic acid reduced PA12-Au sample imaged with SEM-EDS (a). Gold spectral image (green) overlaid with the image of the analyzed area (b). Reproduced with kind permission from the American Chemical Society.^{III}

The size distribution observed from the HIM imaging was also further confirmed as the different PA12-Au objects were analyzed with Powder X-ray Diffractometry. The PXRD analysis (**Fig. 34**) showed that, depending on the reduction method, the gold particles were in the range of 9 to 70 nm when estimated with the Scherrer method. It should be kept in mind that the PXRD analysis is a rather qualitative method of determining nanoparticle sizes in samples. Regardless, the PXRD results can be seen to suggest that the particles are in the same size range than what was observed with the HIM imaging. Additionally, the PA12-Au filter where the gold was derived from PCB leachate (**Fig. 33 g.**) also showed more similar results than the other PA12-Au filters which were made using synthetic tetrachloroaurate solution (**Fig. 34 a-f**).

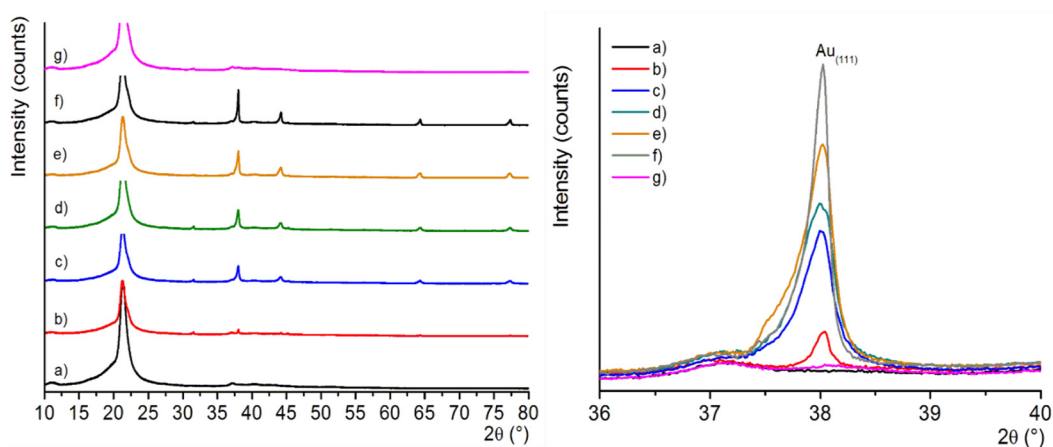


FIGURE 34 Left: PXRD patterns of PA12-Au filters with following reducing agents: a) Plain PA12 without Au, b) PA12-Au with UV-light reduction, c) NaBH_4 , d) thermal treatment, e) ascorbic acid, f) H_2O_2 , and g) a PA12-Au sample, with PCB derived gold followed by NaBH_4 reduction. Right: zoomed in 2θ range showing the $\text{Au}_{(111)}$ peak on the pattern of each sample. Reproduced with kind permission from the American Chemical Society. ^{III}

To obtain additional information of the size of the Au nanoparticles in the material, SP-ICP-MS analysis was performed. The experiment was conducted by shaking the different PA12-Au objects in water, followed by nanoparticle analysis of the solution. The results (**Fig. 35**) suggest that most of the different types of PA12-Au plates possess nanoparticles with a diameter of around 14-32 nm. Some variance in the size distribution can be observed, but given the uncertainty present in the analysis, the samples can be seen to possess mostly particles of roughly 20 nm of size. Additionally, the sample that was made using the PCB leachate and then reduced using NaBH_4 showed roughly the same size nanoparticles than the other PA12-Au filters. This further demonstrates that the waste-derived gold can be efficiently utilized to produce SLS 3D printed nanocatalysts.

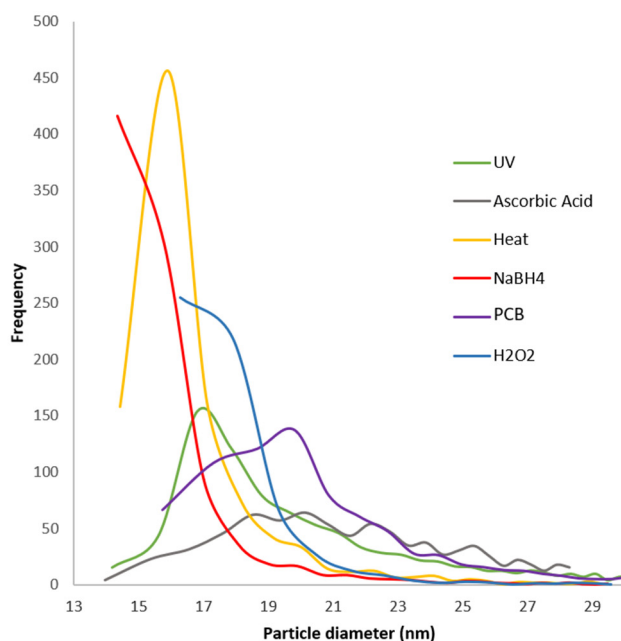


FIGURE 35 Particle diameter distribution diagram of the different PA12-Au filters received from the SP-ICP-MS measurement. Reproduced with kind permission from the American Chemical Society.^{III}

Finally, the catalytic performance of the different PA12-Au plates was evaluated in a simple reduction reaction of 4-nitrophenol to 4-aminophenol. The reaction was performed with an excess of NaBH_4 as a reducing agent to ensure that the changes in the concentration of the reductant would not affect the reaction. Samples of 0.1 mM 4-nitrophenol in water were contacted with the PA12-Au plates prepared with different reduction methods. Reference reactions were carried out without a catalyst and PA12 plate without Au as a catalyst. After two hours of stirring, most of the reactions can be seen to reach completeness as the absorbance, measured using UV-Vis spectrometer, diminishes as the 4-nitrophenol is reduced to 4-aminophenol (Fig. 36). While most of the reactions happened more rapidly, reaction time was increased to ensure that the control reactions would not proceed, thereby confirming the catalytic activity of PA12-Au plates. Most of the PA12-Au plates can be seen to effectively catalyze the reaction. However, the nanoparticles produced by heating the PA12-Au plate appear to possess slightly slower reaction kinetics, which is most likely due to the vastly different reduction process utilized for particle generation. Additionally, the PCB waste-derived PA12-Au filter (PCB- NaBH_4 in Fig. 34) can be seen to perform identically when compared to the PA12-Au filters produced using the synthetic tetrachloroaurate solution.

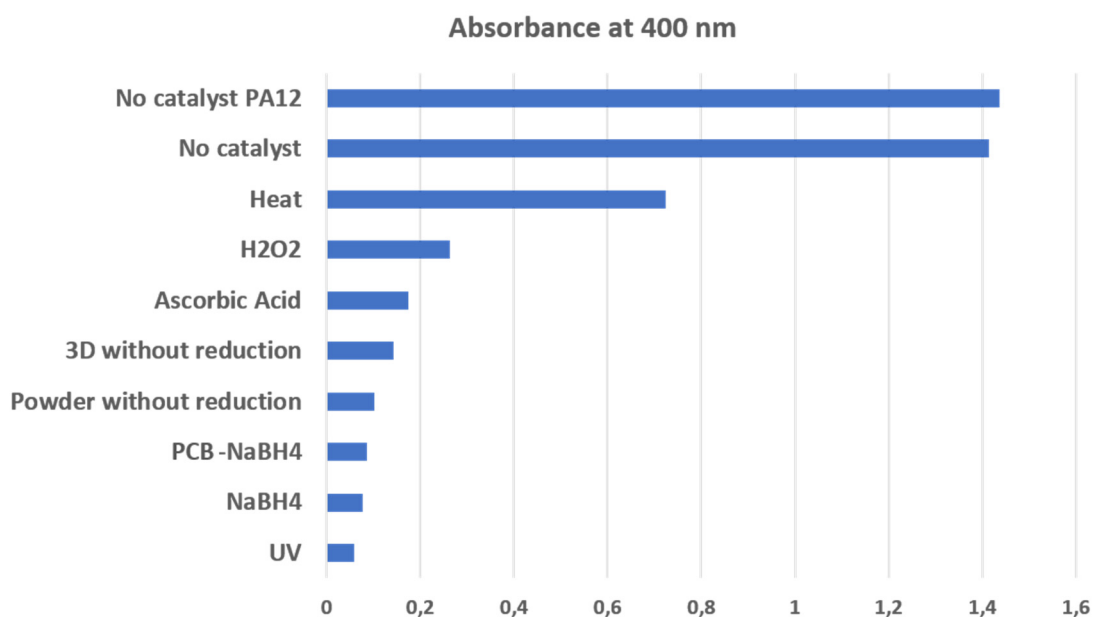


FIGURE 36 UV-Vis absorbance at 400 nm for the gold-catalyzed reduction of 4-nitrophenol to 4-aminophenol in the presence of NaBH_4 .^{III}

While the catalytic activity of the PA12-Au plates that were fabricated using different reduction methods were not exhaustively studied here, the results still suggest the catalytic activity of the SLS 3D printed PA12-Au plates. The different characterization methods confirmed that the nanoparticle distribution is rather homogeneous both in terms of the particle size and the distribution throughout the objects. Furthermore, the ability to obtain the gold from waste material makes the method an appealing option also in terms of the circular economy. The method removes many of the typically laborious steps from the process of converting the waste-derived material back into a functional product. This combined with the inherent ability to fully customize the physical structure of the SLS 3D printed catalyst makes the method a powerful technique for catalyst fabrication.

SUMMARY

The work here ventured into the field of chemically functional 3D printing. The aim was to see whether or not the SLS 3D printing could be utilized for this purpose. Especially, the interest was in the development of a new metal separation technique by utilizing SLS 3D printing. The requirements for the new method were customizability, efficiency, and ease-of-use as well as the ability to compete with existing methods in these categories.

The first project included the SLS 3D printing of the highly selective, tetrachloroaurate scavenging filters. This was achieved by the utilization of the high selectivity of PA12 towards tetrachloroaurate under acidic conditions. The SLS 3D printed PA12 filters were successfully utilized in the separation of gold from an extremely challenging matrix, the PCB leachate. The filters were able to selectively scavenge gold and therefore, provided the first proof-of-concept-level results for the chemically functional SLS 3D printing project.

Next, the customizability of the printing material was investigated. Previously, the use of plain PA12 provided the functionality, but for more widespread use of the technique, the functionality of the material should be customizable. The rudimentary approach of simply mixing the functional additive into chemically inert PP powder was found to lead to objects possessing the chemical functionality of the additive. This was tested by incorporating an anion exchange resin, namely Dowex 21K, into the printing material and by utilizing the resulting PP-21K for successful separation of palladium and platinum from the PCB leachate. By combining the aforementioned PA12 filters with the PP-21K filters, the separation of the noble metals from the PCB leachate was achieved.

A different approach towards metal separation was also investigated. It included the conversion of the scavenged metal into functional nanocatalysts. Instead of further separating the metal into its own separate fraction, catalytically active objects could be fabricated with the SLS 3D printing method by using the PA12 filters for the adsorption of tetrachloroaurate, followed by the reduction of the gold into nanoparticles. These PA12-Au objects could be utilized as catalysts due to the catalytically active nature of the gold nanoparticles. This method represents the so-called "from waste to product" approach that could easily be incorporated with today's view of the circular economy, which is mostly focused just on the separation of different elements to different fractions.

The results here show that SLS 3D printing can be utilized for preparing chemically functional objects. The customizability of the chemical functionality of the objects is made easy as providing the functionality to the objects simply requires mixing the additive with desired properties into the building material. Additionally, the printing method itself places very minimal requirements on the additives. However, the customizability is not limited to just the chemical properties. The ability to design the shape, size, and geometry of the object is inherent to 3D printing. In addition to that, the SLS 3D printing also enables the possibility to adjust the physical properties, such as porosity, of the object by

altering the printing parameters. This gives the user the ability to customize both the chemical and physical properties of the object for the needs of the specific application.

All in all, the proof-of-concept results here demonstrate that SLS 3D printing has immense potential as a fabrication method for metal separation devices. Even though the work here focused on the treatment of PCB leachate, the customizability of the objects enables easy fabrication of tailor-made objects to match the chemical and physical requirements of a wide range of different applications.

REFERENCES

- 1 V. Jegatheesan, J. L. Liow, L. Shu, S. H. Kim, C. Visvanathan, *J. Clean. Prod.* 2009, **17**, 637.
- 2 R. M. Izatt, *Metal Sustainability: Global Challenges, Consequences, and Prospects*, John Wiley & Sons, 2016.
- 3 R. M. Izatt, S. R. Izatt, R. L. Bruening, N. E. Izatt, B. A. Moyer, *Chem. Soc. Rev.* 2014, **43**, 2451.
- 4 D. A. Singer, *Econ. Geol.* 1995, **90**, 88.
- 5 J. R. Dodson, A. J. Hunt, H. L. Parker, Y. Yang, J. H. Clark, *Chem. Eng. Process. Process Intensif.* 2012, **51**, 69.
- 6 A. Tuncuk, V. Stazi, A. Akcil, E. Y. Yazici, H. Deveci, *Miner. Eng.* 2012, **25**, 28.
- 7 F. L. Bernardis, R. A. Grant, D. C. Sherrington, *React. Funct. Polym.* 2005, **65**, 205.
- 8 A. Chagnes, G. Cote, C. Ekberg, M. Nilsson, T. Retegan, *WEEE Recycling: Research, Development, and Policies*, Elsevier, 2016.
- 9 J. Tang, M. Su, Q. Wu, L. Wei, N. Wang, E. Xiao, H. Zhang, Y. Wei, Y. Liu, C. Ekberg, B.-M. Steenari, T. Xiao, *J. Clean. Prod.* 2019, **234**, 139.
- 10 S. Dupin, O. Lame, C. Barrès, J.-Y. Charneau, *Eur. Polym. J.* 2012, **48**, 1611.
- 11 S. F. S. Shirazi, S. Gharekhani, M. Mehrali, H. Yarmand, H. S. C. Metselaar, N. Adib Kadri, N. A. A. Osman, *Sci. Technol. Adv. Mater.* 2015, **16**, 33502.
- 12 F. Fina, C. M. Madla, A. Goyanes, J. Zhang, S. Gaisford, A. W. Basit, *Int. J. Pharm.* 2018, **541**, 101.
- 13 T. Stichel, T. Frick, T. Laumer, F. Tenner, T. Hausotte, M. Merklein, M. Schmidt, *J. Mater. Process. Technol.* 2018, **252**, 537.
- 14 F. Fu, Q. Wang, *J. Environ. Manage.* 2011, **92**, 407.
- 15 Y. Ku, I.-L. Jung, *Water Res.* 2001, **35**, 135.
- 16 M. A. Barakat, *Arab. J. Chem.* 2011, **4**, 361.
- 17 J. G. Dean, F. L. Bosqui, K. H. Lanouette, *Environ. Sci. Technol.* 1972, **6**, 518.
- 18 C. I. C. Silvestre, J. L. M. Santos, J. L. F. C. Lima, E. A. G. Zagatto, *Anal. Chim. Acta* 2009, **652**, 54.
- 19 A. P. Lim, A. Z. Aris, *Rev. Environ. Sci. Bio/Technology* 2014, **13**, 163.
- 20 A. Dańbrowski, Z. Hubicki, P. Podkościelny, E. Robens, *Chemosphere* 2004, **56**, 91.
- 21 A. A. Zagorodni, *Ion Exchange Materials: Properties and Applications*, Elsevier, 2006.
- 22 K. Dorfner, *Ion Exchangers*, Walter De Gruyter, 2011.
- 23 K. W. Pepper, *J. Appl. Chem.* 1951, **1**, 124.
- 24 F. G. Helfferich, *Ion Exchange*, Courier Corporation, 1962.
- 25 C. E. Harland, *Ion Exchange: Theory and Practice*, Royal Society Of Chemistry, 1994.
- 26 S. E. Jørgensen, in *Math. Submodels Water Qual. Syst.* (Eds.: S.E. Jørgensen, M.J.B.T.-D. in E.M. Gromiec), Elsevier, 1989, pp. 65–81.

- 27 C. E. Harland, *Ion Exchange: Theory and Practice*, Royal Society Of Chemistry, 2007.
- 28 I. Ali, M. Asim, T. A. Khan, *J. Environ. Manage.* 2012, **113**, 170.
- 29 I. G. Lalov, I. I. Guerginov, M. A. Krysteva, K. Fartsov, *Water Res.* 2000, **34**, 1503.
- 30 I. Šafařík, *Water Res.* 1995, **29**, 101.
- 31 W. S. Wan Ngah, L. C. Teong, M. A. K. M. Hanafiah, *Carbohydr. Polym.* 2011, **83**, 1446.
- 32 M. Kumar, B. P. Tripathi, V. K. Shahi, *J. Hazard. Mater.* 2009, **172**, 1041.
- 33 M.-W. Wan, C.-C. Kan, B. D. Rogel, M. L. P. Dalida, *Carbohydr. Polym.* 2010, **80**, 891.
- 34 G. Zhang, R. Qu, C. Sun, C. Ji, H. Chen, C. Wang, Y. Niu, *J. Appl. Polym. Sci.* 2008, **110**, 2321.
- 35 V. Nair, A. Panigrahy, R. Vinu, *Chem. Eng. J.* 2014, **254**, 491.
- 36 G. Mckay, *Use of Adsorbents for the Removal of Pollutants from Wastewater*, CRC Press, 1995.
- 37 W. S. Wan Ngah, M. A. K. M. Hanafiah, *Bioresour. Technol.* 2008, **99**, 3935.
- 38 S. De Gisi, G. Lofrano, M. Grassi, M. Notarnicola, *Sustain. Mater. Technol.* 2016, **9**, 10.
- 39 G. Crini, *Prog. Polym. Sci.* 2005, **30**, 38.
- 40 D. Mohan, C. U. Pittman, *J. Hazard. Mater.* 2007, **142**, 1.
- 41 R. Zhang, T. Leiviskä, J. Tanskanen, B. Gao, Q. Yue, *Chem. Eng. J.* 2019, **361**, 680.
- 42 E. Abu-Danso, S. Peräniemi, T. Leiviskä, T. Kim, K. M. Tripathi, A. Bhatnagar, *J. Hazard. Mater.* 2020, **381**, 120871.
- 43 G. Blanchard, M. Maunaye, G. Martin, *Water Res.* 1984, **18**, 1501.
- 44 S. Babel, T. A. Kurniawan, *J. Hazard. Mater.* 2003, **97**, 219.
- 45 E. Da'na, *Microporous Mesoporous Mater.* 2017, **247**, 145.
- 46 S. Sen Gupta, K. G. Bhattacharyya, *Adv. Colloid Interface Sci.* 2011, **162**, 39.
- 47 K. S. Hui, C. Y. H. Chao, S. C. Kot, *J. Hazard. Mater.* 2005, **127**, 89.
- 48 M. Luqman, *Ion Exchange Technology I: Theory and Materials*, Springer Science & Business Media, 2012.
- 49 T. Xu, *J. Memb. Sci.* 2005, **263**, 1.
- 50 J. Ran, L. Wu, Y. He, Z. Yang, Y. Wang, C. Jiang, L. Ge, E. Bakangura, T. Xu, *J. Memb. Sci.* 2017, **522**, 267.
- 51 N. Guo, M. C. Leu, *Front. Mech. Eng.* 2013, **8**, 215.
- 52 D. Dimitrov, K. Schreve, N. de Beer, *Rapid Prototyp. J.* 2006, **12**, 136.
- 53 B. Berman, *Bus. Horiz.* 2012, **55**, 155.
- 54 X. Wang, M. Jiang, Z. Zhou, J. Gou, D. Hui, *Compos. Part B Eng.* 2017, **110**.
- 55 D. Chen, S. Heyer, S. Ibbotson, K. Salonitis, J. G. Steingrímsson, S. Thiede, *J. Clean. Prod.* 2015, **107**, 615.
- 56 J. W. Stansbury, M. J. Idacavage, *Dent. Mater.* 2016, **32**, 54.
- 57 A. Pirjan, D.-M. Petroşanu, *J. Inf. Syst. Oper. Manag.* 2013, **7**, 360.
- 58 P. Wu, J. Wang, X. Wang, *Autom. Constr.* 2016, **68**, 21.
- 59 I. Kothman, N. Faber, *J. Manuf. Technol. Manag.* 2016, **27**, 932.

- 60 R. A. Buswell, R. C. Soar, A. G. F. Gibb, A. Thorpe, *Autom. Constr.* 2007, **16**, 224.
- 61 F. Kotz, K. Arnold, W. Bauer, D. Schild, N. Keller, K. Sachsenheimer, T. M. Nargang, C. Richter, D. Helmer, B. E. Rapp, *Nature* 2017, **544**, 337.
- 62 S. C. Ligon, R. Liska, J. Stampfl, M. Gurr, R. Mülhaupt, *Chem. Rev.* 2017, **117**, 10212.
- 63 D. Xie, H. Zhang, X. Shu, J. Xiao, S. Cao, *Sci. China Technol. Sci.* 2010, **53**, 1605.
- 64 C. Ladd, J.-H. So, J. Muth, M. D. Dickey, *Adv. Mater.* 2013, **25**, 5081.
- 65 G. C. Anzalone, C. Zhang, B. Wijnen, P. G. Sanders, J. M. Pearce, *IEEE Access* 2013, **1**, 803.
- 66 L. E. Murr, E. Martinez, K. N. Amato, S. M. Gaytan, J. Hernandez, D. A. Ramirez, P. W. Shindo, F. Medina, R. B. Wicker, *J. Mater. Res. Technol.* 2012, **1**, 42.
- 67 N. G. Tanikella, B. Wittbrodt, J. M. Pearce, *Addit. Manuf.* 2017, **15**, 40.
- 68 P. Parandoush, D. Lin, *Compos. Struct.* 2017, **182**, 36.
- 69 K. Gnanasekaran, T. Heijmans, S. van Bennekom, H. Woldhuis, S. Wijnia, G. de With, H. Friedrich, *Appl. Mater. Today* 2017, **9**, 21.
- 70 R. Matsuzaki, M. Ueda, M. Namiki, T.-K. Jeong, H. Asahara, K. Horiguchi, T. Nakamura, A. Todoroki, Y. Hirano, *Sci. Rep.* 2016, **6**, 23058.
- 71 X. Wei, D. Li, W. Jiang, Z. Gu, X. Wang, Z. Zhang, Z. Sun, *Sci. Rep.* 2015, **5**, 11181.
- 72 S. J. Leigh, R. J. Bradley, C. P. Pursell, D. R. Billson, D. A. Hutchins, *PLoS One* 2012, **7**, e49365.
- 73 A. Goyanes, M. Kobayashi, R. Martínez-Pacheco, S. Gaisford, A. W. Basit, *Int. J. Pharm.* 2016, **514**, 290.
- 74 S. Waheed, J. M. Cabot, N. P. Macdonald, T. Lewis, R. M. Guijt, B. Paull, M. C. Breadmore, *Lab Chip* 2016, **16**, 1993.
- 75 J. R. C. Dizon, A. H. Espera, Q. Chen, R. C. Advincula, *Addit. Manuf.* 2018, **20**, 44.
- 76 Z. Muwaffak, A. Goyanes, V. Clark, A. W. Basit, S. T. Hilton, S. Gaisford, *Int. J. Pharm.* 2017, **527**, 161.
- 77 C. Parra-Cabrera, C. Achille, S. Kuhn, R. Ameloot, *Chem. Soc. Rev.* 2018, **47**, 209.
- 78 B. Gross, S. Y. Lockwood, D. M. Spence, *Anal. Chem.* 2017, **89**, 57.
- 79 J.-Y. Lee, J. An, C. K. Chua, *Appl. Mater. Today* 2017, **7**, 120.
- 80 C. L. Manzanares Palenzuela, M. Pumera, *TrAC Trends Anal. Chem.* 2018, **103**, 110.
- 81 C. R. Tubío, J. Azuaje, L. Escalante, A. Coelho, F. Guitián, E. Sotelo, A. Gil, *J. Catal.* 2016, **334**, 110.
- 82 A. S. Díaz-Marta, C. R. Tubío, C. Carbajales, C. Fernández, L. Escalante, E. Sotelo, F. Guitián, V. L. Barrio, A. Gil, A. Coelho, *ACS Catal.* 2018, **8**, 392.
- 83 J. Azuaje, C. R. Tubío, L. Escalante, M. Gómez, F. Guitián, A. Coelho, O. Caamaño, A. Gil, E. Sotelo, *Appl. Catal. A Gen.* 2017, **530**, 203.
- 84 P. J. Kitson, S. Glatzel, W. Chen, C.-G. Lin, Y.-F. Song, L. Cronin, *Nat. Protoc.*

- 2016, **11**, 920.
- 85 P. J. Kitson, M. D. Symes, V. Dragone, L. Cronin, *Chem. Sci.* 2013, **4**, 3099.
- 86 M. D. Symes, P. J. Kitson, J. Yan, C. J. Richmond, G. J. T. Cooper, R. W. Bowman, T. Vilbrandt, L. Cronin, *Nat. Chem.* 2012, **4**, 349.
- 87 P. J. Kitson, G. Marie, J.-P. Francoia, S. S. Zaleskiy, R. C. Sigerson, J. S. Mathieson, L. Cronin, *Science (80-.)*. 2018, **359**, 314.
- 88 U. Kalsoom, P. N. Nesterenko, B. Paull, *TrAC Trends Anal. Chem.* 2018, **105**, 492.
- 89 M. Belka, S. Ulenberg, T. Bączek, *Anal. Chem.* 2017, **89**, 4373.
- 90 M. Yan, X. Tian, G. Peng, Y. Cao, D. Li, *Mater. Des.* 2017, **135**, 62.
- 91 A. Ambrosi, M. Pumera, *Chem. Soc. Rev.* 2016, **45**, 2740.
- 92 K. Fu, Y. Yao, J. Dai, L. Hu, *Adv. Mater.* 2017, **29**, 1603486.
- 93 H. Watschke, K. Hilbig, T. Vietor, *Appl. Sci.* 2019, **9**.
- 94 K. Fu, Y. Wang, C. Yan, Y. Yao, Y. Chen, J. Dai, S. Lacey, Y. Wang, J. Wan, T. Li, Z. Wang, Y. Xu, L. Hu, *Adv. Mater.* 2016, **28**, 2587.
- 95 A. Maurel, M. Courty, B. Fleutot, H. Tortajada, K. Prashantha, M. Armand, S. Grugeon, S. Panier, L. Dupont, *Chem. Mater.* 2018, **30**, 7484.
- 96 K. Sun, T.-S. Wei, B. Y. Ahn, J. Y. Seo, S. J. Dillon, J. A. Lewis, *Adv. Mater.* 2013, **25**, 4539.
- 97 C. Zhu, T. Liu, F. Qian, T. Y.-J. Han, E. B. Duoss, J. D. Kuntz, C. M. Spadaccini, M. A. Worsley, Y. Li, *Nano Lett.* 2016, **16**, 3448.
- 98 E. García-Tuñón, S. Barg, J. Franco, R. Bell, S. Eslava, E. D'Elia, R. C. Maher, F. Guitian, E. Saiz, *Adv. Mater.* 2015, **27**, 1688.
- 99 F. P. W. Melchels, J. Feijen, D. W. Grijpma, *Biomaterials* 2010, **31**, 6121.
- 100 J. Z. Manapat, Q. Chen, P. Ye, R. C. Advincula, *Macromol. Mater. Eng.* 2017, **302**, 1600553.
- 101 G. Comina, A. Suska, D. Filippini, *Angew. Chemie Int. Ed.* 2015, **54**, 8708.
- 102 J. S. Mohammed, *Methods Oceanogr.* 2016, **17**, 97.
- 103 B. C. Gross, J. L. Erkal, S. Y. Lockwood, C. Chen, D. M. Spence, *Anal. Chem.* 2014, **86**, 3240.
- 104 F. Wang, Y. Chong, F. Wang, C. He, *J. Appl. Polym. Sci.* 2017, **134**, 44988.
- 105 E. Kukkonen, E. Lahtinen, P. Myllyperkiö, J. Konu, M. Haukka, *ACS Omega* 2018, **3**, 11558.
- 106 M. T. W. Hearn, *Curr. Opin. Chem. Eng.* 2017, **18**, 90.
- 107 C.-K. Su, P.-J. Peng, Y.-C. Sun, *Anal. Chem.* 2015, **87**, 6945.
- 108 C. Calderilla, F. Maya, V. Cerdà, L. O. Leal, *Talanta* 2017, **175**, 463.
- 109 C. Calderilla, F. Maya, V. Cerdà, L. O. Leal, *Talanta* 2018, **184**, 15.
- 110 Q. Ge, A. H. Sakhaei, H. Lee, C. K. Dunn, N. X. Fang, M. L. Dunn, *Sci. Rep.* 2016, **6**, 31110.
- 111 K. H. Tan, C. K. Chua, K. F. Leong, C. M. Cheah, P. Cheang, M. S. Abu Bakar, S. W. Cha, *Biomaterials* 2003, **24**, 3115.
- 112 F. L. Amorim, A. Lohrengel, V. Neubert, C. F. Higa, T. Czelusniak, *Rapid Prototyp. J.* 2014, **20**, 59.
- 113 G. V Salmoria, P. Klauss, R. A. Paggi, L. A. Kanis, A. Lago, *Polym. Test.* 2009, **28**, 648.

- 114 K. C. R. Kolan, M. C. Leu, G. E. Hilmas, M. Velez, *J. Mech. Behav. Biomed. Mater.* 2012, **13**, 14.
- 115 M. M. Savalani, L. Hao, P. M. Dickens, Y. Zhang, K. E. Tanner, R. A. Harris, *Rapid Prototyp. J.* 2012, **18**, 16.
- 116 E. Lahtinen, M. M. Hänninen, K. Kinnunen, H. M. Tuononen, A. Väisänen, K. Rissanen, M. Haukka, *Adv. Sustain. Syst.* 2018, **2**, 1800048.
- 117 W. Jamróz, J. Szafraniec, M. Kurek, R. Jachowicz, *Pharm. Res.* 2018, **35**, 176.
- 118 A. J. Capel, S. Edmondson, S. D. R. Christie, R. D. Goodridge, R. J. Bibb, M. Thurstans, *Lab Chip* 2013, **13**, 4583.
- 119 H. N. Chia, B. M. Wu, *J. Biol. Eng.* 2015, **9**, 4.
- 120 E. Lahtinen, E. Kukkonen, J. Jokivartio, J. Parkkonen, J. Virkajärvi, L. Kivijärvi, M. Ahlskog, M. Haukka, *ACS Appl. Energy Mater.* 2019.
- 121 E. Lahtinen, R. L. M. Precker, M. Lahtinen, E. Hey-Hawkins, M. Haukka, *Chempluschem* 2019, **84**, 222.
- 122 E. Lahtinen, L. Turunen, M. M. Hänninen, K. Kolari, H. M. Tuononen, M. Haukka, *ACS Omega* 2019, **4**, 12012.
- 123 X. Liu, H. Xu, H. Xia, D. Wang, *Langmuir* 2012, **28**, 13720.



ORIGINAL PAPERS

I

SELECTIVE RECOVERY OF GOLD FROM ELECTRONIC WASTE USING 3D-PRINTED SCAVENGER

by

Elmeri Lahtinen, Lauri Kivijärvi, Rajendhraprasad Tatikonda, Ari Väisänen,
Kari Rissanen and Matti Haukka

ACS Omega, 2017, 2, 10, 7299-7304.

Reproduced with kind permission from American Chemical Society.



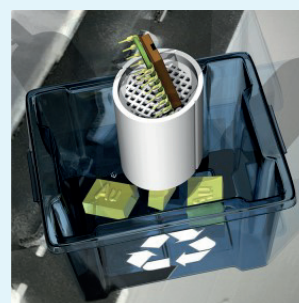
Selective Recovery of Gold from Electronic Waste Using 3D-Printed Scavenger

Elmeri Lahtinen,[†] Lauri Kivijärvi,[†] Rajendhrasrad Tatikonda,[†] Ari Väisänen,^{*,†} Kari Rissanen,^{*,†} and Matti Haukka^{*,†}

[†]Department of Chemistry and [‡]Nanoscience Center, University of Jyväskylä, P.O. Box 35, FI-40014 Jyväskylä, Finland

S Supporting Information

ABSTRACT: Around 10% of the worldwide annual production of gold is used for manufacturing of electronic devices. According to the European Commission, waste electric and electronic equipment is the fastest growing waste stream in the European Union. This has generated the need for an effective method to recover gold from electronic waste. Here, we report a simple, effective, and highly selective nylon-12-based three-dimensional (3D)-printed scavenger objects for gold recovery directly from an aqua regia extract of a printed circuit board waste. Using the easy to handle and reusable 3D-printed meshes or columns, gold can be selectively captured both in a batch and continuous flow processes by dipping the scavenger into the solution or passing the gold-containing solution through the column. The possibility to optimize the shape, size, and flow properties of scavenger objects with 3D printing enables the gold scavengers to match the requirements of any processing plants.



INTRODUCTION

The development of three-dimensional (3D) printing techniques and printing materials has been booming over the past decades.¹ Materials from resins to metals can nowadays be printed to produce complex objects with precise dimensions and desired mechanical properties. The focus of interest is slowly expanding toward 3D-printed objects that possess additional physical or chemical functionalities. Currently, the 3D printing technique has been utilized for antimicrobial composites² and ion-exchange membranes,^{3,4} as well as for pH-sensitive and catalytically active materials.^{5–7} Even polymer-bonded rare-earth metal magnets⁸ and quantum dot light-emitting diodes have been successfully printed.⁹ Despite the progress in the field of functional 3D objects, the true potential of the technique has not been fully exploited, e.g., in chemistry. The use of 3D printing techniques in production of continuous flow reactors, chromatographic, or ion-exchange columns using an active material would open up a completely new level of control, e.g., of the reagent flow. If the conventional columns filled with active powder or beads are replaced with a column in which the adsorbent is also printed, practical pitfalls, such as unfavorable adsorbent packing and uneven eluent flow through the column, could be completely avoided. In the current work, we have used this approach in hydrometallurgy of electronic waste to prepare an efficient, selective, and simple collector for capturing gold from a complex mixture of dissolved metal ions.

Gold is widely used in the electronic industry, and with the waste electric and electronic equipment (WEEE) stream generated in the European Union predicted to be over 12 million tons by 2020,¹⁰ an effective recovery method for gold is needed. Currently, used gold recovery methods include physical, pyrometallurgical, or hydrometallurgical treatments,

or their combinations.^{11–14} However, most of these methods suffer from environmental risks and from the need for extensive preprocessing of the material.^{15–17} Hydrometallurgical processes have proven to be successful for leaching^{13,18,19} of gold from WEEE, but the recovery of gold from solution is often laborious, containing several steps.^{12,20,21} After the leaching, ion-exchange resins are often being used as an adsorbent for the gold, as has been widely reported.^{18,22–26} There have also been reports of polymers, such as polypyrrole and polyaniline, being used to recover gold.^{27–29} Because of lack of selectivity of the adsorbents and various other recovery methods, extensive preprocessing of the sample is often required.^{17,30} Typical scavenger materials used to adsorb the dissolved gold consist of small particles and hence a filtration system is often required, either to recover the used adsorbent or to purify the solution stream of remaining particles. The above difficulties make recycling the adsorbent challenging or even impossible.

These problems can be avoided by using 3D printing.³¹ The scavenger material is printed in a form of a column or a mesh, and the ion-containing solution is either flowed through it or the object is simply dipped into the solution. The captured metal ions can then be recovered by elution with a suitable solution, after which the scavenger is reusable for metal capturing. We used inexpensive 50 μm nylon-12 (N12) powder for printing scavengers and tested these scavengers to selectively adsorb gold from aqua regia solutions containing up to 500 times higher concentrations of other metal ions. The binding of gold as $[\text{AuCl}_4]^-$ on nylon has been previously

Received: August 20, 2017

Accepted: October 17, 2017

Published: October 27, 2017

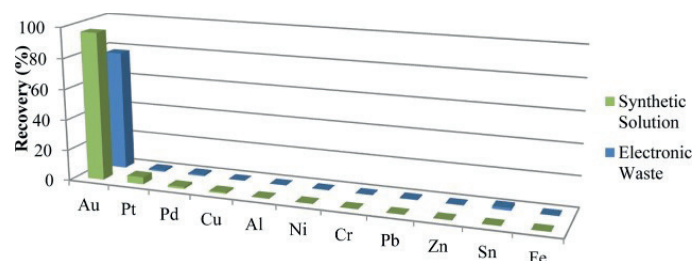


Figure 1. Recovery percentages of the metals by nylon-12 powder from the synthetic 5% HCl test solution (green) and from a 1:1 diluted aqua regia leached true electronic waste sample (blue). As can be seen, nylon-12 retains its efficiency and selectivity even in harsh oxidizing conditions.

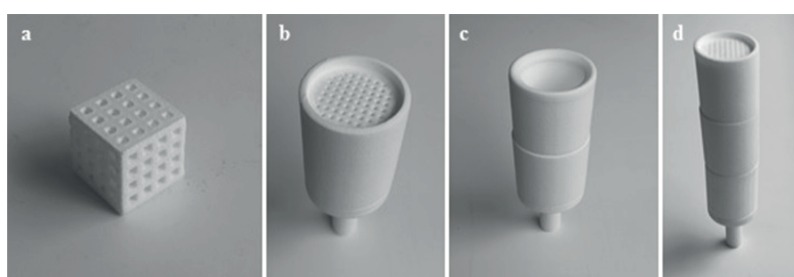


Figure 2. (a) Three-dimensionally printed cube-shaped mesh with dimensions of 18 mm x 18 mm x 18 mm used for batch tests. (b) Structure of the scavenger unit (length 35 mm and diameter 27 mm) with a flow restricting funnel used for continuous flow processes (c). The complete column consists of three interlocking parts: the funnel at the bottom, the main gold scavenging unit in the middle and the reservoir cylinder at the top used for loading the sample (c). (d) An extended column with three scavenging units and the funnel.

noted,³² but to our knowledge, the excellent selectivity of nylon toward gold has not been reported. The binding mechanism between the amide group and $[\text{AuCl}_4]^-$ has been predicted to be related to hydrogen bonding between the hydrogen of the protonated amide group and the chlorides of the gold complex.³³ The cause for selectivity toward gold could potentially be because of -1 charge of the complex and square planar geometry of the $[\text{AuCl}_4]^-$. The only other species possessing square planar geometries in the solution would be chloride complexes of Pt(II) and Pd(II). These, however, would have a charge of -2 . The selectivity of the material will be investigated further in future by using molecular modeling.

RESULTS AND DISCUSSION

To find out the impact of 3D printing by the selective laser sintering (SLS) technique on the properties of nylon-12, we first tested the gold-capturing efficiency of the powder. The selectivity was tested using a solution mimicking the high concentrations of other metals typically present in acid-leached electronic waste (100 ppm of Ni, Zn, Fe, and Cu and 50 ppm of Al, Cr, Pb, and Sn along with 5 ppm of Pd, Pt, and Au in 5% hydrochloric acid). The 10 mL samples were treated with 50 mg of N12 powder, and the slurry was stirred at room temperature for 4 h after which the powder was filtered off. The PerkinElmer inductively coupled plasma optical emission spectrometry (ICP-OES) Optima 8300 DV was used to determine the metal-ion concentrations in solution before and after the adsorption experiments. All in all, 96.4% of gold was adsorbed by the N12 powder together with 4.6% of the platinum, whereas noticeable adsorption of any of the other metals was not observed (Figure 1, green columns). To compare adsorption properties of different nylon polymers,

nylon-11 (N11) and one of the most commonly used commercial grade of nylon, nylon-6,6 (N66), were also tested under the same conditions as that of N12. The N11 behaves much like N12, showing comparable selectivity with N12, but N66 was found to be less selective, adsorbing 25.6% of platinum and 13.8% of palladium along with 93.6% of the gold (Table S1). As nylon polymers are extensively used by the clothing industry, the typical fabric used, for example, for sport socks (82% of nylon, 16% of polypropylene, and 2% of elastane), was also tested and found to have similar properties as those of the N66 powder (Table S1). The comparisons indicate clearly that the highest selectivity can be achieved by using longer carbon chain nylon polymers N12 and N11.

To test the N12 powder with real electronic waste, a sample of aqua regia leached printed circuit boards (PCBs) was used. The PCB sample used contained 25 000 mg L^{-1} copper, 2700 mg L^{-1} iron, 1700 mg L^{-1} zinc, 1600 mg L^{-1} nickel, and 850 mg L^{-1} tin, along with high concentrations of other metal ions. The gold concentration in PCB was 73 mg L^{-1} . PCB leachate also contains silver, but the presence of chloride in the leaching solution accompanied by dilution leads to precipitation of silver chloride. Therefore, changes in silver concentration were not monitored. Silver precipitate can be simply filtered off before using a nylon scavenger. In N12 powder adsorption experiments, the PCB samples were diluted in a 1:1 ratio with ultrapure water and then stirred with 50 mg of N12 for 4 h. From the PCB sample, 77.8% of the gold was adsorbed, whereas tin (1.6%) was the only other metal-ion adsorbed (Figure 1, blue columns), showing the excellent selectivity of N12 toward gold. The maximum gold-adsorbing capacity of the N12 powder was tested by mixing 25 mg of N12 with 10 mL of a solution containing 200 ppm of $[\text{AuCl}_4]^-$ in 5% hydrochloric

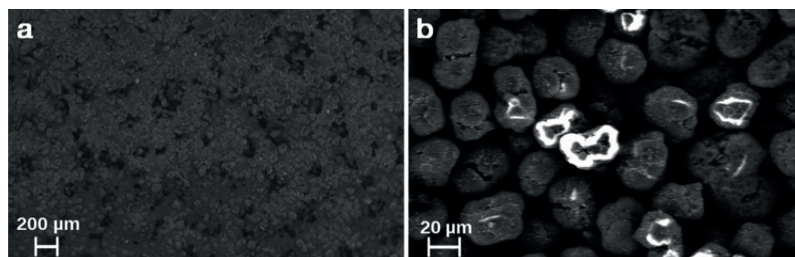


Figure 3. Scanning electron microscopy (SEM) images of the surface of solid objects printed with low laser power.

acid for 24 h. A capacity higher than 66 mg of gold per 1 g of N12 powder was observed.

The actual 3D-printed scavengers were prepared by using N12 powder and a selective laser sintering (SLS) 3D printing technique. Both cube-shaped meshes for batch processes and column-shaped scavengers for continuous flow processes were printed (Figure 2). The selectivity and recovery capability of the 3D-printed mesh (Figure 2a) in a batch process were tested using the same test solution as that for the N12 powder. Soaking the mesh into the test solution for 4 h yielded gold recovery of 90.4% with no noticeable amounts of other metals adsorbed into the mesh.

The continuous flow behavior of the short 3D-printed column shown in Figure 2b (35 mm long scavenger part with 27 mm diameter) was tested by passing the test solution through the column. With the tested short column, the flow rate was ca. 3 mL s^{-1} . The high flow rate leads to overall contact times of ca. 3–5 s with a 10 mL sample. Even with this very short contact time, the tested scavenger adsorbed 27.2% of gold with only traces of other metals. With a column consisting of three scavenger units (total length 105 mm) 47.8% and with a column of 10 scavenger units (total length 350 mm), 82.7% of gold was captured. Even in the last case, the contact time remained very short (30s). The results can be even further improved by adjusting the flow rate through to the column. This can be done either by restricting the flow rate by using a valve or by redesigning and optimizing the flow channels in the scavenger units. The total recovery percentage can also be increased by recycling the solution through the column.

The capacity of the 3D-printed objects depends on the structure of the object and the printing parameters used. Because the specific surface area and capacity is dependent on the shape, size, and the design of the flow channels, it is difficult to give a simple figure for the capacity of the printed scavenger. Therefore, we tested the capacity of small solid rectangular printed plates with no elaborated pore structure to get a limiting value for the capacity. The capacity of these solid objects ranged from 13 to 18 mg per 1 g of the 3D-printed object. However, the surface area and thereof capacity of the 3D-printed object can be improved considerably by careful design of the surface structure.

One of the advantages of the scavenger objects is that gold can be nearly quantitatively removed from them by a simple elution process. Elution can be carried out by using nitric acid as eluent if acidic conditions are preferred (see the Methods section). Effective elution can also be obtained by using organic eluents such as diethylene glycol dibutyl ether. In both cases, the 3D-printed scavenger is fully reusable after gold has been removed.

The results show that 3D printing retains the excellent gold recovering properties of nylon-12. Obviously, 3D printing reduces the surface area of the object compared to the same amount of powder. However, the surface structure of the printed objects can be controlled up to a point by adjusting the 3D printing conditions: low laser power will produce an object with higher porosity and larger surface area (Figure 3). High laser power will increase the durability of the object but reduce the surface area, as the sintering of the material is more extensive (Figure S1).

The main advantage of the use of 3D-printed scavengers is that the gold can be separated directly from the diluted leachate with no tedious preprocessing steps. Scavengers can be easily scaled (Figure S2c) and modified accordingly to meet the users' requirements even up to the industrial scale. It is expected that by using other printable polymers with other functional groups or hybrid materials, other metals can also be captured by using 3D-printed scavengers. In such a case, scavenger modules with different selectivity could be linked together to obtain multimetal scavengers with detachable ion-specific modules. Because the 3D-printed scavengers are highly selective, they can be used for recovering gold from leachates originating from sources other than electronic waste as well. In general, the use of chemically functional printing materials can extend considerably the use of 3D printing in manufacturing of chemically active devices.

METHODS

Chemicals and Solvents. Synthetic solutions were prepared from stock spectroscopy standard solutions (1000 ppm) purchased from PerkinElmer. Nylon-12 was purchased from EOS and Advanc3d Materials and was in the form of powder, with an average particle diameter of $50 \mu\text{m}$. Nylon-11 powder having an average particle diameter of $50 \mu\text{m}$ was purchased from Advanc3d Materials. Nylon-6,6 was purchased from Sigma-Aldrich and had an average particle diameter of $15\text{--}20 \mu\text{m}$. Nitric acid ($\geq 65\%$) and hydrochloric acid ($\geq 37\%$) were purchased from Sigma-Aldrich. All of the chemicals were used as received. High-purity water of $18.2 \text{ M}\Omega \text{ cm}$ resistivity produced by a Purelab Ultra water purification system supplied by Elga (Buckinghamshire, U.K.) was used in all experiments. No unexpected or unusually high safety hazards were encountered.

Sample Preparation. The sample solution for the synthetic tests was prepared by diluting the 1000 ppm PerkinElmer spectroscopy standards. The solution prepared contained 100 ppm of Ni, Zn, Fe, and Cu and 50 ppm of Al, Cr, Pb, and Sn along with 5 ppm of Pd, Pt, and Au in 5% hydrochloric acid. The electronic waste sample was prepared by

milling printed circuit boards (PCBs) down to fine particles and ashing them for 4 h at the temperature of 950 °C. One gram of the ashed sample was placed in a 50 mL centrifuge tube along with 10 mL of aqua regia. Ultrasound-assisted leaching was performed at room temperature using six cycles lasting 3 min each. Between the cycles, the pressure was released from the reaction containers. The ultrasound water bath used was Elma Elmasonic P. Leached samples were filtered (Whatman 41) and diluted in a 1:1 ratio with ultrapure water.

Recovery from Synthetic Solution. A 10 mL sample of the synthetic solution was placed in a 15 mL centrifuge tube. Fifty milligrams of nylon-12 powder was added into the tube. The tube was sealed and then stirred using Stuart SF1 at 500 osc min⁻¹ for 4 h at room temperature. Nylon-12 was removed from the sample solution by filtration (Whatman 41). The same procedure was used for testing nylon-11 (N11), nylon-6,6 (N66), and the fabric samples. All of the tests discussed in this article were performed in triplicate. Recovery percentages of the metals with significant decrease in concentration are presented in Table S1.

Recovery from Synthetic Solution Using Acid-Washed N12 Powder. A 1 g sample of the N12 powder was placed in a glass column and 200 mL of 10% aqua regia, followed by 200 mL of water being passed through it. The N12 powder was dried at 105 °C for 4 h and was then used for adsorption tests. Ten milliliters of the synthetic solution was placed in a 15 mL centrifuge tube. Washed and dried N12 powder (50 mg) was added into the tube. The tube was sealed and then agitated using Stuart SF1 at 500 osc min⁻¹ for 4 h at room temperature. Nylon-12 was removed from the sample solution by filtration (Whatman 41). Recovery percentages of the metals with significant decrease in concentrations are presented in Table S1.

Recovery from Leached Electronic Waste. Leached electronic waste samples were diluted with ultrapure water in a ratio of 1:1 before gold recovery was performed. The recovery process was conducted by adding 50 mg of the N12 powder into the centrifuge tube containing 10 mL of the solution. The container was sealed, and the sample was agitated for 4 h using Stuart SF1 at 500 osc min⁻¹ at room temperature. Samples were filtered (Whatman 41) to remove the nylon-12.

Capacity of the Material. Solution containing 200 ppm of [AuCl₄]⁻ in 5% hydrochloric acid was prepared by diluting the PerkinElmer spectroscopy standard of gold (1000 ppm). Ten milliliters of the solution was placed in a 15 mL centrifuge tube, and 25 mg of nylon-12 was added. The tube was sealed and agitated using Stuart SF1 at 500 osc min⁻¹ for 24 h at room temperature. Samples were filtered (Whatman 41) to remove the nylon-12. A similar test was performed for small, 3D-printed, rectangle-shaped solid objects having average mass of 8 mg. Additionally, the capacity of slightly larger 3D-printed objects, with an average mass of 131 mg, was tested by reacting the objects with 50 mL of the synthetic solution used to test the capacity of the nylon-12 powder.

Recovery from Synthetic Solution Using 3D-Printed Mesh. The test conducted using 3D-printed mesh cube was done by contacting the synthetic solution containing 100 ppm of Ni, Zn, Fe, and Cu and 50 ppm of Al, Cr, Pb, and Sn along with 5 ppm of Pd, Pt, and Au in 5% hydrochloric acid with the object. Twenty milliliters of the synthetic solution was placed in a 50 mL centrifuge tube containing the mesh. The tube was sealed and agitated using Stuart SF1 at 500 osc min⁻¹ for 4 h at

room temperature. Recovery percentages of the metals that had significant decrease in concentration are presented in Table S2.

Recovery from Synthetic Solution Using 3D-Printed Column. The test conducted using 3D-printed columns was done by letting synthetic solution containing 100 ppm of Ni, Zn, Fe, and Cu and 50 ppm of Al, Cr, Pb, and Sn along with 5 ppm of Pd, Pt, and Au in 5% hydrochloric acid flow through the column. A 10 mL sample size was used for the tests. The length of the column was varied. In initial tests, a column containing one functional middle piece with the length of 35 mm and the diameter of 27 mm was used. To further improve the recovery, following tests were done utilizing a column with three functional middle pieces attached and a total length of 105 mm (Figure S2a). Additionally, a column with 10 functional middle pieces and total length of 350 mm was tested (Figure S2b). For the 350 mm long column, a sample size of 20 mL was used. The size of the column can be easily scaled, as illustrated in Figure S2c. Recovery percentages of the metals that had significant decrease in concentration are presented in Table S2.

Removal of Gold from Scavenger Objects. Gold removal tests were conducted using a 3D-printed column consisting of three functional units (Figure S2a). First, the column was loaded by letting 10 mL of 5% hydrochloric acid solution, containing 10 ppm of Au, run through the column. This loading solution was prepared by diluting the 1000 ppm PerkinElmer spectroscopy standard of gold. About 30% nitric acid (prepared by diluting nitric acid so that the concentration of the removal eluent was 45% of the concentration of concentrated nitric acid) was then used as the gold removal eluent. The removal eluent was let to flow through the collector column in 15 mL pulses. The first 15 mL pulse recovered 47.9% of the adsorbed gold. By using four 15 mL pulses, 99% of the adsorbed gold was recovered. To confirm the ability to use organic eluents, a similar elution test was carried out by using diethylene glycol dibutyl ether as the removal eluent. With one 15 mL pulse, about 15% of gold was recovered. By repeating the pulses, the recovery percentage could be improved, as in the case of nitric acid eluent.

Three-dimensional Printing. Designing of the 3D-printed objects was done using FreeCAD v0.16. Designed objects were prepared for the printer using Slic3r v1.2.9. Images of the designed pieces are presented in Figures S3–S6. Three-dimensional printing was done by using ShareBot SnowWhite SLS 3D printer. Nylon-12 was used as printing powder. A layer thickness of 0.1 mm was used for printing the objects. The laser power used was 50–55%, with a rate of 64 000 (2560 mm s⁻¹). The build plate temperature was set to 173 °C and was changed to 161 °C at an object height of 0.5 mm. The environment temperature was set to 144 °C. Five warming layers were used for the print, and the wait time between each layer was set to 12 s.

Objects were cleared thoroughly of any unsintered powder remaining on the surfaces before being taken for adsorption tests. The column used for the tests consisted of several pieces that could be linked together to form the actual column.

ICP-OES Measurements. Measurements were done with PerkinElmer ICP-OES Optima 8300 DV using a GemCone low flow nebulizer and a cyclonic spray chamber. For all measurements, argon gas flow of 8 L min⁻¹, nebulizer gas flow of 0.6 L min⁻¹, auxiliary gas flow of 0.2 L min⁻¹, and a sample flow rate of 1.5 L min⁻¹ was used. The radio frequency power used for all of the measurements was 1500 W. Method detection limits (MDLs) were established using the United

States Environmental Protection Agency method 200.7.³⁴ The metals analyzed, MDLs, chosen wavelengths, calibration ranges, and *R* values for methods used for synthetic solution and for leached electronic waste are presented in Tables S3 and S4.

Concentrations of the metals present in the solutions were measured before and after the recovery process. Metal recovery rates were calculated from the change in concentration

$$\text{recovery (\%)} = \frac{c_i - c}{c_i} \times 100 \quad (1)$$

where c_i is the concentration of the analyte before the gold recovery process and c is the concentration of the analyte after the recovery.

SEM. Scanning electron microscope measurements were done using Zeiss EVO-50XVP. Three-dimensionally printed objects were cleared thoroughly of any unsintered powder before the SEM measurements. Figure S1 shows the surface of a 3D-printed object that was manufactured using high laser power.

Statistical Analysis. Results were statistically analyzed on a confidence interval of 95%. The analysis was done as follows

$$t = \frac{|\bar{x} - \mu|}{s/\sqrt{n}} \quad (2)$$

where \bar{x} is the average of the analyte concentration after the recovery process. μ is the average of the analyte concentration before the recovery process. s is the standard deviation of the analyte concentration after the recovery process and n is the number of replicates. The number of replicates used for all experiments was three. The hypothesis of the *t*-tests was that whether the concentrations after the recovery process resulted in significantly lower concentrations than those of the original sample; thus, the one tailed *t*-test was performed.

■ ASSOCIATED CONTENT

Supporting Information

The Supporting Information is available free of charge on the ACS Publications website at DOI: 10.1021/acsomega.7b01215.

Metal recovery percentages; ICP-OES measurement parameters; SEM figure; figures of the scavenger columns; figures of the designed columns (PDF)

■ AUTHOR INFORMATION

Corresponding Authors

*E-mail: ari.o.vaisanen@jyu.fi (A.V.).

*E-mail: kari.t.rissanen@jyu.fi (K.R.).

*E-mail: matti.o.haukka@jyu.fi (M.H.).

ORCID

Rajendhrasasad Tatikonda: 0000-0003-1277-3492

Kari Rissanen: 0000-0002-7282-8419

Matti Haukka: 0000-0002-6744-7208

Author Contributions

M.H., A.V., and K.R. conceptualized the use of scavenging materials, the design, and 3D printing of the reported scavengers, and supervised the characterization work. E.L. carried out the adsorption tests and metal-ion analytics; E.L. and L.K. prepared the 3D models of the scavenger and performed the 3D printing. R.T. did the SEM measurements. E.L., L.K., A.V., K.R., and M.H. wrote the manuscript.

Notes

The authors declare no competing financial interest.

■ ACKNOWLEDGMENTS

The research reported in this publication was solely performed at the Department of Chemistry, University of Jyväskylä, Finland, and was supported by the funding from Centennial Foundation of Technology Industries of Finland and Jane and Aatos Erkkö foundation as a part of The Future Makers program. The research was also supported by the Academy of Finland (grant nos: 295581 (M.H.), 263256, 265328, and 292746 (K.R.)) and the University of Jyväskylä.

■ REFERENCES

- (1) Gross, B. C.; Erkal, J. L.; Lockwood, S. Y.; Chen, C.; Spence, D. M. Evaluation of 3D Printing and Its Potential Impact on Biotechnology and the Chemical Sciences. *Anal. Chem.* **2014**, *86*, 3240–3253.
- (2) Yue, J.; Zhao, P.; Gerasimov, J. Y.; van de Lagemaat, M.; Grotenhuis, A.; Rustema-Abbing, M.; van der Mei, H. C.; Busscher, H. J.; Herrmann, A.; Ren, Y. 3D-Printable Antimicrobial Composite Resins. *Adv. Funct. Mater.* **2015**, *25*, 6756–6767.
- (3) Seo, J.; Kushner, D. I.; Hickner, M. A. 3D Printing of Micropatterned Anion Exchange Membranes. *ACS Appl. Mater. Interfaces* **2016**, *8*, 16656–16663.
- (4) Philamore, H.; Rossiter, J.; Walters, P.; Winfield, J.; Ieropoulos, I. Cast and 3D Printed Ion Exchange Membranes for Monolithic Microbial Fuel Cell Fabrication. *J. Power Sources* **2015**, *289*, 91–99.
- (5) Nadgorny, M.; Xiao, Z.; Chen, C.; Connal, L. A. Three-Dimensional Printing of pH-Responsive and Functional Polymers on an Affordable Desktop Printer. *ACS Appl. Mater. Interfaces* **2016**, *8*, 28946–28954.
- (6) Coupland, D. R. Catalyst Manufacturing Method. U.S. Patent 9,278,338 B2, March 8, 2016.
- (7) Tubío, C. R.; Azuaje, J.; Escalante, L.; Coelho, A.; Guitián, F.; Sotelo, E.; Gil, A. 3D Printing of a Heterogeneous Copper-Based Catalyst. *J. Catal.* **2016**, *334*, 110–115.
- (8) Huber, C.; Abert, C.; Bruckner, F.; Groenefeld, M.; Muthsam, O.; Schuschnigg, S.; Sirak, K.; Thanhoffer, R.; Teliban, I.; Vogler, C.; Windl, R.; Suess, D. 3D Print of Polymer Bonded Rare-Earth Magnets, and 3D Magnetic Field Scanning with an End-User 3D Printer. *Appl. Phys. Lett.* **2016**, *109*, No. 162401.
- (9) Kong, Y. L.; Tamargo, I. A.; Kim, H.; Johnson, B. N.; Gupta, M. K.; Koh, T.-W.; Chin, H.-A.; Steingart, D. A.; Rand, B. P.; McAlpine, M. C. 3D Printed Quantum Dot Light-Emitting Diodes. *Nano Lett.* **2014**, *14*, 7017–7023.
- (10) Waste Electrical & Electronic Equipment (WEEE), 2017. http://ec.europa.eu/environment/waste/weee/index_en.htm (accessed July 18, 2017).
- (11) Kaya, M. Recovery of Metals and Nonmetals from Electronic Waste by Physical and Chemical Recycling Processes. *Waste Manage.* **2016**, *57*, 64–90.
- (12) Akcil, A.; Erust, C.; Gahan, C. S.; Ozgun, M.; Sahin, M.; Tuncuk, A. Precious Metal Recovery from Waste Printed Circuit Boards Using Cyanide and Non-Cyanide Lixiviants—A Review. *Waste Manage.* **2015**, *45*, 258–271.
- (13) Jadhav, U.; Hocheng, H. Hydrometallurgical Recovery of Metals from Large Printed Circuit Board Pieces. *Sci. Rep.* **2015**, *5*, No. 14574.
- (14) Cayumil, R.; Khanna, R.; Rajarao, R.; Mukherjee, P. S.; Sahajwalla, V. Concentration of Precious Metals during Their Recovery from Electronic Waste. *Waste Manage.* **2016**, *57*, 121–130.
- (15) Donato, D. B.; Nichols, O.; Possingham, H.; Moore, M.; Ricci, P. F.; Noller, B. N. A Critical Review of the Effects of Gold Cyanide-Bearing Tailings Solutions on Wildlife. *Environ. Int.* **2007**, *33*, 974–984.
- (16) Hilson, G.; Monhemius, A. J. Alternatives to Cyanide in the Gold Mining Industry: What Prospects for the Future? *J. Cleaner Prod.* **2006**, *14*, 1158–1167.
- (17) Alguacil, F. J.; Adeva, P.; Alonso, M. Processing of Residual Gold(III) Solutions via Ion Exchange. *Gold Bull.* **2005**, *38*, 9–13.

- (18) Kim, E.-y.; Kim, M.-s.; Lee, J.-c.; Pandey, B. D. Selective Recovery of Gold from Waste Mobile Phone PCBs by Hydro-metallurgical Process. *J. Hazard. Mater.* **2011**, *198*, 206–215.
- (19) Yue, C.; Sun, H.; Liu, W.-J.; Guan, B.; Deng, X.; Zhang, X.; Yang, P. Environmentally Benign, Rapid, and Selective Extraction of Gold from Ores and Waste Electronic Materials. *Angew. Chem., Int. Ed.* **2017**, *56*, 9331–9335.
- (20) Cui, J.; Zhang, L. Metallurgical Recovery of Metals from Electronic Waste: A Review. *J. Hazard. Mater.* **2008**, *158*, 228–256.
- (21) Tuncuk, A.; Stazi, V.; Akcil, A.; Yazici, E. Y.; Deveci, H. Aqueous Metal Recovery Techniques from E-Scrap: Hydrometallurgy in Recycling. *Miner. Eng.* **2012**, *25*, 28–37.
- (22) Trochimczuk, A. W. Uptake of Gold from Hydrochloric Acid Solutions by Polymeric Resins Bearing Various Phosphorus Containing Ligands. *Sep. Sci. Technol.* **2002**, *37*, 3201–3210.
- (23) Fujiwara, K.; Ramesh, A.; Maki, T.; Hasegawa, H.; Ueda, K. Adsorption of Platinum(IV), Palladium(II) and Gold(III) from Aqueous Solutions onto L-Lysine Modified Crosslinked Chitosan Resin. *J. Hazard. Mater.* **2007**, *146*, 39–50.
- (24) Ramesh, A.; Hasegawa, H.; Sugimoto, W.; Maki, T.; Ueda, K. Adsorption of gold(III), platinum(IV) and palladium(II) onto Glycine Modified Crosslinked Chitosan Resin. *Bioresour. Technol.* **2008**, *99*, 3801–3809.
- (25) Parajuli, D.; Khunathai, K.; Adhikari, C. R.; Inoue, K.; Ohto, K.; Kawakita, H.; Funaoka, M.; Hirota, K. Total Recovery of Gold, Palladium, and Platinum Using Lignophenol Derivative. *Miner. Eng.* **2009**, *22*, 1173–1178.
- (26) Piłśniak, M.; Trochimczuk, A. W.; Apostoluk, W. The Uptake of Gold(I) from Ammonia Leaching Solution by Imidazole Containing Polymeric Resins. *Sep. Sci. Technol.* **2009**, *44*, 1099–1119.
- (27) Kang, E. T.; Ting, Y. P.; Neoh, K. G.; Tan, K. L. Electroless Recovery of Precious Metals from Acid Solutions by N-Containing Electroactive Polymers. *Synth. Met.* **1995**, *69*, 477–478.
- (28) Neoh, K. G.; Tan, K. K.; Goh, P. L.; Huang, S. W.; Kang, E. T.; Tan, K. L. Electroactive polymer-SiO₂ Nanocomposites for Metal Uptake. *Polymer* **1999**, *40*, 887–893.
- (29) Neoh, K. G.; Young, T. T.; Looi, N. T.; Kang, E. T.; Tan, K. L. Oxidation–Reduction Interactions between Electroactive Polymer Thin Films and Au(III) Ions in Acid Solutions. *Chem. Mater.* **1997**, *9*, 2906–2912.
- (30) Reck, B. K.; Graedel, T. E. Challenges in Metal Recycling. *Science* **2012**, *337*, 690–695.
- (31) Haukka, M.; Väisänen, A.; Rissanen, K.; Lahtinen, E.; Kivijärvi, L. A Porous Body, Method for Manufacturing It and Its Use for Collecting Substance from Source Material. Finland Patent Application no. 20175652, 2017.
- (32) Cheval, N.; Gindy, N.; Flowkes, C.; Fahmi, A. Polyamide 66 Microspheres Metallised with in Situ Synthesised Gold Nanoparticles for a Catalytic Application. *Nanoscale Res. Lett.* **2012**, *7*, 182.
- (33) Doidge, E. D.; Carson, I.; Tasker, P. A.; Ellis, R. J.; Morrison, C. A.; Love, J. B. A Simple Primary Amide for the Selective Recovery of Gold from Secondary Resources. *Angew. Chem., Int. Ed.* **2016**, *55*, 12436–12439.
- (34) Martin, T. D.; Brockhoff, C. A.; Creed, J. T.; Long, S. E. Determination of Metals and Trace Elements in Water and Wastes by Inductively Coupled Plasma-Atomic Emission Spectrometry. *Methods for the Determination of Metals in Environmental Samples*; CRC Press Inc.: Boca Raton, 1992; pp 33–91.



II

POROUS 3D PRINTED SCAVENGER FILTERS FOR SELECTIVE RECOVERY OF PRECIOUS METALS FROM ELECTRONIC WASTE

by

Elmeri Lahtinen, Mikko M. Hänninen, Kimmo Kinnunen, Heikki M.
Tuononen, Ari Väisänen, Kari Rissanen and Matti Haukka

Adv. Sustainable Syst. **2018**, 2, 1800048

Reproduced with kind permission from John Wiley & Sons.

Porous 3D Printed Scavenger Filters for Selective Recovery of Precious Metals from Electronic Waste

*Elmeri Lahtinen, Mikko M. Hänninen, Kimmo M. Kinnunen, Heikki M. Tuononen, Ari Väisänen, Kari Rissanen, Matti Haukka**

E. Lahtinen, Dr. M. M. Hänninen, Prof. H. M. Tuononen, Adj. Prof. A. Väisänen, Prof. K. Rissanen, Prof. M. Haukka

Department of Chemistry, University of Jyväskylä, P.O. Box 35, FI-40014 University of Jyväskylä, Finland

E-mail: matti.o.haukka@jyu.fi

Dr. K. M. Kinnunen

Nanoscience Center, Department of Physics, University of Jyväskylä, P.O. Box 35, FI-40014 University of Jyväskylä, Jyväskylä, Finland

Keywords: Functional materials, 3D printing, platinum group metals, gold, metal scavenging, selective laser sintering

Abstract

Selective Laser Sintering (SLS) 3D printing technique was used to fabricate highly porous ion scavenger filters for recovery of Pd and Pt from electronic waste. The scavengers were printed by using a mixture of polypropylene with 10 wt-% of type-1 anion exchange resin as the printing material. Porosities and the flow-through properties of the filters were controlled by adjusting the SLS printing parameters. The cylinder-shaped filters were used in selective recovery of the target metals, Pd and Pt, from acidic leachate of electronic waste simply by passing the solution through the object at room temperature. Under such conditions, the scavenger filters were able to capture Pd and Pt with high efficiency and selectivity from a complex solution of metal ions that contained up to 100 times higher concentrations of other metals, such as copper. By using the Pd/Pt scavenger together with previously reported, highly selective nylon based Au scavenger, the most precious metals *i.e.* Au, Pd and Pt could all be recovered from the electronic waste leachate in a single flow-through process. One of the main advantages of the employed printed scavengers is that all recovered metals can be easily extracted from the filters as separate fractions by using aqueous solutions of thiourea or

diluted nitric acid. After removal of the captured metals, the scavengers are reusable without significant loss in their ion capturing performance.

Introduction

Development of 3D printing techniques has enabled the preparation of chemically and/or physically functional materials and devices.^[1] Fascinating examples have been reported where the potential, industrially relevant applications range from antimicrobial composites to catalytically active materials and even light emitting diodes.^[2] Advances in printing material development have opened the field for intriguing discoveries such as new energy storage devices or drug delivery systems.^[3] Typically, these products have been obtained by utilizing printing techniques such as stereolithography, extrusion-based methods or inkjet printing.^[1a, 4] The chemical activity is often obtained only via post processing the printed object.^[2b, 5] In most of these cases, the porosity, and thus the specific surface area, of the printed material itself is low and cannot be adjusted.

In powder-based printing methods, *e.g.* selective laser sintering (SLS), small, typically 50-100 μm , particles are fused together by laser. This allows, at least up to a point, control over the porosity of the material by fine-tuning the printing parameters including laser power, exposure time, printing temperature and cooling rate.^[6] When the particles are sintered in such a way that only their surfaces are partially melted, a solid structure containing accessible voids between the sintered grains is obtained. Such porous materials can be utilized directly in chemical applications. For example, if a porous column is printed, a fluid (liquid or gas) can flow through the object, interacting with the surface of the partially fused particles. When this type system is compared to a column packed with loose particles, the advantages are obvious. First of all, as the positions of the particles are fixed, they cannot be rearranged by the flowing fluid. Thus, any unwanted channeling is prevented. Second, the porosity can be adjusted,

which can be utilized in controlling the back-pressure of the object. Third, the possibilities to design the shape, interior structure and the size of the object are almost limitless due to the printing technique. Hence, if the printing material is chemically active, the object can be used as a chemically functional device. In principle, the potential applications of such devices are limited only by the chemical functionality of the printing material.

We have recently published a study concerning recovery of gold from acidic leachate of Waste Electrical and Electronic Equipment (WEEE) by using pure nylon (polyamide 12, PA) based 3D printed scavenger object. Herein, we extend this approach to a hybrid printing material consisting of polypropylene and type-1 anion exchange resin. The goal was to develop a 3D printed scavenger filters for recovering Pd and Pt from WEEE leachate and to show that even very low concentrations of metals can be cost-effectively and selectively captured by using simple, reusable scavenger devices.

Results and Discussion

To prepare 3D printed functional filters with precious metal scavenging properties, swollen beads of additive **1** (type-1 anion exchange resin, Dowex 21K) were dried at 90 °C overnight and grinded to a fine powder in a ball mill. The chemically active resin (10 wt-%) was mixed with readily available and easily printable polypropylene (PP), which was chosen as the supporting matrix for the chemically active component. The mixture was then used to print filters with desired shape, size (5 mm tall disc with 16.5 mm diameter) and porosity (see the Experimental section) by using Sharebot SnowWhite SLS 3D printer. The final filters were analyzed using microscopic techniques and X-Ray tomography.

Scanning electron microscopy (SEM) is commonly utilized to acquire information about the porosity and composition of novel materials. Unfortunately, non-conducting samples, like

organic polymers, are known to have notable charging problem during SEM experiments. This charging effect can be reduced, for example, by image post-processing or by coating the sample with metal, but important information about surface structure could be lost during the treatment. Thus, imaging of insulating samples is challenging using standard electron microscopic methods. In helium ion microscopy (HIM) imaging is based on usage of positive He ions when the aforementioned charge problem can be circumvented by utilization of charge compensating low voltage electron beam (a flood gun), enabling the imaging of insulating samples.^[7] Hence, the surfaces of the printed objects were thoroughly investigated using HIM (**Figure 1**). By inspecting the images acquired from the break surfaces of PP/resin filter (1-PP) (**Figure 1**, left), it is evident that the filters are highly porous throughout the sample. In general, the material appears to be composed of polypropylene beads partially sintered together forming a macroporous structure. Extensive melting of the polymer beads is not observed either in printed pure PP (supplementary **Figure S1**) or 1-PP. When zooming in, the particles of anion exchange resin additive **1** can be seen firmly attached to the surface of sintered polypropylene (**Figure 1**, middle). However, the additive is not encapsulated by the polypropylene matrix. The active resin is thus available for chemical interactions. In addition to overall porosity, using SLS technique different density material can be printed in a single object enabling fabrication of entirely functioning products with solvent impermeable edges and chemically active interior (**Figure S2**).

Detailed and comprehensive information about the the interior structure of the objects and the distribution of the active component was acquired using X-ray tomography (**Figure 1**, right). The overall porosity of the objects was established from the high estimated porosity percent (~32 %). The pore size distribution is relatively even, as the diameter of most of the pores falls between 20 and 60 micrometers (**Figure S3**). The data obtained from this analysis demonstrates that the inside structure of the filters corresponds to the HIM images and, even

more importantly, that the active material (Dowex 21K) is evenly distributed over the whole object.

The chemical performance of the printed scavengers was evaluated by using a synthetic test solution containing 100 mg L⁻¹ of Ni, Zn, Fe and Cu and 50 mg L⁻¹ of Al, Cr, Pb and Sn along with 5 mg L⁻¹ of Pd and Au and 1 mg L⁻¹ of Pt in 5% *aqua regia*. The chosen composition mimics the metal ratio in an average sample of an *aqua regia* dissolved Printed Circuit Board (PCB) waste.^[8] Synthetic test solution was used due to the fact that the metal concentrations in true WEEE leachates vary considerably depending on the actual waste material. Hence, analysis of a well-defined synthetic mimic solution is needed for estimating the true capacity and the overall performance of the printed scavengers. It should also be noted that the main part of the metal scavenging experiments with 1-PP Pd/Pt scavenging hybrid material were conducted with a test solution without two key components, Ag and Au, found in electronic waste. From authentic PCB waste, silver can precipitate in presence of chloride, hence it was not included in any of the test solutions. Similarly, gold can be removed completely and selectively by using the 3D printed nylon scavenger prior to 1-PP filter (see below and **Table S4**).^[8] Hence, the synthetic test solution mimics the leachate after removal of Au and Ag. The scavengers were also tested with authentic WEEE solutions, which were prepared by using ultrasound assisted *aqua regia* leaching to dissolve metals from crushed PCB waste. The efficiency of the scavenger was determined by analyzing the metal content of the solution before and after it was passed through the filter. In all experiments, 8 mL of metal solution were passed through three separate 5 mm thick cylinder-shaped 1-PP filters with a diameter of 16.5 mm. This was carried out by placing the tightly fitting filters into a 10 mL syringe and pressing the solution gently through them (**Figure S4**).

For the synthetic test solution over, 96 % of Pd and 98% of Pt were captured from the solution with high selectivity. The most concentrated metal ions, such as aluminium, iron and copper were not retained by the filter while about 50 % of Sn and 10-22 % of Pb and Zn were initially adsorbed (**Figure 2**). However, practically all of zinc and lead as well as most of tin and traces of other metals trapped inside the filters during experiments could be easily removed by subsequent water washes (6 times 8 ml), and only a small amount of tin remained as the main impurity. Excellent efficiency and selectivity for capturing Pd and Pt was also obtained when an authentic WEEE leachate was used instead of the synthetic test solution. These results are summarized in the supplementary data (**Table S6**).

By using a sequence of nylon filters and the **1-PP** filters, the most valuable metals, *i.e.* Au, Pt and Pd, could be captured selectively even from an authentic WEEE solution (**Figure 3**). In this process, the solution was first passed through gold scavenging filters (pure 3D printed nylon) followed by a set of **1-PP** filters. Over 98 % of Au could be removed from the authentic WEEE solution with three 5 mm thick nylon filters with a diameter of 16.5 mm, and over 79 % of Pd and 89 % of Pt could be captured by using three subsequent **1-PP** hybrid filters.

Both Au and Pd/Pt scavengers are fully reusable as the recovered metals can be removed from the filters without destroying their ability to capture ions. Because Au and Pd/Pt were captured in discrete filters, the stripping could be performed separately to produce cleaner end-products. Au was extracted from the nylon filter by using 7 M nitric acid as reported earlier.^[8] Pd and Pt were removed from **1-PP** hybrid filter one-by-one with thiourea solutions. Pd was extracted first with 0.1 M aqueous thiourea followed by extraction of Pt with 0.3 M aqueous thiourea solution (**Table S2**). Total of about 83 and 85 % of adsorbed Pd and Pt, respectively, were recovered with thiourea washes (see the experimental section). This

process allowed separation and isolation of Pd and Pt as separate fractions. In the end, the residual Sn, also trapped by the **1-PP** (see above), was removed also as a separate fraction by using 4.5 M nitric acid. Unlike nylon scavenger for Au, which was ready to be re-used immediately after removal of the captured metal, the **1-PP** filters needed to be regenerated with 0.1 M hydrochloric acid before reuse. However, neither the stripping of the metals nor the regeneration of the filters caused significant reduction in adsorption efficiency (**Table S3**). Maximum adsorption capacity of the **1-PP** filters was studied by passing 10 ml of solution containing 400 mg L⁻¹ of Pd and Pt in 5 % *aqua regia* through one 5 mm filter five times (**Table S5**). Pd and Pt scavenging capacity of the filters was calculated to be about 11 wt-% relative to the mass of the additive in the filter. Performance of the 3D printed filter was compared with similar weight (520 mg) of powderous, non-printed mixture of type-1 anion exchanger resin (Dowex 21K) and polypropylene. The powder mixture was stirred in 10 ml of concentrated Pd/Pt solution and the maximum capacity was found to be *ca.* 13 wt-%. The results show that printing decreases the maximum capacity of the resin only slightly, again highlighting the high porosity of the objects and the availability of the chemically active component **1**.

Conclusions

The presented results clearly demonstrate that SLS 3D printing can be utilized to fabricate porous but still rigid chemically functional objects. These objects can be printed by using a hybrid material such as **1-PP** in which the chemically active component is printed together with easily printable supporting matrix. The results also show that the printing does not destroy the chemical functionality of the active component. The **1-PP** filters introduced in this paper can be used as effective and selective scavengers for Pd and Pt from complex mixtures of metal ions such as acidic leachate of WEEE waste. The captured metals can be removed from the scavenger filter in a stepwise manner, enabling the separation of Pd and Pt as

individual fractions. After removal of the metal ions, the objects can be regenerated, which makes them fully re-usable.

Although we have used WEEE leachate as an example, the scavengers could also be used to capture metal ions from various other source materials. In a broader scope, the concept of using functional printing materials could be extended even beyond scavenging of ions. By developing new, chemically active printing materials it is possible to open entirely new chapter in design of chemically functional devices for various chemical processes.

Experimental Section

Chemicals and solvents: Synthetic solutions used were prepared from PerkinElmer spectroscopy standards (1000 mg L⁻¹). Polymers used for 3D printing were purchased from Advanc3d Materials. Dowex 21K, thiourea, nitric acid ($\geq 65\%$) and hydrochloric acid ($\geq 37\%$) were purchased from Merck. High purity water of 18.2 M Ω cm resistivity was used throughout the experiments. Water was purified using Elga Purelab Ultra.

Sample preparation: Synthetic solution containing 100 mg L⁻¹ of Ni, Zn, Fe and Cu and 50 mg L⁻¹ of Al, Cr, Pb and Sn along with 5 mg L⁻¹ of Pd (and Au for a solution for synthetic test with gold, see **Table S4**) and 1 mg L⁻¹ of Pt in 5% *aqua regia* was prepared by using PerkinElmer spectroscopy standards. Synthetic solution used for capacity tests containing 400 mg L⁻¹ of Pd and Pt in 5% *aqua regia* was also prepared using PerkinElmer spectroscopy standards. The authentic WEEE solution was prepared by ashing milled printed circuit boards for 4 hours at 950 °C. 1 g of the ashed WEEE was placed in a 50 ml centrifuge tube and 10 ml of *aqua regia* was added. Ultrasound assisted leaching was conducted at 25 °C by performing six three-minute cycles. Pressure was released from the tubes between the cycles. Elma Elmasonic P was used as the ultrasound bath. Samples were filtered using Whatman 41 filter papers and diluted in 1:5 ratio before being used for adsorption tests. Detailed descriptions of

HIM imaging, X-ray tomography and ICP-OES measurements can be found from Supporting Information.

Metal recovery and stripping: Recovery experiments were conducted by placing three 5 mm thick and 16.5 mm diameter tightly fitting filters in a 10 ml syringe. Before the adsorption tests, were prepared by passing 8 ml of water through them. 8 ml of the synthetic or authentic solution was then pushed through the filters and metal concentrations were measured before and after the adsorption experiment. To consider the amount of solution trapped in the objects, the final metal concentrations were compared to those of solution that had been passed through a syringe containing three 5 mm thick and 16.5 mm diameter pure PP filters. Hence, the recovery efficiency was calculated as the percentage difference in metal concentrations between initial solution (synthetic or authentic) passed through the pure PP filters and the concentration detected after 1-PP treatment. After water washes, recovery efficiency (**Table S1**) was obtained by adding the concentrations present in water wash fraction to the metal concentrations left in the solution after the treatment with 1-PP and by comparing this value to the initial metal concentration of untreated synthetic solution.

Stripping tests were performed by using filters that had been used for recovery tests with synthetic solution. First, six washing cycles were performed by using water (5 times 8 ml), followed by four 8 ml washes of 0.1 M thiourea. Next, four 8 ml washes of 0.3 M thiourea were conducted, followed by four 8 ml washes of 4.5 M nitric acid. Finally, filters were regenerated by passing through 16 ml of 0.1 M hydrochloric acid. All experiments presented in this paper were performed in triplicate.

Capacity experiment was conducted by placing one 5 mm thick and 16.5 mm diameter filter in 10 ml syringe and passing 10 ml of the synthetic solution containing 400 mg L⁻¹ of Pd and Pt in 5 % *aqua regia* through the filter for five times. Results of this experiment were compared to the result received by stirring the same weight (520 mg) of powder used for manufacturing the filters with 10 ml of the same synthetic solution for 30 minutes.

3D printing: Filters were designed using FreeCad v. 0.16 and sliced by using Slic3r v 1.2.9. Printing was done using ShareBot SnowWhite SLS 3D-printer. 0.1 mm layer thickness was used for all 3D printed objects. For PP and 1-PP, the used laser power was 40 % with a rate of 60000 (2400 mm s⁻¹). Build plate temperature of 119-123 °C was used. For nylon, laser power of 40 % with a rate of 64000 (2560 mm s⁻¹) was used. Build plate temperature was set to 160-163 °C for the duration of the print.

Acknowledgements

Financial support from the Centennial Foundation of Technology Industries of Finland and Jane and Aatos Erkkö foundation as a part of The Future Makers program is greatly appreciated. The research was also supported by the Academy of Finland (grant numbers: 295581 (M.H.), 282499 (H.M.T), 263256, 265328, and 292746 (K.R.)) and the University of Jyväskylä. We also want to thank Joni Parkkonen and Jussi Virkajärvi for performing the X-ray tomography measurement and analyses.

References

- [1] a) C. Parra-Cabrera, C. Achille, S. Kuhn, R. Ameloot, *Chem. Soc. Rev.* **2018**, *47*, 209-230; b) B. C. Gross, J. L. Erkal, S. Y. Lockwood, C. Chen, D. M. Spence, *Anal. Chem.* **2014**, *86*, 3240-3253; c) P. J. Kitson, G. Marie, J. P. Francoia, S. S. Zalesskiy, R. C. Sigerson, J. S. Mathieson, L. Cronin, *Science* **2018**, *359*, 314-319; d) P. J. Kitson, S. Glatzel, W. Chen, C. G. Lin, Y. F. Song, L. Cronin, *Nat. Protoc.* **2016**, *11*, 920-936.
- [2] a) J. Yue, P. Zhao, J. Y. Gerasimov, M. van de Lagemaat, A. Grotenhuis, M. Rustema-Abbing, H. C. van der Mei, H. J. Busscher, A. Herrmann, Y. Ren, *Adv. Funct. Mater.* **2015**, *25*, 6756-6767; b) C. R. Tubío, J. Azuaje, L. Escalante, A. Coelho, F. Guitián, E. Sotelo, A. Gil, *J. Catal.* **2016**, *334*, 110-115; c) C. Hurt, M. Brandt, S. S. Priya, T. Bhatelia, J. Patel, P. R. Selvakannan, S. Bhargava, *Catal. Sci. Technol.* **2017**, *7*, 3421-3439; d) Y. L. Kong, I. A. Tamargo, H. Kim, B. N. Johnson, M. K. Gupta, T. W. Koh, H. A. Chin, D. A. Steingart, B. P. Rand, M. C. McAlpine, *Nano Lett.* **2014**, *14*, 7017-7023.
- [3] a) S. C. Ligon, R. Liska, J. Stampfl, M. Gurr, R. Mulhaupt, *Chem. Rev.* **2017**, *117*, 10212-10290; b) C. W. Foster, M. P. Down, Y. Zhang, X. Ji, S. J. Rowley-Neale, G. C. Smith, P. J. Kelly, C. E. Banks, *Sci Rep* **2017**, *7*, 42233; c) S. E. Moulton, G. G. Wallace, *J Control Release* **2014**, *193*, 27-34; d) J. Goole, K. Amighi, *Int. J. Pharm.* **2016**, *499*, 376-394.
- [4] X. Zhou, C.-j. Liu, *Adv. Funct. Mater.* **2017**, *27*, 1701134.
- [5] a) B. Bian, D. Shi, X. Cai, M. Hu, Q. Guo, C. Zhang, Q. Wang, A. X. Sun, J. Yang, *Nano Energy* **2018**, *44*, 174-180; b) A. S. Díaz-Marta, C. R. Tubío, C. Carbajales, C. Fernández, L. Escalante, E. Sotelo, F. Guitián, V. L. Barrio, A. Gil, A. Coelho, *ACS*

- Catalysis* **2017**, *8*, 392-404; c) A. E. Jakus, S. L. Taylor, N. R. Geisendorfer, D. C. Dunand, R. N. Shah, *Adv. Funct. Mater.* **2015**, *25*, 6985-6995.
- [6] a) S. Dupin, O. Lame, C. Barrès, J.-Y. Charneau, *Eur. Polym. J.* **2012**, *48*, 1611-1621; b) S. F. Shirazi, S. Gharekhani, M. Mehrali, H. Yarmand, H. S. Metselaar, N. Adib Kadri, N. A. Osman, *Sci Technol Adv Mater* **2015**, *16*, 033502; c) A. Danezan, G. Delaizir, N. Tessier-Doyen, G. Gasgnier, J. M. Gaillard, P. Duport, B. Nait-Ali, *J. Eur. Ceram. Soc.* **2018**, *38*, 769-775; d) F. Fina, A. Goyanes, S. Gaisford, A. W. Basit, *Int. J. Pharm.* **2017**, *529*, 285-293; e) L. C. Hwa, S. Rajoo, A. M. Noor, N. Ahmad, M. B. Uday, *Curr. Opin. Solid State Mater. Sci.* **2017**, *21*, 323-347; f) T. Stichel, T. Frick, T. Laumer, F. Tenner, T. Hausotte, M. Merklein, M. Schmidt, *J. Mater. Process. Technol.* **2018**, *252*, 537-545; g) M. Yan, X. Tian, G. Peng, Y. Cao, D. Li, *Mater. Des.* **2017**, *135*, 62-68.
- [7] M. S. Joens, C. Huynh, J. M. Kasuboski, D. Ferranti, Y. J. Sigal, F. Zeitvogel, M. Obst, C. J. Burkhardt, K. P. Curran, S. H. Chalasani, L. A. Stern, B. Goetze, J. A. J. Fitzpatrick, *Sci. Rep.* **2013**, *3*, 3514.
- [8] E. Lahtinen, L. Kivijärvi, R. Tatikonda, A. Väisänen, K. Rissanen, M. Haukka, *ACS Omega* **2017**, *2*, 7299-7304.
- [9] L. A. Feldkamp, L. C. Davis, J. W. Kress, *J. Opt. Soc. Am. A.* **1984**, *1*, 612-619.

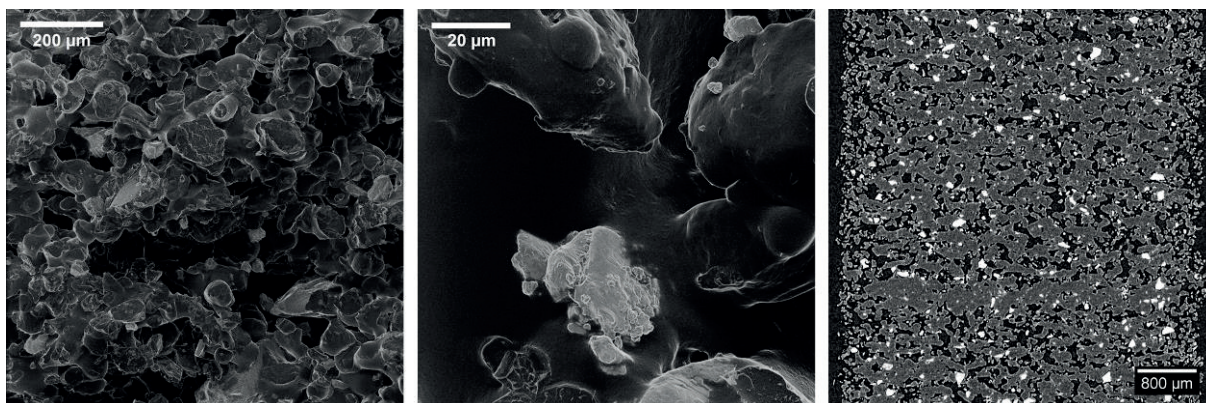


Figure 1. HIM image of break surface of 1-PP (left), zoomed in view of 1-PP (middle) and X-ray tomography image of 1-PP showing the additive in white and supporting polypropylene in grey (right).

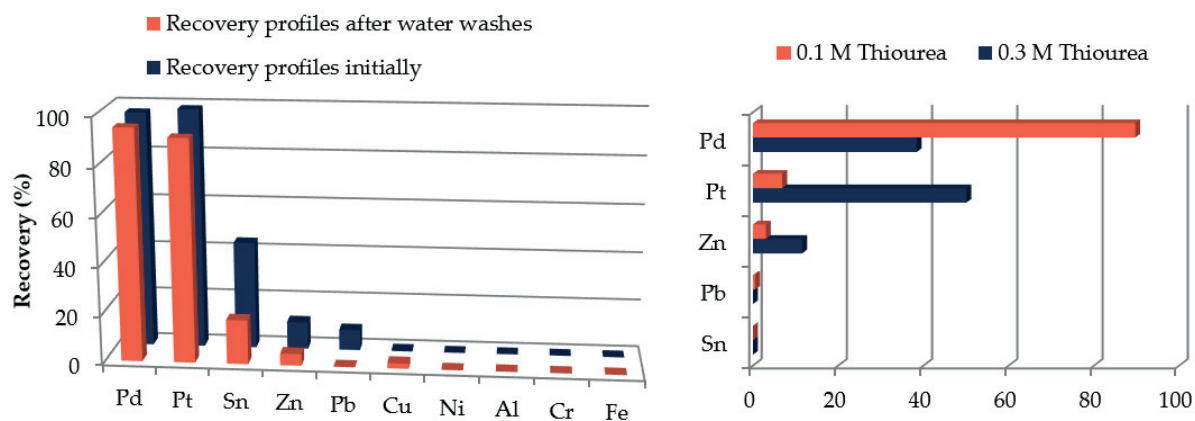


Figure 2. Recovery profiles after treatment with three 1-PP 5mm filters (left) and compositions of stripping solutions (right).

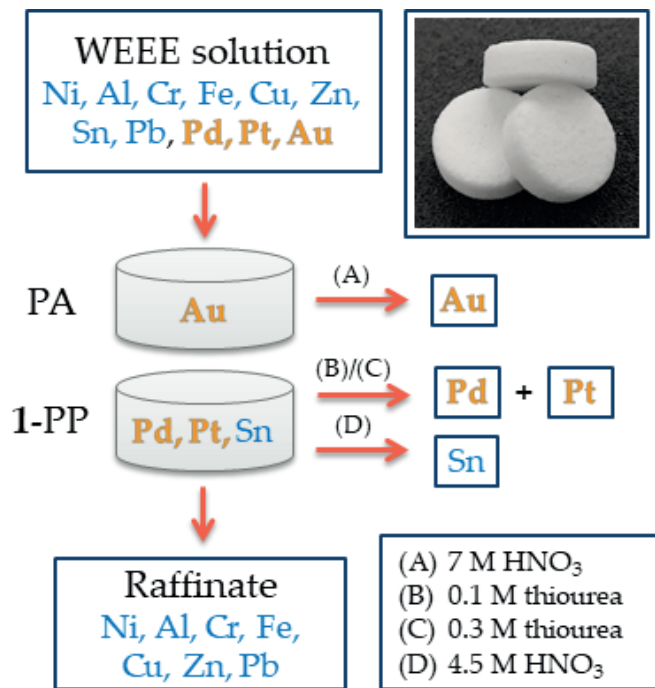


Figure 3. Complete route for extraction and stripping of gold and platinum group metals from WEEE solution using PA and 1-PP filters.



III

GOLD NANOPARTICLES ON 3D-PRINTED FILTERS: FROM WASTE TO CATALYSTS

by

Elmeri Lahtinen, Esa Kukkonen, Virva Kinnunen, Manu Lahtinen, Kimmo
Kinnunen, Sari Suvanto, Ari Väisänen and Matti Haukka

ACS Omega, 2019, 4, 16, 16891-16898.

Reproduced with kind permission from American Chemical Society.



Gold Nanoparticles on 3D-Printed Filters: From Waste to Catalysts

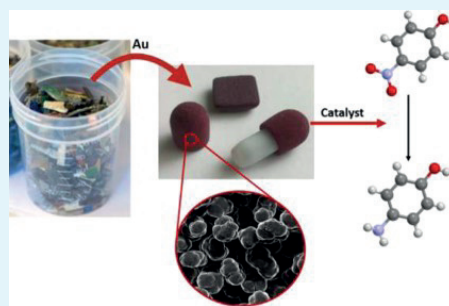
Elmeri Lahtinen,[†] Esa Kukkonen,[†] Virva Kinnunen,[†] Manu Lahtinen,[†] Kimmo Kinnunen,[‡] Sari Suvanto,[§] Ari Väisänen,[†] and Matti Haukka^{*,†}

[†]Department of Chemistry and [‡]Department of Physics, Nanoscience Center, University of Jyväskylä, P.O. Box 35, Jyväskylä FI-40014, Finland

[§]Department of Chemistry, University of Eastern Finland, P.O. Box 111, Joensuu FI-80101, Finland

Supporting Information

ABSTRACT: Three-dimensionally printed solid but highly porous polyamide-12 (PA12) plate-like filters were used as selective adsorbents for capturing tetrachloroaurate from acidic solutions and leachates to prepare PA12–Au composite catalysts. The polyamide-adsorbed tetrachloroaurate can be readily reduced to gold nanoparticles by using sodium borohydride, ascorbic acid, hydrogen peroxide, UV light, or by heating. All reduction methods led to polyamide-anchored nanoparticles with an even size distribution and high dispersion. The particle sizes were somewhat dependent on the reduction method, but the average diameters were typically about 20 nm. Particle sizes were determined by using a combination of single-particle inductively coupled plasma mass spectrometry, helium ion microscopy, and powder X-ray diffraction. Dispersion of the particles was analyzed by scanning electron microscopy with energy-dispersive spectroscopy. Due to the high adsorption selectivity of polyamide-12 toward tetrachloroaurate, the three-dimensional-printed filters were first used as selective gold scavengers for the acidic leachate of electronic waste (WEEE). The supported nanoparticles were then generated directly on the filter via a simple reduction step. These objects were used as catalysts for the reduction of 4-nitrophenol to 4-aminophenol. The described method provides a direct route from waste to catalysts. The selective laser sintering method can be used to customize the flow properties of the catalytically active filter object, which allows the optimization of the porous catalytic object to meet the requirements of catalytic processes.



INTRODUCTION

Gold nanoparticles have received an immense amount of attention during the past decades as they possess a range of fascinating properties and can be used for a variety of different applications.^{1–4} Especially gold-nanoparticle-mediated catalysis has emerged as a promising application.^{5–8} However, the use of gold nanoparticles as a suspension is problematic due to challenges faced in handling and recovering the particles. Therefore, immobilization of nanoparticles onto different polymers,^{9–11} resins,^{12,13} and even gels¹⁴ has been suggested as a potential solution to this problem. These solutions often rely on the use of novel or expensive materials that lack selectivity toward gold and therefore need to be prepared by using pure gold solutions. The use of a material with high selectivity toward gold could solve this issue as even gold-containing waste could be used as a source for gold nanoparticles. Additionally, the previously reported immobilization methods often lack possibilities to control the shape, size, and flow properties of the supporting matrix. This, in turn, sets limitations to their usability in different types of reactions and flow environments.

Polyamide-12 (PA12) has been previously reported to have a high adsorption selectivity toward gold, as tetrachloroaurate,

from acidic waste electrical and electronic equipment (WEEE) leachate.¹⁵ The captured tetrachloroaurate can be removed from polyamide by a simple elution step, which allows PA12 to be used as a reusable scavenger material. However, it is also possible to reduce the captured tetrachloroaurate to zero-valent gold directly on the polymer surface. In other words, the reduction process produces polyamide-anchored gold nanoparticles.¹¹ The reduced gold particles are firmly attached onto the polyamide support, which make the metallized materials potential catalysts. This approach opens up a route for the preparation of supported nanoparticle catalysts directly from waste materials.

Three-dimensional (3D) printing enables the alteration of the shape and size of the nanoparticle-bearing objects. It is also possible to fabricate flow channels into the printed objects. This has been previously demonstrated with methods such as stereolithography and ink-jet printing.^{16,17} However, these methods produce surfaces that are not inherently porous. Furthermore, they also often require specifically customized

Received: July 9, 2019

Accepted: August 29, 2019

Published: October 1, 2019

printing materials. These problems can be avoided by using powder-based 3D-printing methods, such as selective laser sintering (SLS). With the SLS technique, it is possible to produce objects that are inherently porous. In SLS-printing, small particles with a typical diameter of 50–100 μm are fused together by a laser, which gives control over the physical characteristics such as the porosity and mechanical strength of the printed material by fine-tuning the printing parameters such as laser power, exposure time, and printing temperature.^{18–22} When the particles are sintered in such a way that only their surfaces are partially melted, a solid structure containing accessible voids between the sintered grains is obtained.^{5,18,23} Also, a wide range of chemically active printing materials can be used without complicated preprocessing steps ranging from functional polymers to mixtures of functional additives and supporting polymer matrices.^{23,24}

In this paper, SLS 3D-printed PA12 filters were functionalized into PA12–Au composites by gold adsorption followed by reduction. The gold was adsorbed as tetrachloroaurate, from either acidic leachate of WEEE or a synthetic tetrachloroaurate solution. The reduction and formation of gold nanoparticles with various sizes were investigated with helium ion microscopy (HIM), scanning electron microscopy energy-dispersive spectroscopy (SEM-EDS), powder X-ray diffraction (XRD), and single-particle inductively coupled plasma mass spectrometry (SP-ICP-MS). A range of different reduction methods were used to investigate their impact on the particle size. The autoreduction process with no specific reduction agent was also followed. The catalytic activity of the supported gold nanoparticle filters was tested in the reduction of 4-nitrophenol to 4-aminophenol, which is a commonly used model reaction for gold-nanoparticle-mediated catalysis.^{25–27}

RESULTS AND DISCUSSION

The porous SLS 3D-printed plate-like filters were fabricated using a Sharebot SnowWhite 3D printer, using PA12 powder consisting of c.a. 50 μm diameter particles as printing material. After the printing process, the filters were carefully cleaned of any unsintered powder and adsorption of tetrachloroaurate was performed either from a synthetic solution or from acid-leached printed circuit board (PCB) waste. After the adsorption, the SLS 3D-printed filters were washed extensively with water before being used in reduction experiments. Even though the samples used for the studies were simple plate-shaped objects, different shapes and forms can also be produced and functionalized with gold nanoparticles (Figure S1).

The SLS 3D-printed PA12–Au filters were reduced using a variety of different reducing agents. First, PA12–Au filters were treated with 20 mL of 0.5 M NaBH_4 . By changing the reduction time between 1 and 15 min, the color of the resulting PA12–Au filter could be altered. The shorter contact times led to filter plates with a red to light purple color, whereas longer contact times led to dark purple filters (Figure 1a). The color changes indicated changes in the nanoparticle sizes. NaBH_4 reduction was also carried out for PA12–Au filters, where the gold was adsorbed from acid leachate of WEEE (Figure S2, see the Experimental Section). The resulting metallized filters were identical to the ones obtained by using pure tetrachloroaurate solution. The results show that it is possible to use electronic waste as a gold source for supported nanoparticles.

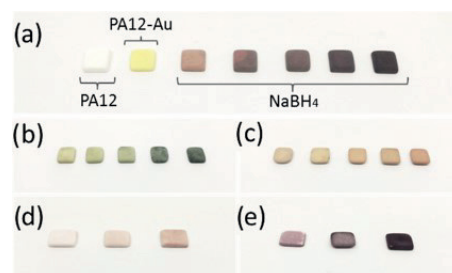


Figure 1. Images of SLS 3D-printed PA12 filters ($10 \times 10 \times 2 \text{ mm}^3$). (a) Pure filter (PA12) and a filter immediately after gold adsorption (PA12–Au). NaBH_4 : PA12–Au filters reduced with 0.5 M NaBH_4 for 1, 3, 5, 10, and 15 min, respectively. (b) PA12–Au filters reduced with 0.5 M ascorbic acid for 1, 3, 5, 10, and 15 min, respectively. (c) PA12–Au filters reduced with 30% H_2O_2 for 5, 10, 15, 30, and 60 min, respectively. (d) PA12–Au filters reduced by using UV light (405 nm) for 20, 40, and 60 min. (e) PA12–Au filters reduced by heating them in the oven ($110 \text{ }^\circ\text{C}$) for 30, 60, and 90 min.

The second tested reduction method, that is, reduction with ascorbic acid, yielded gray to greenish PA12–Au filters. Also, in this case, the intensity of the color was dependent on the reduction time (Figure 1b). However, after the reduction, the color of the filters started to change to purple over a longer period of storage, typically over several days. The next method of reduction was more unconventional as it included treating the PA12–Au filter with hydrogen peroxide. Hydrogen peroxide is known to produce gold nanoparticles²⁸ and in the case of SLS 3D-printed PA12–Au filters, it resulted in filters with red to light brown colors (Figure 1c). The last two methods tested were treating the filters with UV light (405 nm) and heating them in the oven at $110 \text{ }^\circ\text{C}$, respectively. Both methods yielded PA12–Au filters with a red to purple color. In general, the heating treatment produced a much more intense color than the light-induced reduction (Figure 1d,e). However, it should be noted that even storing the PA12–Au filters at room temperature in ambient light was enough for slow conversion of the adsorbed gold into nanoparticles. This was observed as the color of the filters slowly turned light purple over an extended period of time.

HIM imaging of the PA12–Au samples was conducted to study the nanoparticle sizes and their distribution within the SLS 3D-printed filters. Figure 2 shows the HIM images of PA12–Au filters prepared from synthetic tetrachloroaurate solution and reduced with H_2O_2 (Figure 2a,b) and ascorbic acid-reduced PA12–Au filters prepared from acidic WEEE leachate (Figure 2c,d). From the zoomed-out images, it can be seen that distributions of the gold nanoparticles on the surfaces of the fused PA12 particles in PA12–Au filters are rather even for both of the samples. As it has been previously shown, SLS 3D-printing can be used to fabricate solid but highly porous structures, where a fluid can flow through the voids between the partially fused particles.^{23,24} This particle-like structure can also be seen in Figure 2a,c and in Figure S3 given as a Supporting Information. Furthermore, the gold nanoparticles are attached only on the surfaces of the fused particles and they are not encapsulated by the polymer. This means that the gold nanoparticles are also distributed in the inner structure of the printed objects, but they are still able to interact with fluids running through the object material. The more detailed HIM images (Figure 2b,d) confirm the even spatial distribution of

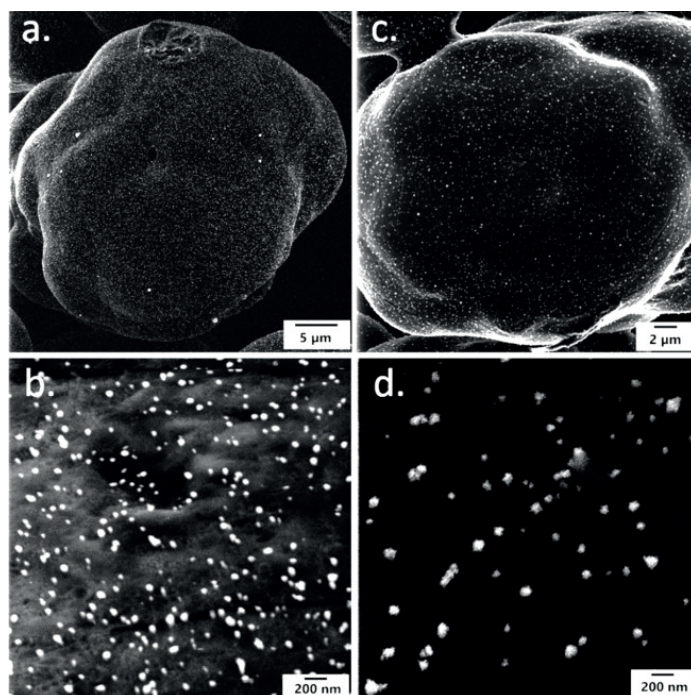


Figure 2. HIM images of the surfaces of the H_2O_2 -reduced PA12–Au filters prepared using synthetic tetrachloroaurate solution (a, b) and of the ascorbic acid-reduced, WEEE-derived PA12–Au filters (c, d).

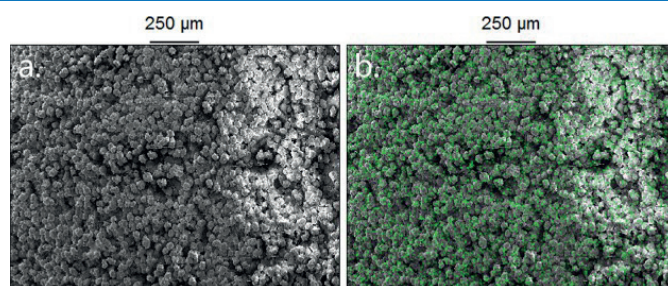


Figure 3. SEM-EDS image of the analyzed area of the ascorbic acid-reduced PA12–Au sample (a). Overlaid image of the obtained gold spectral image (green) and the initial image of the analyzed area (b).

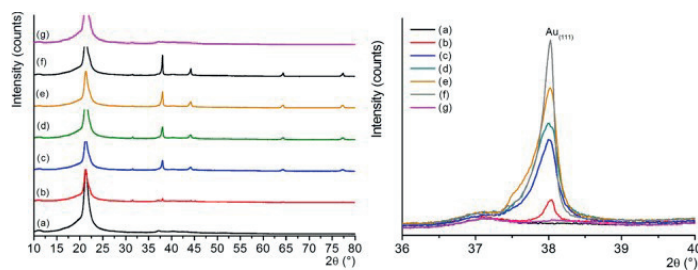


Figure 4. Left: XRD patterns of PA12–Au filters with different reducing agents used: (a) reference filter without Au; PA12–Au reduced with (b) UV light, (c) NaBH_4 , (d) heating, (e) ascorbic acid, and (f) H_2O_2 ; and (g) PA12–Au sample, where gold is derived from WEEE and reduced with NaBH_4 . Right: zoomed 2θ range showing the $\text{Au}_{(111)}$ peak on each pattern.

the gold particles. The even size distribution of the nanoparticles can also be seen in Figures 2b,d. Even if HIM is not the optimal method for particle size analysis, it clearly indicates that most of the nanoparticles are within the range of 10–100 nm in both samples. The HIM images of the samples reduced by other methods are given in the Supporting Information (Figures S4 and S5).

The even distribution of the gold nanoparticles on the surfaces of the SLS 3D-printed objects is somewhat surprising since the nanoparticles are not end-capped with ligands. However, it could be reasoned that interactions between gold and the functional groups of the PA12 polymer are responsible for the high dispersion and even size distribution. This has also been suggested as the reason for the even distribution of gold nanoparticles on PA66 surfaces.¹¹ Most likely, the amide groups of PA12 provide sufficiently strong interactions with the nanoparticles to prevent excessive agglomeration.

Additional analyses for the dispersion of the gold nanoparticles on the printed filters were carried out by performing spectral imaging using SEM-EDS. The ascorbic acid-reduced PA12–Au filter was covered with silver particles prior to SEM-EDS analysis. Spectral imaging was then performed, and the results are shown in Figure 3. The image of the analyzed area of the sample (Figure 3a) is overlaid with the spectral imaging map received for the gold (Figure 3b). Together with the HIM imaging results, the SEM-EDS analysis confirms that the distribution of the gold nanoparticles on the PA12–Au filters is uniform.

Powder X-ray diffraction (XRD) patterns of the PA12–Au filters are shown in Figure 4. All of the XRD patterns show characteristic peaks of the PA12 polymer matrix, which can be confirmed based on the peaks observed in the pattern of the reference filter of pristine PA12 (reference pattern for PA12 was not available in the PDF4 database²⁹). In case of filters with reduced gold nanoparticles, the characteristic diffraction peaks at 38.1, 44.39, 64.62, and 77.59° 2 θ could be assigned (PDF4 entry: 00-066-0091)² to metallic gold in a face-centered cubic crystal system (*Fm $\bar{3}$ m*). In addition to the characteristic peaks of PA12 and gold, there were no other peaks in the patterns, indicating that only gold was reduced onto the filters. This was also the case with the NaBH₄-reduced sample where WEEE was used as the gold source. It means that the other metals present in the WEEE solution (e.g., Cu, Fe, Al...) were not adsorbed to the PA12 filters. However, it should be noted that the gold content in that particular sample was also considerably lower, due to a much lower concentration of gold being available for adsorption from the acid-leached WEEE compared to the synthetic tetrachloroaurate solution. Comparison of the XRDs of the different reduction techniques revealed that the H₂O₂ reduction showed the highest intensity for gold particles, followed by others in the order of ascorbic acid > heat treatment \geq NaBH₄ > UV light (Figure 4).

To get a coarse estimate of the dispersion of gold in the filter, the average crystallite size of the gold particles was estimated by the Scherrer method as shown in eq 1

$$D = \frac{\kappa\lambda}{\beta_s \cos \theta} \quad (1)$$

in which D is the average crystallite size, K is the shape-dependent Scherrer constant (0.90 for spherical crystallites with a cubic symmetry), λ is the X-ray wavelength (1.5406 Å),

β_s is the full peak-width at half-maximum intensity (given in radians) corresponding to structural broadening (instrumental broadening taken into account), and θ is the diffraction angle. For each sample, the strongest Au peak (38.1° 2 θ) with Miller indices (111) was taken for an indicative crystal size analysis, and the resulting values are shown in the Supporting Information (Table S1). Generally, the average crystal size of gold particles ranged from 30 to 70 nm. It is noticeable that UV light-treated and H₂O₂-treated samples exhibit similar-sized particles, even though in terms of quantity they represent the two extremes of the series. In all the rest of the samples, the crystal size of gold is about the same (~30 nm) regardless of the quantity of the gold phase per sample. However, it should be kept in mind that these results represent a rather qualitative estimation of the particle size as an accurate peak profile analysis of a low crystalline phase that is mixed with a low-crystalline organic matrix is challenging for reasons such as the degree of peak overlap and uncertainties to define the proper peak profile tailing versus baseline signals. Second, the crystallographic crystal size analysis tends to skew on larger average sizes due to the fact that larger particles have a somewhat higher diffraction power than the smaller ones. However, the XRD results are well in line with the HIM analyses above.

The SP-ICP-MS analyses were used to study further the size distribution of the nanoparticles. SP-ICP-MS is a highly sensitive method for the characterization of nanoparticles from solutions. Even if the leaching of gold from the gold-functionalized filters was low, the removed particles could be analyzed. The nanoparticle size distribution diagram observed during the analysis is represented in Figure 5. The majority of

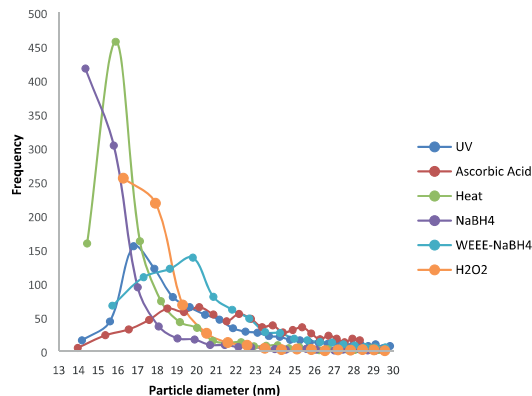


Figure 5. Nanoparticle size distribution diagram of the PA12–Au filters reduced with different methods obtained from the SP-ICP-MS measurement. The observed particle frequencies are not strictly comparable to each other due to different dilution factors and run times.

the observed particles were in the size range of 14–32 nm ($\geq 90\%$ detected particles). Typically, most of the nanoparticles observed appeared to have an average diameter of around 20 nm. Among the different reduction methods, NaBH₄ seems to lead to the smallest nanoparticles with average sizes of 16 \pm 1 nm observed, while ascorbic acid, heating, and UV light led to average particle sizes of 20 \pm 5, 20 \pm 4, and 20 \pm 3 nm, respectively. Reduction with H₂O₂ led to particles with an average diameter of 21 \pm 2 nm. The PA12–Au filters where

the $[\text{AuCl}_4]^-$ was adsorbed from the acidic WEEE leachate followed by reduction using NaBH_4 produced nanoparticles of 21 ± 4 nm diameter (Table S2).

As can be seen from the average diameters observed, most of the reduction methods led to PA12–Au filters having rather uniformly sized nanoparticles. In addition, the normal analytical uncertainty might explain the observed differences in the average diameters. Even the WEEE-derived PA12–Au filters possessed nanoparticles of around the same size than the other PA12–Au filters produced by using synthetic tetrachloroaurate solutions. Such results confirm the suitability of secondary gold sources for generating supported nanoparticles. The particle size distribution based on SP-ICP-MS results are in good agreement with the sizes of the nanoparticles observed in the HIM images (Figures 2, S4, and S5) and the results obtained by XRD (Figure 4 and Table S1). It should be emphasized that no severe leaching of gold was observed. This was tested by shaking the catalyst object vigorously in ultrapure water and analyzing the released Au-NPs by SP-ICP-MS. The amount of released Au was found to be at most 0.1 wt %. The results of the leaching tests support further the firm attachment of gold nanoparticles on the PA12 matrix.

The catalytic activity of the gold nanoparticle-functionalized SLS 3D-printed filters was tested in the simple reduction of 4-nitrophenol to 4-aminophenol in the presence of NaBH_4 following the previously reported method.²⁵ The completeness of the reactions were then determined by UV–vis spectroscopy. Based on the obtained results (Figure 6), it is evident

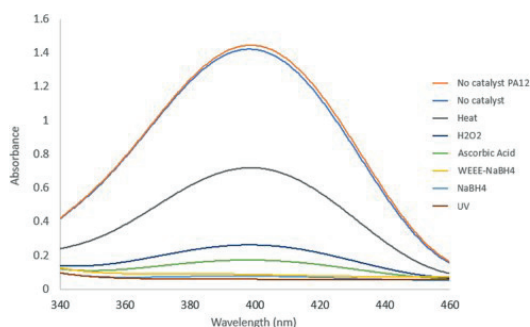


Figure 6. UV–vis results for the gold-catalyzed reduction of 4-nitrophenol to 4-aminophenol in the presence of NaBH_4 .

that the PA12–Au filters are able to effectively catalyze the conversion. The solutions without Au catalysts show no signs of a reaction, whereas most PA12–Au filters have catalyzed the reactions to completeness within the 2 h reaction time. The filter treated by heating shows slightly deviating results compared to others. However, all of the reactions with the catalysts were found to reach completeness if let to react over a longer period of time. In addition to the simple plate-shaped PA12–Au filters, stir bar sleeve-shaped catalysts (Figure S1) were also tested and found to perform similar to the other filters tested.

The reusability of the catalysts was tested by performing 10 consecutive catalytic cycles with the PA12–Au filter reduced with NaBH_4 . No significant decrease in the catalytic activity was observed, which further shows the strong attachment of the gold nanoparticles onto the SLS 3D-printed PA12 filter. Additionally, the PA12–Au filter where gold was adsorbed

from acid-leached WEEE, followed by reduction with NaBH_4 , was also tested (WEEE- NaBH_4). The filter performed just like the ones prepared using pure tetrachloroaurate solution, further confirming that waste materials such as WEEE can be used as a feedstock for the preparation of gold nanoparticle catalysts.

CONCLUSIONS

In this paper, we introduce a method for manufacturing SLS 3D-printed polyamide-12 objects functionalized with gold nanoparticles. This can be achieved by adsorbing gold as tetrachloroaurate onto the polyamide-12 matrix, followed by a reduction. A variety of reduction methods can be used to produce highly dispersed and evenly sized gold nanoparticles with an average diameter of around 20 nm on the polyamide filters. The functionalized filters can be used as effective catalysts in the reduction of 4-nitrophenol to 4-aminophenol. Since PA12 is a highly selective adsorbent for gold, it is possible to use various gold-containing solutions as the source of gold. This opens up a direct route from waste materials to catalysts. For example, the acidic leachate of circuit board waste can be used as the gold source for the preparation of PA12-supported gold nanoparticle catalysts with no additional purification steps and without any interference by the other metals. SLS-printing provides an attempting technique for preparing heterogeneous catalysts. The chemical activity can be optimized by the choice of the printing material, while the printing technique allows fine-tuning of the shape, size, porosity, and flow properties of the printed object. Although we have used SLS-printing for the preparation of catalysts with supported gold nanoparticles, the same approach can be extended to other metals as well. This can be achieved by replacing PA12 with another printing material that can selectively adsorb the desired metal.

EXPERIMENTAL SECTION

Chemicals and Materials. Hydrogen peroxide (AnalaR NORMAPUR) and ascorbic acid (AnalaR NORMAPUR) were purchased from VWR. Sodium borohydride (>98%) was supplied by Acros Organics, and 4-nitrophenol (98%), nitric acid ($\geq 65\%$), and hydrochloric acid ($\geq 37\%$) were purchased from Merck. Polyamide-12 was obtained from ADVANC3D materials and used without any additional pretreatment. All chemicals were used as received.

3D-Printing of the PA12 Filters. The PA12 filters ($10 \times 10 \times 2$ mm³) were printed using a Sharebot SnowWhite SLS 3D printer. Highly porous objects with good physical durability were obtained using the following parameters during the printing process: 161 °C environmental temperature, 40% laser power (a maximum of 14 W), 2400 mm s⁻¹ laser speed, and 0.1 mm layer height. The 3D-printed objects were thoroughly cleaned of any nonsintered powder after the printing process. No further pretreatment was performed prior to the gold adsorption experiments.

Adsorption of Tetrachloroaurate onto PA12 Filters. The gold was adsorbed as tetrachloroaurate onto the SLS 3D-printed filters either from a synthetic solution or from acid-leached PCB waste. The synthetic tetrachloroaurate solution was prepared by diluting a Perkin Elmer 1000 mg L⁻¹ spectroscopy standard until the concentration of gold was around 200 mg L⁻¹. The solution was adjusted to have 10 vol % HCl. The PCB sample was prepared by ashing the milled

PCB waste at 950 °C for 4 h. The sample was then dissolved using ultrasound-assisted leaching with aqua regia. The leachate was diluted before the gold was adsorbed onto the 3D-printed filters. Both with synthetic and authentic solutions, the filter plates were kept in contact with the solution for 8 h. This was done to ensure the saturation, even though the adsorption process itself is rather fast.¹⁵ After the adsorption, the filters were thoroughly washed with water. The PA12–Au objects, prepared from the synthetic tetrachloroaurate solution, were adjusted to possess around 0.5 wt % of gold. After the adsorption, the objects were reduced. The samples that were analyzed using the following methods were reduced using 0.5 M NaBH₄, 0.5 M ascorbic acid, 30% H₂O₂ solution, UV light, or thermal treatment for 15 min (NaBH₄ and ascorbic acid), 60 min (H₂O₂ and UV), or 90 min (thermal treatment).

Helium Ion Microscopy. Imaging was performed with a Carl Zeiss ORION NanoFab helium ion microscope. The beam energy used was roughly 30 keV, and the beam current was set between 0.32 and 0.38 pA. The dwell time of the scans was altered between 0.2 and 50 μs for optimal picture quality. The working distance was generally around 6.2–8.3 mm. Samples were not treated in any way before imaging aside from the use of pressurized air to clear any loose particles from the surfaces of the samples.

Scanning Electron Microscopy Energy-Dispersive X-Ray Spectroscopy. The SEM-EDS analysis was performed by using Hitachi S-4800 field emission scanning electron microscopy with a Thermo Electron Noran System Sic EDS (NSS200) detector. The samples were coated with silver particles prior to analysis to overcome the challenges faced with nonconductive samples. An acceleration voltage of 10 kV was used for the analysis. Around 10 min of spectral imaging data were gathered during the imaging process for the gold dispersion analysis.

Powder X-ray Diffractometry. X-ray powder diffraction patterns were measured by a PANalytical X'Pert PRO diffractometer in Bragg–Brentano geometry using Cu Kα₁ radiation (Johannsson type monochromator, λ = 1.5406 Å, 45 kV, 40 mA). A sample filter was first set on a silicon filter (zero background signal filter) that was placed on a steel-made sample holder with a height-adjustable cavity. The pattern was recorded from a spinning sample by an X'Celerator detector in the 2θ range of 3–80° with a step size of 0.017° and a counting time of 400 s per step (4 h 10 min overall time). Diffraction data were processed with the Malvern Panalytical HighScore Plus v. 4.7 program.³⁰

Single-Particle Inductively Coupled Plasma Mass Spectrometry. SP-ICP-MS measurements were performed on a NexION350D ICP-MS spectrometer operating in the single-particle mode using the Syngistix Nano Application Module (PerkinElmer Inc., Massachusetts). Instrumental parameters are shown in Table 1. The nebulizer gas flow was optimized to gain maximum response for ¹⁹⁷Au. The sample uptake rate was measured daily by quantifying the mass of sample uptake after 3 min in duplicate. The transport efficiency (i.e., the fraction of nebulized sample entering the plasma) was determined using the particle size method. Citrate-stabilized 30 and 60 nm gold nanoparticles (NanoComposix, San Diego, CA) were used for particle calibration after dilution with ultrapure water with a resistivity of 18.2 MΩ cm (UP-water, PURELAB Ultra, ELGA LabWater, Buckinghamshire, U.K.). Dissolved gold calibration solutions were prepared from a standard stock solution of 100 μg mL⁻¹ Au in 2% HCl (Pure

Table 1. NexION350D Instrumental Parameters

parameter	condition
nebulizer	ESI PFA concentric
spray chamber	baffled cyclonic, glass
injector	1.8 mm i.d. sapphire
power	1600 W
nebulizer gas flow	0.97–0.99 L min ⁻¹
sample uptake rate	0.333–0.337 g min ⁻¹
dwell time	100 μs
sampling time	60–6000 s
transport efficiency	6.38–6.73%

Plus, Perkin Elmer, Massachusetts) by dilution in a thiourea solution (0.1 mol % thiourea (≥99.0%, VWR International, Pennsylvania), 2.4 vol % HCl, and 0.05 vol % HNO₃). High-purity (Analpure) hydrochloric acid and nitric acid were obtained from Analytika spol. s r.o. (Prague, Czech Republic). All dilutions were performed gravimetrically.

All samples were placed in 50 mL polypropylene containers and 20 mL of UP-water was added. The samples were vigorously shaken for 30 s for particle release. For every sample, at least three different dilutions were made with UP-water to minimize the contribution of dissolved signal possibly overlapping the particle signal. The sampling time was adjusted to 60–6000 s depending on the sample to gain a sufficient number of detected peaks for reliable particle concentration calculation (>500 peaks). All dilutions were performed gravimetrically, and samples were analyzed as soon as possible after the initial sample preparation to minimize changes in the original sample composition over time.

The Syngistix Nano Application Module was used for data processing. The intensity of detected particles was related to the particle mass (μg) using a particle calibration curve and transformed to the particle diameter (nm) assuming a spherical particle geometry. The mean particle diameter and particle concentration for each sample were calculated as an average for the results obtained for different dilutions (*n* = 1–3) and replicate readings and were reported as average ± standard deviation (1 s). The instrumental drift causing the level of measured intensity to decrease over time was corrected with a drift correction standard (Pt 1 μg kg⁻¹ in 1 + 1% HCl/HNO₃). The total mass of particulate gold in the samples was calculated based on the measured sample particle concentration (particles/g) and mean particle diameter (nm).

UV–Vis Spectroscopy. UV–vis spectra of the catalytically reduced 4-nitrophenol solutions were measured from 700 to 340 nm using a Perkin Elmer Lambda 25 UV/Vis-spectrophotometer. A slit of 1.0 nm was used with a scan speed of 240 nm min⁻¹ and a data interval of 3.0 nm. Ultrapure water was used as a reference sample in the reference cuvette.

Catalysis. A 0.1 mM solution of 4-nitrophenol was prepared by dissolving roughly 7 mg of 4-nitrophenol in 500 mL of deionized water. Next, 5 mL of the obtained solution was pipetted to eight small glass beakers, and 10 mg of NaBH₄ was added to each beaker to act as the reducing agent. Excess of NaBH₄ was used to avoid any kind of effect the change of concentration of the reductant could have on the reaction. One PA12–Au filter each treated with a different gold reduction method (as described earlier) was placed in the beaker containing 4-nitrophenol and NaBH₄. Two beakers, one containing just the starting material and the reductant and the other also containing the PA12 filter with no gold, acted as

references. The mixtures were then stirred for 2 h, even though many of the reactions could be seen to happen much faster. Excessive reaction time was chosen to further confirm that the reaction would not proceed without the catalyst. The reusability of the catalysts was determined by performing 10 reaction cycles with a PA12–Au filter that had been reduced using NaBH₄. No significant drop in the catalytic activity was observed. Samples were then analyzed by using UV–vis spectroscopy.

■ ASSOCIATED CONTENT

Supporting Information

The Supporting Information is available free of charge on the ACS Publications website at DOI: 10.1021/acsomega.9b02113.

Additional images of the PA12–Au objects; HIM images of the structure of the PA12–Au objects; XRD and SP-ICP-MS result tables (PDF)

■ AUTHOR INFORMATION

Corresponding Author

*E-mail: matti.o.haukka@jyu.fi.

ORCID

Elmeri Lahtinen: 0000-0002-8414-9915

Manu Lahtinen: 0000-0001-5561-3259

Matti Haukka: 0000-0002-6744-7208

Author Contributions

E.L. and E.K. printed the objects and performed the gold reduction and catalysis experiments as well as measured the UV–vis spectra. V.K. conducted the SP-ICP-MS measurements. M.L. performed the powder XRD analysis of the samples. K.K. and E.L. conducted the HIM imaging of the PA12–Au filters, while S.S. and E.L. performed the SEM-EDS imaging. M.H. and A.V. supervised the project. The initial manuscript was written by E.L. and E.K. and was then jointly revised by all authors.

Notes

The authors declare no competing financial interest.

■ ACKNOWLEDGMENTS

The funding received from the Centennial Foundation of Technology industries of Finland as well as the Jane and Aatos Erkko foundation is greatly appreciated. The research was also supported by the Academy of Finland (grant number: 295581 (M.H.)) and by the Department of Chemistry, University of Jyväskylä.

■ REFERENCES

- (1) Giljohann, D. A.; Seferos, D. S.; Daniel, W. L.; Massich, M. D.; Patel, P. C.; Mirkin, C. A. Gold Nanoparticles for Biology and Medicine. *Angew. Chem., Int. Ed.* **2010**, *49*, 3280–3294.
- (2) Boisselier, E.; Astruc, D. Gold Nanoparticles in Nanomedicine: Preparations, Imaging, Diagnostics, Therapies and Toxicity. *Chem. Soc. Rev.* **2009**, *38*, 1759–1782.
- (3) Ghosh, P.; Han, G.; De, M.; Kim, C. K.; Rotello, V. M. Gold Nanoparticles in Delivery Applications. *Adv. Drug Delivery Rev.* **2008**, *60*, 1307–1315.
- (4) Guo, S.; Wang, E. Synthesis and Electrochemical Applications of Gold Nanoparticles. *Anal. Chim. Acta* **2007**, *598*, 181–192.
- (5) Corma, A.; Garcia, H. Supported Gold Nanoparticles as Catalysts for Organic Reactions. *Chem. Soc. Rev.* **2008**, *37*, 2096–2126.
- (6) Chen, Y.; Qiu, J.; Wang, X.; Xiu, J. Preparation and Application of Highly Dispersed Gold Nanoparticles Supported on Silica for Catalytic Hydrogenation of Aromatic Nitro Compounds. *J. Catal.* **2006**, *242*, 227–230.
- (7) Panigrahi, S.; Basu, S.; Praharaj, S.; Pande, S.; Jana, S.; Pal, A.; Ghosh, S. K.; Pal, T. Synthesis and Size-Selective Catalysis by Supported Gold Nanoparticles: Study on Heterogeneous and Homogeneous Catalytic Process. *J. Phys. Chem. C* **2007**, *111*, 4596–4605.
- (8) Tran, T. D.; Nguyen, M. T. T.; Le, H. V.; Nguyen, D. N.; Truong, Q. D.; Tran, P. D. Gold Nanoparticles as an Outstanding Catalyst for the Hydrogen Evolution Reaction. *Chem. Commun.* **2018**, *54*, 3363–3366.
- (9) Ofir, Y.; Samanta, B.; Rotello, V. M. Polymer and Biopolymer Mediated Self-Assembly of Gold Nanoparticles. *Chem. Soc. Rev.* **2008**, *37*, 1814–1825.
- (10) Corbierre, M. K.; Cameron, N. S.; Sutton, M.; Mochrie, S. G. J.; Lurio, L. B.; Rühm, A.; Lennox, R. B. Polymer-Stabilized Gold Nanoparticles and Their Incorporation into Polymer Matrices. *J. Am. Chem. Soc.* **2001**, *123*, 10411–10412.
- (11) Cheval, N.; Gindy, N.; Flowkes, C.; Fahmi, A. Polyamide 66 Microspheres Metallised with in Situ Synthesised Gold Nanoparticles for a Catalytic Application. *Nanoscale Res. Lett.* **2012**, *7*, No. 182.
- (12) Shah, D.; Kaur, H. Resin-Trapped Gold Nanoparticles: An Efficient Catalyst for Reduction of Nitro Compounds and Suzuki-Miyaura Coupling. *J. Mol. Catal. A: Chem.* **2014**, *381*, 70–76.
- (13) Praharaj, S.; Nath, S.; Ghosh, S. K.; Kundu, S.; Pal, T. Immobilization and Recovery of Au Nanoparticles from Anion Exchange Resin: Resin-Bound Nanoparticle Matrix as a Catalyst for the Reduction of 4-Nitrophenol. *Langmuir* **2004**, *20*, 9889–9892.
- (14) Kumar Vemula, P.; Aslam, U.; Ajay Mallia, V.; John, G. In Situ Synthesis of Gold Nanoparticles Using Molecular Gels and Liquid Crystals from Vitamin-C Amphiphiles. *Chem. Mater.* **2007**, *19*, 138–140.
- (15) Lahtinen, E.; Kivijärvi, L.; Tatikonda, R.; Väisänen, A.; Rissanen, K.; Haukka, M. Selective Recovery of Gold from Electronic Waste Using 3D-Printed Scavenger. *ACS Omega* **2017**, *2*, 7299–7304.
- (16) Kamyshny, A.; Ben-Moshe, M.; Aviezer, S.; Magdassi, S. Ink-Jet Printing of Metallic Nanoparticles and Microemulsions. *Macromol. Rapid Commun.* **2005**, *26*, 281–288.
- (17) Fantino, E.; Chiappone, A.; Roppolo, I.; Manfredi, D.; Bongiovanni, R.; Pirri, C. F.; Calignano, F. 3D Printing of Conductive Complex Structures with In Situ Generation of Silver Nanoparticles. *Adv. Mater.* **2016**, *28*, 3712–3717.
- (18) Lahtinen, E.; Kukkonen, E.; Jokivartio, J.; Parkkonen, J.; Virkajärvi, J.; Kivijärvi, L.; Ahlskog, M.; Haukka, M. Preparation of Highly Porous Carbonous Electrodes by Selective Laser Sintering. *ACS Appl. Energy Mater.* **2019**, *2*, 1314–1318 DOI: 10.1021/acsaem.8b01881.
- (19) Shi, D.; Gibson, I. Material Properties and Fabrication Parameters in Selective Laser Sintering Process. *Rapid Prototyping J.* **1997**, *3*, 129–136.
- (20) Shirazi, S. F. S.; Gharehkhani, S.; Mehrali, M.; Yarmand, H.; Metselaar, H. S. C.; Adib Kadri, N.; Osman, N. A. A. A Review on Powder-Based Additive Manufacturing for Tissue Engineering: Selective Laser Sintering and Inkjet 3D Printing. *Sci. Technol. Adv. Mater.* **2015**, *16*, No. 33502.
- (21) Fina, F.; Goyanes, A.; Gaisford, S.; Basit, A. W. Selective Laser Sintering (SLS) 3D Printing of Medicines. *Int. J. Pharm.* **2017**, *529*, 285–293.
- (22) Dizon, J. R. C.; Espera, A. H.; Chen, Q.; Advincula, R. C. Mechanical Characterization of 3D-Printed Polymers. *Addit. Manuf.* **2018**, *20*, 44–67.
- (23) Lahtinen, E.; Hänninen, M. M.; Kinnunen, K.; Tuononen, H. M.; Väisänen, A.; Rissanen, K.; Haukka, M. Porous 3D Printed Scavenger Filters for Selective Recovery of Precious Metals from Electronic Waste. *Adv. Sustainable Syst.* **2018**, *2*, No. 1800048.
- (24) Lahtinen, E.; Precker, R. L. M.; Lahtinen, M.; Hey-Hawkins, E.; Haukka, M. Selective Laser Sintering of Metal-Organic Frameworks:

Production of Highly Porous Filters by 3D Printing onto a Polymeric Matrix. *ChemPlusChem* **2019**, *84*, 222–225.

(25) Yang, M.-Q.; Pan, X.; Zhang, N.; Xu, Y.-J. A Facile One-Step Way to Anchor Noble Metal (Au, Ag, Pd) Nanoparticles on a Reduced Graphene Oxide Mat with Catalytic Activity for Selective Reduction of Nitroaromatic Compounds. *CrystEngComm* **2013**, *15*, 6819–6828.

(26) Li, J.; Liu, C.; Liu, Y. Au/Graphene Hydrogel: Synthesis, Characterization and Its Use for Catalytic Reduction of 4-Nitrophenol. *J. Mater. Chem.* **2012**, *22*, 8426–8430.

(27) Kuroda, K.; Ishida, T.; Haruta, M. Reduction of 4-Nitrophenol to 4-Aminophenol over Au Nanoparticles Deposited on PMMA. *J. Mol. Catal. A: Chem.* **2009**, *298*, 7–11.

(28) Liu, X.; Xu, H.; Xia, H.; Wang, D. Rapid Seeded Growth of Monodisperse, Quasi-Spherical, Citrate-Stabilized Gold Nanoparticles via H₂O₂ Reduction. *Langmuir* **2012**, *28*, 13720–13726.

(29) International Centre for Diffraction Data, ICDD-PDF4+, Release 2018, 12 CampusBoulevard, Newton Square, Pennsylvania, 2018.

(30) Degen, T.; Sadki, M.; Bron, E.; König, U.; Nénert, G. The HighScore Suite. *Powder Diffr.* **2014**, *29*, S13–S18.

DEPARTMENT OF CHEMISTRY, UNIVERSITY OF JYVÄSKYLÄ
RESEARCH REPORT SERIES

1. Vuolle, Mikko: Electron paramagnetic resonance and molecular orbital study of radical ions generated from (2.2)metacyclophane, pyrene and its hydrogenated compounds by alkali metal reduction and by thallium(III)trifluoroacetate oxidation. (99 pp.) 1976
2. Pasanen, Kaija: Electron paramagnetic resonance study of cation radical generated from various chlorinated biphenyls. (66 pp.) 1977
3. Carbon-13 Workshop, September 6-8, 1977. (91 pp.) 1977
4. Laihia, Katri: On the structure determination of norbornane polyols by NMR spectroscopy. (111 pp.) 1979
5. Nyrönen, Timo: On the EPR, ENDOR and visible absorption spectra of some nitrogen containing heterocyclic compounds in liquid ammonia. (76 pp.) 1978
6. Talvitie, Antti: Structure determination of some sesquiterpenoids by shift reagent NMR. (54 pp.) 1979
7. Häkli, Harri: Structure analysis and molecular dynamics of cyclic compounds by shift reagent NMR. (48 pp.) 1979
8. Pitkänen, Ilkka: Thermodynamics of complexation of 1,2,4-triazole with divalent manganese, cobalt, nickel, copper, zinc, cadmium and lead ions in aqueous sodium perchlorate solutions. (89 pp.) 1980
9. Asunta, Tuula: Preparation and characterization of new organometallic compounds synthesized by using metal vapours. (91 pp.) 1980
10. Sattar, Mohammad Abdus: Analyses of MCPA and its metabolites in soil. (57 pp.) 1980
11. Bibliography 1980. (31 pp.) 1981
12. Knuuttila, Pekka: X-Ray structural studies on some divalent 3d metal compounds of picolinic and isonicotinic acid N-oxides. (77 pp.) 1981
13. Bibliography 1981. (33 pp.) 1982
14. 6th National NMR Symposium, September 9-10, 1982, Abstracts. (49 pp.) 1982
15. Bibliography 1982. (38 pp.) 1983
16. Knuuttila, Hilikka: X-Ray structural studies on some Cu(II), Co(II) and Ni(II) complexes with nicotinic and isonicotinic acid N-oxides. (54 pp.) 1983
17. Symposium on inorganic and analytical chemistry May 18, 1984, Program and Abstracts. (100 pp.) 1984
18. Knuutinen, Juha: On the synthesis, structure verification and gas chromatographic determination of chlorinated catechols and guaiacols occurring in spent bleach liquors of kraft pulp mill. (30 pp.) 1984
19. Bibliography 1983. (47 pp.) 1984
20. Pitkänen, Maija: Addition of BrCl, B₂ and Cl₂ to methyl esters of propenoic and 2-butenic acid derivatives and ¹³C NMR studies on methyl esters of saturated

DEPARTMENT OF CHEMISTRY, UNIVERSITY OF JYVÄSKYLÄ
RESEARCH REPORT SERIES

- aliphatic mono- and dichlorocarboxylic acids. (56 pp.) 1985
21. Bibliography 1984. (39 pp.) 1985
22. Salo, Esa: EPR, ENDOR and TRIPLE spectroscopy of some nitrogen heteroaromatics in liquid ammonia. (111 pp.) 1985
23. Humppi, Tarmo: Synthesis, identification and analysis of dimeric impurities of chlorophenols. (39 pp.) 1985
24. Aho, Martti: The ion exchange and adsorption properties of sphagnum peat under acid conditions. (90 pp.) 1985
25. Bibliography 1985 (61 pp.) 1986
26. Bibliography 1986. (23 pp.) 1987
27. Bibliography 1987. (26 pp.) 1988
28. Paasivirta, Jaakko (Ed.): Structures of organic environmental chemicals. (67 pp.) 1988
29. Paasivirta, Jaakko (Ed.): Chemistry and ecology of organo-element compounds. (93 pp.) 1989
30. Sinkkonen, Seija: Determination of crude oil alkylated dibenzothiophenes in environment. (35 pp.) 1989
31. Kolehmainen, Erkki (Ed.): XII National NMR Symposium Program and Abstracts. (75 pp.) 1989
32. Kuokkanen, Tauno: Chlorocymenes and Chlorocymenenes: Persistent chlorocompounds in spent bleach liquors of kraft pulp mills. (40 pp.) 1989
33. Mäkelä, Reijo: ESR, ENDOR and TRIPLE resonance study on substituted 9,10-anthraquinone radicals in solution. (35 pp.) 1990
34. Veijanen, Anja: An integrated sensory and analytical method for identification of off-flavour compounds. (70 pp.) 1990
35. Kasa, Seppo: EPR, ENDOR and TRIPLE resonance and molecular orbital studies on a substitution reaction of anthracene induced by thallium(III) in two fluorinated carboxylic acids. (114 pp.) 1990
36. Herve, Sirpa: Mussel incubation method for monitoring organochlorine compounds in freshwater recipients of pulp and paper industry. (145 pp.) 1991
37. Pohjola, Pekka: The electron paramagnetic resonance method for characterization of Finnish peat types and iron (III) complexes in the process of peat decomposition. (77 pp.) 1991
38. Paasivirta, Jaakko (Ed.): Organochlorines from pulp mills and other sources. Research methodology studies 1988-91. (120 pp.) 1992
39. Veijanen, Anja (Ed.): VI National Symposium on Mass Spectrometry, May 13-15, 1992, Abstracts. (55 pp.) 1992
40. Rissanen, Kari (Ed.): The 7. National Symposium on Inorganic and Analytical Chemistry, May 22, 1992, Abstracts and Program. (153 pp.) 1992
41. Paasivirta, Jaakko (Ed.): CEOEC'92, Second

- Finnish-Russian Seminar:
Chemistry and Ecology of
Organo-Element Compounds.
(93 pp.) 1992
42. Koistinen, Jaana: Persistent polychloroaromatic compounds in the environment: structure-specific analyses. (50 pp.) 1993
43. Virkki, Liisa: Structural characterization of chlorolignins by spectroscopic and liquid chromatographic methods and a comparison with humic substances. (62 pp.) 1993
44. Helenius, Vesa: Electronic and vibrational excitations in some biologically relevant molecules. (30 pp.) 1993
45. Leppä-aho, Jaakko: Thermal behaviour, infrared spectra and x-ray structures of some new rare earth chromates(VI). (64 pp.) 1994
46. Kotila, Sirpa: Synthesis, structure and thermal behavior of solid copper(II) complexes of 2-amino-2-hydroxymethyl-1,3-propanediol. (111 pp.) 1994
47. Mikkonen, Anneli: Retention of molybdenum(VI), vanadium(V) and tungsten(VI) by kaolin and three Finnish mineral soils. (90 pp.) 1995
48. Suontamo, Reijo: Molecular orbital studies of small molecules containing sulfur and selenium. (42 pp.) 1995
49. Hämäläinen, Jouni: Effect of fuel composition on the conversion of fuel-N to nitrogen oxides in the combustion of small single particles. (50 pp.) 1995
50. Nevalainen, Tapio: Polychlorinated diphenyl ethers: synthesis, NMR spectroscopy, structural properties, and estimated toxicity. (76 pp.) 1995
51. Aittola, Jussi-Pekka: Organochloro compounds in the stack emission. (35 pp.) 1995
52. Harju, Timo: Ultrafast polar molecular photophysics of (dibenzylmethine)borondifluoride and 4-aminophthalimide in solution. (61 pp.) 1995
53. Maatela, Paula: Determination of organically bound chlorine in industrial and environmental samples. (83 pp.) 1995
54. Paasivirta, Jaakko (Ed.): CEOEC'95, Third Finnish-Russian Seminar: Chemistry and Ecology of Organo-Element Compounds. (109 pp.) 1995
55. Huuskonen, Juhani: Synthesis and structural studies of some supramolecular compounds. (54 pp.) 1995
56. Palm, Helena: Fate of chlorophenols and their derivatives in sawmill soil and pulp mill recipient environments. (52 pp.) 1995
57. Rantio, Tiina: Chlorohydrocarbons in pulp mill effluents and their fate in the environment. (89 pp.) 1997
58. Ratilainen, Jari: Covalent and non-covalent interactions in molecular recognition. (37 pp.) 1997
59. Kolehmainen, Erkki (Ed.): XIX National NMR Symposium, June 4-6, 1997, Abstracts. (89 pp.)

DEPARTMENT OF CHEMISTRY, UNIVERSITY OF JYVÄSKYLÄ
RESEARCH REPORT SERIES

- 1997
60. Matilainen, Rose: Development of methods for fertilizer analysis by inductively coupled plasma atomic emission spectrometry. (41 pp.) 1997
 61. Koistinen, Jari (Ed.): Spring Meeting on the Division of Synthetic Chemistry, May 15-16, 1997, Program and Abstracts. (36 pp.) 1997
 62. Lappalainen, Kari: Monomeric and cyclic bile acid derivatives: syntheses, NMR spectroscopy and molecular recognition properties. (50 pp.) 1997
 63. Laitinen, Eira: Molecular dynamics of cyanine dyes and phthalimides in solution: picosecond laser studies. (62 pp.) 1997
 64. Eloranta, Jussi: Experimental and theoretical studies on some quinone and quinol radicals. (40 pp.) 1997
 65. Oksanen, Jari: Spectroscopic characterization of some monomeric and aggregated chlorophylls. (43 pp.) 1998
 66. Häkkänen, Heikki: Development of a method based on laserinduced plasma spectrometry for rapid spatial analysis of material distributions in paper coatings. (60 pp.) 1998
 67. Virtapohja, Janne: Fate of chelating agents used in the pulp and paper industries. (58 pp.) 1998
 68. Airola, Karri: X-ray structural studies of supramolecular and organic compounds. (39 pp.) 1998
 69. Hyötyläinen, Juha: Transport of lignin-type compounds in the receiving waters of pulp mills. (40 pp.) 1999
 70. Ristolainen, Matti: Analysis of the organic material dissolved during totally chlorine-free bleaching. (40 pp.) 1999
 71. Eklin, Tero: Development of analytical procedures with industrial samples for atomic emission and atomic absorption spectrometry. (43 pp.) 1999
 72. Välisaari, Jouni: Hygiene properties of resol-type phenolic resin laminates. (129 pp.) 1999
 73. Hu, Jiwei: Persistent polyhalogenated diphenyl ethers: model compounds syntheses, characterization and molecular orbital studies. (59 pp.) 1999
 74. Malkavaara, Petteri: Chemometric adaptations in wood processing chemistry. (56 pp.) 2000
 75. Kujala Elena, Laihia Katri, Nieminen Kari (Eds.): NBC 2000, Symposium on Nuclear, Biological and Chemical Threats in the 21st Century. (299 pp.) 2000
 76. Rantalainen, Anna-Lea: Semipermeable membrane devices in monitoring persistent organic pollutants in the environment. (58 pp.) 2000
 77. Lahtinen, Manu: *In situ* X-ray powder diffraction studies of Pt/C, CuCl/C and Cu₂O/C catalysts at elevated temperatures in various reaction conditions. (92 pp.) 2000
 78. Tamminen, Jari: Syntheses, empirical and theoretical

- characterization, and metal cation complexation of bile acid-based monomers and open/closed dimers. (54 pp.) 2000
79. Vatanen, Virpi: Experimental studies by EPR and theoretical studies by DFT calculations of Π amino-9,10-anthraquinone radical anions and cations in solution. (37 pp.) 2000
80. Kotilainen, Risto: Chemical changes in wood during heating at 150-260 °C. (57 pp.) 2000
81. Nissinen, Maija: X-ray structural studies on weak, non-covalent interactions in supramolecular compounds. (69 pp.) 2001
82. Wegelius, Elina: X-ray structural studies on self-assembled hydrogen-bonded networks and metallosupramolecular complexes. (84 pp.) 2001
83. Paasivirta, Jaakko (Ed.): CEOEC'2001, Fifth Finnish-Russian Seminar: Chemistry and Ecology of Organo-Element Compounds. (163 pp.) 2001
84. Kiljunen, Toni: Theoretical studies on spectroscopy and atomic dynamics in rare gas solids. (56 pp.) 2001
85. Du, Jin: Derivatives of dextran: synthesis and applications in oncology. (48 pp.) 2001
86. Koivisto, Jari: Structural analysis of selected polychlorinated persistent organic pollutants (POPs) and related compounds. (88 pp.) 2001
87. Feng, Zhinan: Alkaline pulping of non-wood feedstocks and characterization of black liquors. (54 pp.) 2001
88. Halonen, Markku: Lahon havupuun käyttö sulfaattiprosessin raaka-aineena sekä havupuun lahontorjunta. (90 pp.) 2002
89. Falábu, Dezsö: Synthesis, conformational analysis and complexation studies of resorcarene derivatives. (212 pp.) 2001
90. Lehtovuori, Pekka: EMR spectroscopic studies on radicals of ubiquinones Q-*n*, vitamin K3 and vitamine E in liquid solution. (40 pp.) 2002
91. Perkkalainen, Paula: Polymorphism of sugar alcohols and effect of grinding on thermal behavior on binary sugar alcohol mixtures. (53 pp.) 2002
92. Ihalainen, Janne: Spectroscopic studies on light-harvesting complexes of green plants and purple bacteria. (42 pp.) 2002
93. Kunttu, Henrik, Kiljunen, Toni (Eds.): 4th International Conference on Low Temperature Chemistry. (159 pp.) 2002
94. Väisänen, Ari: Development of methods for toxic element analysis in samples with environmental concern by ICP-AES and ETAAS. (54 pp.) 2002
95. Luostarinen, Minna: Synthesis and characterisation of novel resorcarene derivatives. (200 pp.) 2002
96. Louhelainen, Jarmo: Changes in the chemical composition and

- physical properties of wood and nonwood black liquors during heating. (68 pp.) 2003
97. Lahtinen, Tanja: Concave hydrocarbon cyclophane π prismoids. (65 pp.) 2003
98. Laihia, Katri (Ed.): NBC 2003, Symposium on Nuclear, Biological and Chemical Threats – A Crisis Management Challenge. (245 pp.) 2003
99. Oasmaa, Anja: Fuel oil quality properties of wood-based pyrolysis liquids. (32 pp.) 2003
100. Virtanen, Elina: Syntheses, structural characterisation, and cation/anion recognition properties of nano-sized bile acidbased host molecules and their precursors. (123 pp.) 2003
101. Nättinen, Kalle: Synthesis and X-ray structural studies of organic and metallo-organic supramolecular systems. (79 pp.) 2003
102. Lampiselkä, Jarkko: Demonstraatio lukion kemian opetuksessa. (285 pp.) 2003
103. Kallioinen, Jani: Photoinduced dynamics of $\text{Ru}(\text{dcbpy})_2(\text{NCS})_2$ – in solution and on nanocrystalline titanium dioxide thin films. (47 pp.) 2004
104. Valkonen, Arto (Ed.): VII Synthetic Chemistry Meeting and XXVI Finnish NMR Symposium. (103 pp.) 2004
105. Vaskonen, Kari: Spectroscopic studies on atoms and small molecules isolated in low temperature rare gas matrices. (65 pp.) 2004
106. Lehtovuori, Viivi: Ultrafast light induced dissociation of $\text{Ru}(\text{dcbpy})(\text{CO})_2\text{I}_2$ in solution. (49 pp.) 2004
107. Saarenketo, Pauli: Structural studies of metal complexing Schiff bases, Schiff base derived *N*-glycosides and cyclophane π prismoids. (95 pp.) 2004
108. Paasivirta, Jaakko (Ed.): CEOEC'2004, Sixth Finnish-Russian Seminar: Chemistry and Ecology of Organo-Element Compounds. (147 pp.) 2004
109. Suontamo, Tuula: Development of a test method for evaluating the cleaning efficiency of hardsurface cleaning agents. (96 pp.) 2004
110. Güneş, Minna: Studies of thiocyanates of silver for nonlinear optics. (48 pp.) 2004
111. Ropponen, Jarmo: Aliphatic polyester dendrimers and dendrons. (81 pp.) 2004
112. Vu, Mân Thi Hong: Alkaline pulping and the subsequent elemental chlorine-free bleaching of bamboo (*Bambusa procera*). (69 pp.) 2004
113. Mansikkamäki, Heidi: Selfassembly of resorcinarenes. (77 pp.) 2006
114. Tuononen, Heikki M.: EPR spectroscopic and quantum chemical studies of some inorganic main group radicals. (79 pp.) 2005
115. Kaski, Saara: Development of methods and applications of laserinduced plasma

- spectroscopy in vacuum ultraviolet. (44 pp.) 2005
116. Mäkinen, Riika-Mari: Synthesis, crystal structure and thermal decomposition of certain metal thiocyanates and organic thiocyanates. (119 pp.) 2006
117. Ahokas, Jussi: Spectroscopic studies of atoms and small molecules isolated in rare gas solids: photodissociation and thermal reactions. (53 pp.) 2006
118. Busi, Sara: Synthesis, characterization and thermal properties of new quaternary ammonium compounds: new materials for electrolytes, ionic liquids and complexation studies. (102 pp.) 2006
119. Mäntykoski, Keijo: PCBs in processes, products and environment of paper mills using wastepaper as their raw material. (73 pp.) 2006
120. Laamanen, Pirkko-Leena: Simultaneous determination of industrially and environmentally relevant aminopolycarboxylic and hydroxycarboxylic acids by capillary zone electrophoresis. (54 pp.) 2007
121. Salmela, Maria: Description of oxygen-alkali delignification of kraft pulp using analysis of dissolved material. (71 pp.) 2007
122. Lehtovaara, Lauri: Theoretical studies of atomic scale impurities in superfluid ^4He . (87 pp.) 2007
123. Rautiainen, J. Mikko: Quantum chemical calculations of structures, bonding, and spectroscopic properties of some sulphur and selenium iodine cations. (71 pp.) 2007
124. Nummelin, Sami: Synthesis, characterization, structural and retrostructural analysis of self-assembling pore forming dendrimers. (286 pp.) 2008
125. Sopo, Harri: Uranyl(VI) ion complexes of some organic aminobisphenolate ligands: syntheses, structures and extraction studies. (57 pp.) 2008
126. Valkonen, Arto: Structural characteristics and properties of substituted cholanoates and *N* substituted cholanamides. (80 pp.) 2008
127. Lähde, Anna: Production and surface modification of pharmaceutical nano- and microparticles with the aerosol flow reactor. (43 pp.) 2008
128. Beyeh, Ngong Kodiah: Resorcinarenes and their derivatives: synthesis, characterization and complexation in gas phase and in solution. (75 pp.) 2008
129. Väliisaari, Jouni, Lundell, Jan (Eds.): Kemian opetuksen päivät 2008: uusia oppimisympäristöjä ja ongelmalähtöistä opetusta. (118 pp.) 2008
130. Myllyperkiö, Pasi: Ultrafast electron transfer from potential organic and metal containing solar cell sensitizers. (69 pp.) 2009
131. Käkölä, Jaana: Fast chromatographic methods for determining aliphatic carboxylic acids in black liquors. (82 pp.) 2009

DEPARTMENT OF CHEMISTRY, UNIVERSITY OF JYVÄSKYLÄ
RESEARCH REPORT SERIES

132. Koivukorpi, Juha: Bile acid-arene conjugates: from photoswitchability to cancer cell detection. (67 pp.) 2009
133. Tuuttila, Tero: Functional dendritic polyester compounds: synthesis and characterization of small bifunctional dendrimers and dyes. (74 pp.) 2009
134. Salorinne, Kirsi: Tetramethoxy resorcinarene based cation and anion receptors: synthesis, characterization and binding properties. (79 pp.) 2009
135. Rautiainen, Riikka: The use of first-thinning Scots pine (*Pinus sylvestris*) as fiber raw material for the kraft pulp and paper industry. (73 pp.) 2010
136. Ilander, Laura: Uranyl salophens: synthesis and use as ditopic receptors. (199 pp.) 2010
137. Kiviniemi, Tiina: Vibrational dynamics of iodine molecule and its complexes in solid krypton - Towards coherent control of bimolecular reactions? (73 pp.) 2010
138. Ikonen, Satu: Synthesis, characterization and structural properties of various covalent and non-covalent bile acid derivatives of N/O-heterocycles and their precursors. (105 pp.) 2010
139. Siitonen, Anni: Spectroscopic studies of semiconducting singlewalled carbon nanotubes. (56 pp.) 2010
140. Raatikainen, Kari: Synthesis and structural studies of piperazine cyclophanes - Supramolecular systems through Halogen and Hydrogen bonding and metal ion coordination. (69 pp.) 2010
141. Leivo, Kimmo: Gelation and gel properties of two- and threecomponent Pyrene based low molecular weight organogelators. (116 pp.) 2011
142. Martiskainen, Jari: Electronic energy transfer in light-harvesting complexes isolated from *Spinacia oleracea* and from three photosynthetic green bacteria *Chloroflexus aurantiacus*, *Chlorobium tepidum*, and *Prosthecochloris aestuarii*. (55 pp.) 2011
143. Wichmann, Oula: Syntheses, characterization and structural properties of [O,N,O,X'] aminobisphenolate metal complexes. (101 pp.) 2011
144. Ilander, Aki: Development of ultrasound-assisted digestion methods for the determination of toxic element concentrations in ash samples by ICP-OES. (58 pp.) 2011
145. The Combined XII Spring Meeting of the Division of Synthetic Chemistry and XXXIII Finnish NMR Symposium. Book of Abstracts. (90 pp.) 2011
146. Valto, Piia: Development of fast analysis methods for extractives in papermaking process waters. (73 pp.) 2011
147. Andersin, Jenni: Catalytic activity of palladium-based nanostructures in the conversion of simple olefinic hydro- and chlorohydrocarbons from first principles. (78 pp.) 2011

148. Aumanen, Jukka: Photophysical properties of dansylated poly(propylene amine) dendrimers. (55 pp.) 2011
149. Kärnä, Minna: Etherfunctionalized quaternary ammonium ionic liquids – synthesis, characterization and physicochemical properties. (76 pp.) 2011
150. Jurček, Ondřej: Steroid conjugates for applications in pharmacology and biology. (57 pp.) 2011
151. Nauha, Elisa: Crystalline forms of selected Agrochemical actives: design and synthesis of cocrystals. (77 pp.) 2012
152. Ahkola, Heidi: Passive sampling in monitoring of nonylphenol ethoxylates and nonylphenol in aquatic environments. (92 pp.) 2012
153. Helttunen, Kaisa: Exploring the self-assembly of resorcinarenes: from molecular level interactions to mesoscopic structures. (78 pp.) 2012
154. Linnanto, Juha: Light excitation transfer in photosynthesis revealed by quantum chemical calculations and exciton theory. (179 pp.) 2012
155. Roiko-Jokela, Veikko: Digital imaging and infrared measurements of soil adhesion and cleanability of semihard and hard surfaces. (122 pp.) 2012
156. Nojonen, Virpi: Amides of bile acids and biologically important small molecules: properties and applications. (85 pp.) 2012
157. Hulkko, Eero: Spectroscopic signatures as a probe of structure and dynamics in condensed-phase systems – studies of iodine and gold ranging from isolated molecules to nanoclusters. (69 pp.) 2012
158. Lappi, Hanna: Production of Hydrocarbon-rich biofuels from extractives-derived materials. (95 pp.) 2012
159. Nykänen, Lauri: Computational studies of Carbon chemistry on transition metal surfaces. (76 pp.) 2012
160. Ahonen, Kari: Solid state studies of pharmaceutically important molecules and their derivatives. (65 pp.) 2012
161. Pakkanen, Hannu: Characterization of organic material dissolved during alkaline pulping of wood and non-wood feedstocks. (76 pp.) 2012
162. Moilanen, Jani: Theoretical and experimental studies of some main group compounds: from closed shell interactions to singlet diradicals and stable radicals. (80 pp.) 2012
163. Himanen, Jatta: Stereoselective synthesis of Oligosaccharides by *De Novo* Saccharide welding. (133 pp.) 2012
164. Bunzen, Hana: Steroidal derivatives of nitrogen containing compounds as potential gelators. (76 pp.) 2013
165. Seppälä, Petri: Structural diversity of copper(II) amino alcohol complexes. Syntheses,

- structural and magnetic properties of bidentate amino alcohol copper(II) complexes. (67 pp.) 2013
166. Lindgren, Johan: Computational investigations on rotational and vibrational spectroscopies of some diatomics in solid environment. (77 pp.) 2013
167. Giri, Chandan: Sub-component self-assembly of linear and nonlinear diamines and diacylhydrazines, formylpyridine and transition metal cations. (145 pp.) 2013
168. Riisiö, Antti: Synthesis, Characterization and Properties of Cu(II)-, Mo(VI)- and U(VI) Complexes With Diaminotetraphenolate Ligands. (51 pp.) 2013
169. Kiljunen, Toni (Ed.): Chemistry and Physics at Low Temperatures. Book of Abstracts. (103 pp.) 2013
170. Hänninen, Mikko: Experimental and Computational Studies of Transition Metal Complexes with Polydentate Amino- and Aminophenolate Ligands: Synthesis, Structure, Reactivity and Magnetic Properties. (66 pp.) 2013
171. Antila, Liisa: Spectroscopic studies of electron transfer reactions at the photoactive electrode of dye-sensitized solar cells. (53 pp.) 2013
172. Kemppainen, Eeva: MukaiyamaMichael reactions with α substituted acroleins – a useful tool for the synthesis of the pectenotoxins and other natural product targets. (190 pp.) 2013
173. Virtanen, Suvi: Structural Studies of Dielectric Polymer Nanocomposites. (49 pp.) 2013
174. Yliniemelä-Sipari, Sanna: Understanding The Structural Requirements for Optimal Hydrogen Bond Catalyzed Enolization – A Biomimetic Approach. (160 pp.) 2013
175. Leskinen, Mikko V: Remote β functionalization of β' -keto esters. (105 pp.) 2014
176. 12th European Conference on Research in Chemistry Education (ECRICE2014). Book of Abstracts. (166 pp.) 2014
177. Peuronen, Anssi: N-Monoalkylated DABCO-Based N-Donors as Versatile Building Blocks in Crystal Engineering and Supramolecular Chemistry. (54 pp.) 2014
178. Perämäki, Siiri: Method development for determination and recovery of rare earth elements from industrial fly ash. (88 pp.) 2014
179. Chernyshev, Alexander, N.: Nitrogen-containing ligands and their platinum(IV) and gold(III) complexes: investigation and basicity and nucleophilicity, luminescence, and aurophilic interactions. (64 pp.) 2014
180. Lehto, Joni: Advanced Biorefinery Concepts Integrated to Chemical Pulping. (142 pp.) 2015
181. Tero, Tiia-Riikka: Tetramethoxy resorcinarenes as platforms for

- fluorescent and halogen bonding systems. (61 pp.) 2015
182. Löfman, Miika: Bile acid amides as components of microcrystalline organogels. (62 pp.) 2015
183. Selin, Jukka: Adsorption of softwood-derived organic material onto various fillers during papermaking. (169 pp.) 2015
184. Piisola, Antti: Challenges in the stereoselective synthesis of allylic alcohols. (210 pp.) 2015
185. Bonakdarzadeh, Pia: Supramolecular coordination polyhedra based on achiral and chiral pyridyl ligands: design, preparation, and characterization. (65 pp.) 2015
186. Vasko, Petra: Synthesis, characterization, and reactivity of heavier group 13 and 14 metallylenes and metalloid clusters: small molecule activation and more. (66 pp.) 2015
187. Topić, Filip: Structural Studies of Nano-sized Supramolecular Assemblies. (79 pp.) 2015
188. Mustalahti, Satu: Photodynamics Studies of Ligand-Protected Gold Nanoclusters by using Ultrafast Transient Infrared Spectroscopy. (58 pp.) 2015
189. Koivisto, Jaakko: Electronic and vibrational spectroscopic studies of gold-nanoclusters. (63 pp.) 2015
190. Suhonen, Aku: Solid state conformational behavior and interactions of series of aromatic oligoamide foldamers. (68 pp.) 2016
191. Soikkeli, Ville: Hydrometallurgical recovery and leaching studies for selected valuable metals from fly ash samples by ultrasound-assisted extraction followed by ICP-OES determination. (107 pp.) 2016
192. XXXVIII Finnish NMR Symposium. Book of Abstracts. (51 pp.) 2016
193. Mäkelä, Toni: Ion Pair Recognition by Ditopic Crown Ether Based bis-Urea and Uranyl Salophen Receptors. (75 pp.) 2016
194. Lindholm-Lehto, Petra: Occurrence of pharmaceuticals in municipal wastewater treatment plants and receiving surface waters in Central and Southern Finland. (98 pp.) 2016
195. Härkönen, Ville: Computational and Theoretical studies on Lattice Thermal conductivity and Thermal properties of Silicon Clathrates. (89 pp.) 2016
196. Tuokko, Sakari: Understanding selective reduction reactions with heterogeneous Pd and Pt: climbing out of the black box. (85 pp.) 2016
197. Nuora, Piia: Monitapaustutkimus LUMA-Toimintaan liittyvissä oppimisympäristöissä tapahtuvista kemian oppimiskokemuksista. (171 pp.) 2016
198. Kumar, Hemanathan: Novel Concepts on The Recovery of ByProducts from Alkaline Pulping. (61 pp.) 2016
199. Arnedo-Sánchez, Leticia: Lanthanide and Transition Metal

- Complexes as Building Blocks for Supramolecular Functional Materials. (227 pp.) 2016
200. Gell, Lars: Theoretical Investigations of Ligand Protected Silver Nanoclusters. (134 pp.) 2016
201. Vaskuri, Juhani: Oppiennätyksistä opetussuunnitelman perusteisiin - lukion kemian kansallisen opetussuunnitelman kehittyminen Suomessa vuosina 1918-2016. (314 pp.) 2017
202. Lundell Jan, Kiljunen Toni (Eds.): 22nd Horizons in Hydrogen Bond Research. Book of Abstracts. 2017
203. Turunen, Lotta: Design and construction of halogen-bonded capsules and cages. (61 pp.) 2017
204. Hurmalainen, Juha: Experimental and computational studies of unconventional main group compounds: stable radicals and reactive intermediates. (88 pp.) 2017
205. Koivistoinen Juha: Non-linear interactions of femtosecond laser pulses with graphene: photooxidation, imaging and photodynamics. (68 pp.) 2017
206. Chen, Chengcong: Combustion behavior of black liquors: droplet swelling and influence of liquor composition. (39 pp.) 2017
207. Mansikkamäki, Akseli: Theoretical and Computational Studies of Magnetic Anisotropy and Exchange Coupling in Molecular Systems. (190 p. + included articles) 2018.
208. Tatikonda, Rajendhraprasad: Multivalent N-donor ligands for the construction of coordination polymers and coordination polymer gels. (62 pp.) 2018
209. Budhathoki, Roshan: Beneficiation, desilication and selective precipitation techniques for phosphorus refining from biomass derived fly ash. (64 pp.) 2018
210. Siitonen, Juha: Synthetic Studies on 1-azabicyclo[5.3.0]decane Alkaloids. (140 pp.) 2018
211. Ullah, Saleem: Advanced Biorefinery Concepts Related to Non-wood Feedstocks. (57 pp.) 2018
212. Ghalibaf, Maryam: Analytical Pyrolysis of Wood and NonWood Materials from Integrated Biorefinery Concepts. (106 pp.) 2018

DEPARTMENT OF CHEMISTRY, UNIVERSITY OF JYVÄSKYLÄ
DISSERTATIONS PUBLISHED IN THE JYU DISSERTATIONS RESEARCH SERIES

1. Bulatov, Evgeny: Synthetic and structural studies of covalent and non-covalent interactions of ligands and metal center in platinum(II) complexes containing 2,2'-dipyridylamine or oxime ligands. (58 pp.) 2019. JYU Dissertations 70.
2. Annala, Riia: Conformational Properties and Anion Complexes of Aromatic Oligoamide Foldamers. (80 pp.) 2019. JYU Dissertations 84.
3. Isoaho, Jukka Pekka: Dithionite Bleaching of Thermomechanical Pulp - Chemistry and Optimal Conditions. (73 pp.) 2019. JYU Dissertations 85.
4. Nygrén, Enni: Recovery of rubidium from power plant fly ash. (98 pp.) 2019. JYU Dissertations 136.
5. Kiesilä, Anniina: Supramolecular chemistry of anion-binding receptors based on concave macromolecules. (68 pp.) 2019. JYU Dissertations 137.
6. Sokolowska, Karolina: Study of water-soluble p-MBA-protected gold nanoclusters and their superstructures. 2019. JYU Dissertations.